Communication of Blood Vessels and Hepatic Cell Types During Liver Regeneration

Inaugural-Dissertation

zur Erlangung des Doktorgrades
der Mathematisch-Naturwissenschaftlichen Fakultät
der Heinrich-Heine-Universität Düsseldorf

vorgelegt von

Tobias Buschmann
aus Oberhausen

Düsseldorf, Januar 2017

aus dem Institut für
der Heinrich-Heine-Universität Düsseldorf

Gedruckt mit der Genehmigung der
Mathematisch-Naturwissenschaftlichen Fakultät der
Heinrich-Heine-Universität Düsseldorf

Referent: Prof. Dr. Eckhard Lammert

Korreferent: Prof. Dr. Hermann Aberle

Tag der mündlichen Prüfung:
(bitte bei der Abgabe Ihrer Dissertation noch offen lassen)

„Keine Zukunft ohne Kampf -
Lethargie ist Untergang!“

- Callejon

Inhaltsverzeichnis

Zusammenfassung

Die Leber hat eine einzigartige Regenerationsfähigkeit. Nach dem Verlust von Gewebe, zum Beispiel durch einen Unfall, können die verbleibenden Leberzellen (Hepatozyten) durch Proliferation den Verlust innerhalb weniger Tage ausgleichen.
Die partielle Hepatektomie (PHx) ist eine weit verbreitete Methode, um Leberregeneration molekular zu untersuchen. Diese Technik findet auch Anwendung an humanen Patienten, um Lebertumore oder Metastasen zu entfernen.
Während in den letzten Jahrzehnten viele wichtige Faktoren für die Leberregeneration identifiziert wurden, rückten angiokrine Faktoren in den Mittelpunkt der Forschung. Diese Faktoren spielen allerdings erst spät während des Regenerationprozesses eine Rolle. In dieser Arbeit wurde die Hypothese untersucht, dass nach PHx, bedingt durch die kleinere Organmasse, hämodynamische Veränderungen auftreten und dies eine Rolle bei der Induktion der Leberregeneration spielen kann.
Zunächst wurden hämodynamische Veränderungen nach PHx untersucht und später die Folgen dieser auf zellulärer Ebene untersucht. Dazu wurden verschiedene moderne *in vivo-, ex vivo-* und *in vitro*-Methoden angewendet. Mit Hilfe von kontrastmittelverstärktem Ultraschall konnte ein höheres Blutvolumen in der Leber nach PHx nachgewiesen werden.
Das erhöhte Verhältnis von Blutvolumen zur Organmasse korrelierte mit gedehnten Blutgefäßen und dadurch gestreckten Endothelzellen. Die hämodynamischen Veränderungen nach PHx resultierten in mechanischen Kräften, die dazu führten das wichtige Faktoren für die Leberregeneration stärker exprimiert wurden. Sowohl der Makrophagen-Migrations-Inhibitions-Faktor (MIF) wie auch das intrazelluläre Adhesionsmolekül-1 (ICAM-1) wurden durch erhöhte mechanische Kräfte hochreguliert. Dies konnte sowohl *in vivo*, *in vitro* und *ex vivo* gezeigt werden. Des Weiteren wurde gezeigt, dass ICAM-1 durch MIF sowohl *in vivo* wie auch *in vitro* reguliert wird. ICAM-1 wurde in früheren Arbeiten bereits als wichtiger Faktor für die Leberregeneration identifiziert. Durch die Verwendung von genetisch veränderten Mäusen konnte ein relevanter Beitrag von β1 Integrin für die Hochregulierung von MIF als auch für die Leberregeneration festgestellt werden. β1 Integrin wird dabei für die Weiterleitung der mechanischen Kräfte benötigt. Letztendlich konnte MIF als neuer

wichtiger Faktor für die Leberregeneration, durch die Verwendung von MIF Knockout Mäusen, identifiziert werden.
Durch die Ergebnisse konnten zum ersten Mal mechanische Kräfte bedingt durch hämodynamische Veränderungen mit der Leberregeneration in Verbindung gebracht und die molekularen Hintergründe teilweise aufgedeckt werden.

Summary

The liver has a unique capability to regenerate after tissue loss. Partial hepatectomy (PHx) is a common technique to study liver regeneration. This technique is also used in human patients to remove hepatic tumors or metastases. Many important factors for liver regeneration were discovered in the last decades, and here angiocrine factors moved in the focus of research. Notably, these factors play a role in the late regenerative process. In this thesis the hypothesis was examined, that due to the reduced organ mass after PHx, hemodynamic changes may occur and that this would play a role in induction of liver regeneration. At first, hemodynamic changes were examined after PHx, and the molecular effects of these changes were examined on a cellular level using several state-of-the-art *in vivo, ex vivo* and *in vitro* methods. Using contrast enhanced ultrasound, a higher blood volume in the liver could be observed after PHx. This increased blood-to-liver ratio correlates with dilated blood vessels and therefore stretched endothelial cells. The hemodynamic changes after PHx resulted in mechanical forces, which triggered higher expression for important factors for liver regeneration. Both macrophage migration inhibitory factor (MIF) and intracellular adhesion molecule-1 (ICAM-1) were upregulated by elevated mechanical forces. This effect could be demonstrated *in vivo*, *in vitro* and *ex vivo* experiments. Moreover, it was shown that ICAM-1 could be regulated by MIF *in vivo* and *in vitro*. ICAM-1 was already described as an important factor for liver regeneration in previous reports. Using genetically modified mice, a relevant contribution of β1 integrin for the upregulation of MIF and for liver regeneration could be observed. Thereby, β1 integrin is crucial for the transduction of the mechanical forces. Finally, MIF knockout mice were used to identify MIF as a new important factor for liver regeneration. In sum, mechanical forces induced by hemodynamic changes could be linked to liver regeneration and molecular insights into this process were gained.

1 Introduction

1.1 The Liver

The liver is a large gland with essential functions in glucose and lipid homeostasis, detoxification and hormone production. But also other physiological functions e.g. nutrition storage, plasma protein synthesis, bile formation and detoxification[1]. The secretion of bile is important for lipid digestion. Therefore bile secretion is the major exocrine function of the liver[2]. The liver also plays an important role in drug metabolism[3,4]. And it displays the largest reticulo-endothelial cell network in the body[5].
In humans the liver is located in the upper right area of the abdomen, right beneath the diaphragm[6]. It comprises about 2 % of the body weight[5]. In mice the liver occupies the whole subdiaphragmatic space[6] and constitute about 6 % of the bodyweight[6]. But also 3.5-4 % bodyweight are reported for mice livers[7].
Beside the important physiological functions, severe diseases can also affect the liver. This can be acute and chronic hepatitis for example. This disease can evolve into fibrosis. If fibrosis progresses, it can develop into cirrhosis and furthermore even in primary liver cancer (hepatocellular carcinoma, HCC)[8].
The liver also plays an important role in insulin resistance and type 2 diabetes mellitus (T2DM)[9].
The structure of the liver is pretty conserved among mammals. In mice and men the liver is segmented into four lobes. In mice these lobes are termed median, left, right and caudate lobe[7]. In humans, the lobes are termed left, right, caudate and quadrate lobe. In addition in humans, but not in mice the liver lobe is traversed by ligaments (between the right and left liver lobe)[6].
For medical applications the liver is artificially divided in seven lobes. This artificial nomenclature is aligned to areas, which are pervaded by bigger blood vessels. Those vessels display important obstacles for example in metastases surgery.

1.1.1 Microscopic Anatomy

On a microscopic level the functional unit of the liver is represented by the hepatic lobule[10] (also known as acinus[1]). These lobules consist of so called “hepatocyte lines”, strings of 15-25 liver parenchymal cells (hepatocytes), which are lined by liver sinusoids (specialized capillaries). The lobules show a roughly hexagonal shape and have a size of about 1-2mm in diameter in humans[5,11].

On the edges of these lobules, branches of the arterioles, venules, bile ductules, and lymphatics occur in a structure denoted as portal triads (or portal tracts or portal field)[6] (Figure 1A).

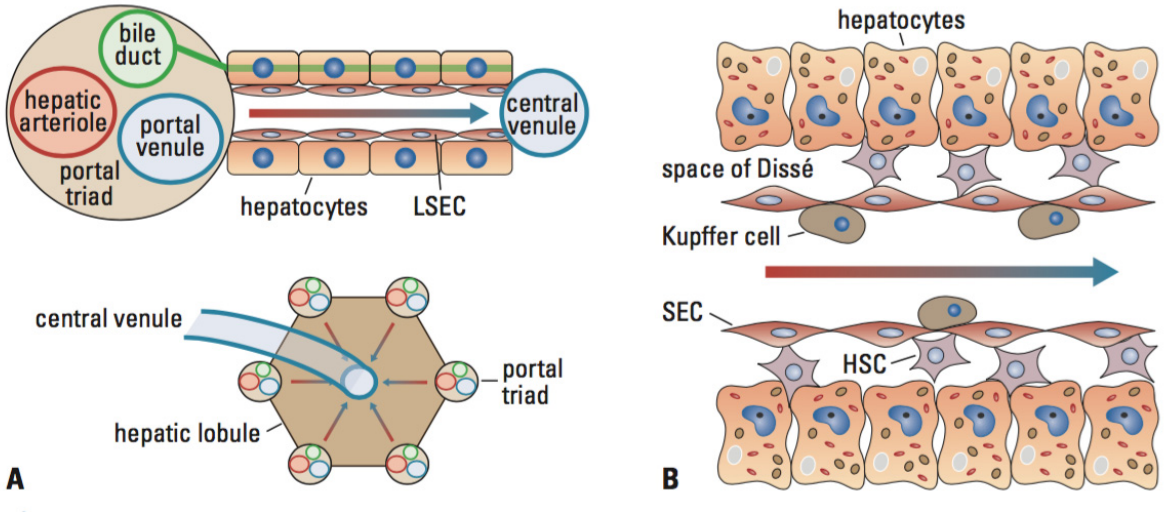

Figure 1: Overview of microscopic liver anatomy. The functional unit of the liver parenchyma is the hepatic lobule (A). These lobules are roughly hexagonal in shape and about 1-2 diameters in size. On the edges of the lobules, ramifications from the hepatic artery, hepatic portal vein und the bilde duct branch into the liver sinusoids (B). Cell types of the liver sinusoids and their schematic arrangement is shown in (B). Liver sinusoids are build of (liver) sinusoidal endothelial cells ((L)SECs) but also hepatic stellate cells (HSC) and Kupffer cells (KC). LSECs are separated from the parenchyma by the space of Disse or perisunusoidal space (B). Figure taken from: Angiogenesis and Liver Regeneration. *Liver Regeneration* 2011, De Gruyter.

1.1.2 Hepatic blood flow

The liver is a well-perfused organ since it receives 25 % of the cardiac output[12] via two large vessels, hence the hepatic portal vein (*vena portae*) and the hepatic artery

(*arteria hepatica propria*) provide blood to the liver. In total the oxygen amount brought to the liver is more or less equal in both vessels[13] but approximately two third of the liver blood is supplied via the portal vein. The hepatic portal vein originates from the merge of the superior mesenteric vein with the splenic vein and inferior mesenteric vein. The portal blood flows through other abdominal organs i.e. pancreas, duodenum, spleen, stomach and colon[10] before perfusing the liver parenchyma. Those organs consume lots of the containing oxygen but accumulate nutrients in the passing blood. On the other hand, the hepatic artery delivers about one third of the liver blood amount. This blood is in contrast to the portal vein blood well oxygenated but low in nutrients[10]. Both blood vessels enter the liver at the liver hilum or transverse fissure of the liver (*porta hepatis*). At this fissure beneath the *lobus caudatus* and *lobus quadratus* the blood vessels enter and the bile duct is leaving the liver[10]. Also nerves[14] and lymph vessels[15] pervade the liver at this anatomic feature.

Rectangular branches from these pervading vessels drain into the sinusoids where the venous and arterial blood mixes. After circulating in this anastomosing capillary network the blood empties into the central vein, the blood collecting venule in the center of the lobule[16]. These venules consolidate to the hepatic vein which ends in the inferior vena cava, who eventually ends in the right atrium of the heart[17]. The sinusoids are a very specialized endothelial bed to support the physiologic functions of the liver. For example those capillaries have a low basement membrane and function as an selective sieve[16]. The discontinuous basement membrane in combination with the fenestrated endothelium with allows an improved exchange of nutrients, hormones and other small molecules between hepatocytes and the blood[10].

In contrast to other vascular beds, the sinusoidal endothelial cells are not directly connected to the tissue but separated by a perisinusoidal space (space of Disse) (Figure 1B). This anatomic feature is named after the German anatomist Joseph Hugo Vincenz Disse (1852-1912) and about 10-15 µm in width.

In general the blood flow in capillaries is slow. This supports the exchange from substances between blood and tissue[17]. In liver sinusoids the blood flow is even slower (0.4-0.45 mm/sec)[18] compared to other organs such as brain (0.79 mm/sec) or skeletal muscle (1.14 mm/sec)[19].

The blood pressure in the hepatic artery is 20 to 40 fold higher than in the sinusoids[18].

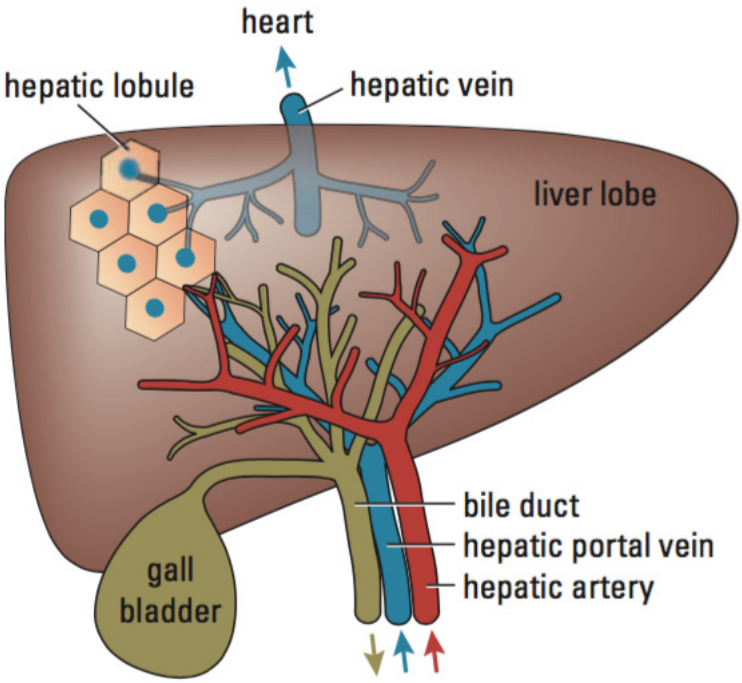

Figure 2: Scheme of blood flow in the liver. The liver receives a dual blood supply. In total 25 % of the cardiac output perfuses the liver, thereby 2/3 is supplied by the portal vein and about 1/3 is supplied by the hepatic artery. The vessels and the bile duct branch inside the liver. After passing hepatic lobules, the blood is drained to the hepatic vein and further to the heart. Branches of the bile duct collect bile, produced by hepatocytes, The bile is stored in the gall bladder. Figure taken from: Angiogenesis and Liver Regeneration. *Liver Regeneration* 2011, De Gruyter.

1.1.3 Liver cell types

The following cell types are represented in the liver:

1.1.3.1 Hepatocytes (Hep)

Hepatocytes are the most abundant cells in the liver, representing about 78 % of the liver volume[5]. These liver parenchymal cells occur polyploid (4n, 8n, 16n and higher) and mono-nucleated as well as bi-nucleated[20]. As parenchymal cells, the hepatocytes accomplish many of the metabolic functions e.g. nutrient storage or bile formation.

Hepatocytes line the liver sinusoids and are separated from liver endothelial cells by the space of Disse (Figure 1B).
Interestingly, the hepatocytes show a metabolic zonation[21] from the portal triad to the central venule. This heterogeneity displays for example in a higher degree of oxygen uptake, gluconeogenesis, cholesterol biosynthesis and ureogenesis periportally, whereas pericentrally the bile acid synthesis, glycolysis, liponeogenesis and glutamine synthesis is higher[22].
Proteins, involved in metabolic zonation could be recently linked to liver regeneration[23].

1.1.3.2 Liver sinusoidal endothelial cells (LSEC)

Liver sinusoidal endothelial cells are very specialized endothelial cells[17]. They occupy about 2.8 % of the liver volume[5] and represent about 50 percent of the non-parenchymal cells[16]. After hepatocytes this cell type occupies the second most liver volume[5] although they are numerically much less. LSECs built sinusoidal blood vessels, which are defined by a fenestration of the endothelial cell membranes and a discontinuous basement membrane (BM).
The fenestrated endothelium in combination with the discontinuous basement membrane allows a better exchange between hepatocytes and the blood.
LSECs show heterogeneity among the sinusoids from periportal (near the portal triad) to center lobular (near the central vein). This heterogeneity results in a shift of fenestrae size and overall porosity. Fenestrae among mice, rats and humans are pretty conserved in numbers per square µm and diameter (in nm)[24,25,26].
Periportally the fenestrae of rat livers have a larger diameter 110.7 ± 0.2 nm vs. 104.8 ± 0.2 nm) but pericentrally the fenestrated area per LSEC is larger (7.94 % vs. 5.96 %)[27].
LSECs also have scavenger functions because they can eliminate soluble waste macromolecules from the portal venous blood[16]. Among others, acetylated low-density lipoprotein (LDL) can be taken up by LSECs. This feature is used to proof the purity of isolated LSECs[28].
Furthermore LSECs fenestrae allow the transfer of lipoproteins and chylomicrons between blood and the space of Disse. In the space of Disse, lipoproteins and chylomicrons can be taken up by hepatocytes via receptor-mediated endocytosis[16].
Interestingly, LSECs share some similarities and express marker, typical for lymphatic endothelial cells. For example lymphatic vascular endothelial hyaluronan receptor-1

(LYVE-1)[29], vascular endothelial growth factor receptor-3 (VEGFR-3)[30]. In contrast LSECs express just low levels of typical blood endothelial markers like platelet endothelial cell adhesion molecule 1 (PECAM-1 / CD31) or von Willebrand factor (vWF)[31].

1.1.3.3 Kupffer cells (KC)

Kupffer cells are liver specific macrophages which represent the largest population of tissue-resident macrophages in the body[32]. The cells are named after the Baltic-German anatomist Karl Wilhelm Ritter von Kupffer (1829-1902) and represent about 2.1 % of the liver volume[5]. Thereby Kupffer cells are the second most non-parenchymal liver cells. They are located in the hepatic sinusoids, more precise in the space of Disse[33]. Kupffer cells are part of the innate immune system and eliminate pathogens like bacteria and parasites[33]. But Kupffer cells also participate in the adaptive immune system by presenting antigens via major histocompatibility complex (MHC) class I and II[34]. Kupffer cells are also supposed to eliminate cancer cells[35].

1.1.3.4 Hepatic stellate cells (HSC)

Hepatic stellate cells are liver specific, contractile pericytes[36] and represent about 1.4 % of the liver volume[5]. HSC are also known as Ito cells or perisinusoidal cells. The term perisinusoidal cell describes the location where these cells occur (space of Disse), whereas Ito cell appreciates the discoverer. Previously they were also called lipocytes or fat storing cells because they show fat droplets which store about 80 % of the vitamin A, present in the human body, in form of retinyl palmitate[37]. HSCs display protrusions whereby they adhere to LSECs or each other[38]. Today this cell type is controversial discussed because of their possible role both in liver disease and regeneration. Whereas the role as myofibroblasts in chronic liver inflammation, contributing in fibrosis is overall accepted in the scientific community, the idea that HSC serve as a liver specific stem cell is still heavily discussed. The current opinion is that HSC become activated (gain a myofibroblastic phenotype) by chronic liver inflammation and start to deposit extracellular matrix (ECM) as a response to the activation. This excessive ECM disturb the blood flow and leads to liver fibrosis[39].

Nevertheless, supporting data for a contributing role in liver regeneration are published[40,41].

1.1.3.5 Pit cells

Pit cells are a population of natural killer (NK) cells in the liver. They are defined as large granular lymphocytes (LGLs)[42]. Pit cells are components of the innate immune system and have the ability to kill certain tumor or viral infected cells without prior sensitization[43]. In contrast to other liver cell types, pit cells have been discovered more recently in 1976[42].

1.2 Liver Regeneration

The liver has a remarkable capacity to regenerate. This feature is required after tissue loss or (chronic) inflammation. In contrast to regeneration of other organs like skin, intestinal epithelium or mucosal tissue from the uterus, liver regeneration is not dependent on stem cells. This is a unique feature among organs in mammals. During liver regeneration first hepatocytes proliferate followed by the other cell types[44]. A wave of mitosis along the sinusoids can be observed from periportal to pericentral areas of the lobule[45]. Liver tissue is challenged to regenerate either by surgical removal of liver tissue e.g. in hepatocellular carcinoma (HCC), respectively metastasis surgery or in conditions of chronic liver disease (CLD). The partial removal of liver tissue is called partial hepatectomy (PHx). Normally a 2/3 PHx is performed in rodents to study liver regeneration (Figure 3). But this technique was also applied to larger animals e.g. dogs[46], pigs[47] and baboons[48]. Even repeated hepatectomy is performed in (human) patients with recurrent HCC[49]. The technique of PHx was established by Higgins and Anderson in 1931[7,50]. The liver mass increases after a loss of tissue very fast. After 2/3 PHx, the organ mass is restored after 5-7 days in rats and 8-15 days in humans[44]. In mice the regenerative process lasts about 7-10days[51]. Liver regeneration after PHx is one of the most used techniques to study organ, cell and tissue regeneration[52].

Most hepatocytes just proliferate one or two times after 2/3 PHx, because theoretically only a proliferation rate of 1.66 is needed per residual hepatocyte[50].

The high regenerative capacity of the liver can also be used in organ transplantation. In contrast to other organs like kidneys, only parts of a liver are sufficient in living donor liver transplants (LDLT). The underlying technique is called split liver and is used since over three decades in adults[53] and children[54] with constant improving survival rates[55]. Today survival rates for living donor transplants are at 100 %[56].

In rats it is possible to remove even more tissue, up to 95 % of liver tissue removal was peformed[57]. But such a severe PHx is not well tolerated by the animals and is accompanied with a high mortality rate. Whereas 90 % PHx is well-tolerated and not associated with decreased survival rates[57].

Actually the proliferation event after PHx or medical induced liver surgery is not regeneration in the narrower sense but more compensatory liver hyperplasia. Hyperplasia is the medical term for organ or tissue growth by proliferation. To fulfill the definition of regeneration, the removed liver lobes ought grow back. However the remaining liver lobes just expand in mass but no growth at the pinch off sides can be observed.

A classical example for regeneration is the limb regeneration in the axolotl (*Ambystoma mexicanum*)[58]. Despite this, in the scientific community, regeneration is the established term for the proliferative events after tissue removal in the liver.

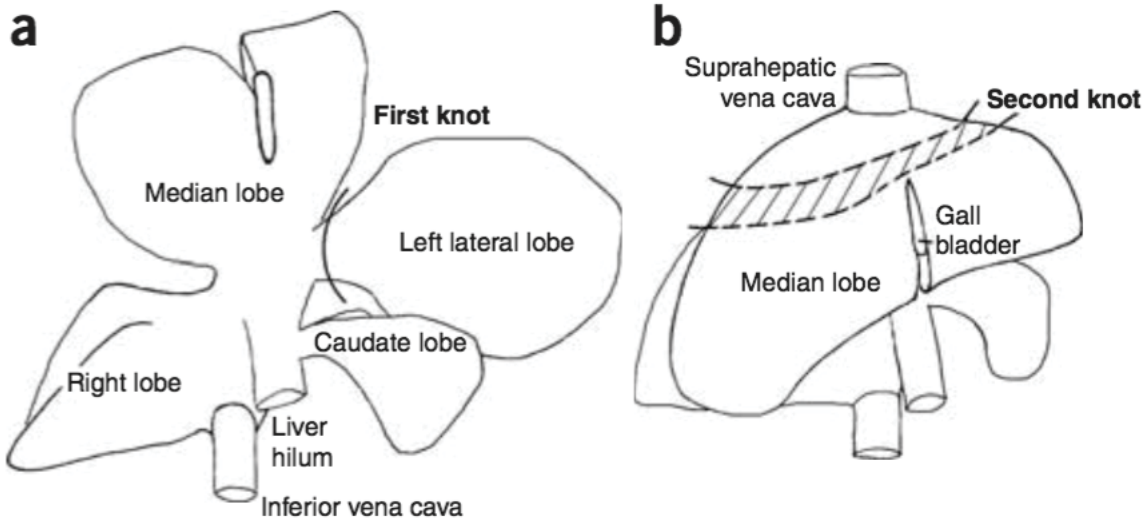

Figure 3: Schematic overview of mice liver lobes and the respective pinch-off sides for PHx. To perform 2/3 partial hepatectomy in mice, first the left lateral liver lobe is ligated with a silk suture and afterwards cut out (A). The second pinch-off side is across the median lobe,

just above the gall bladder (B). Figure is taken from Mitchell & Willenbring, 2008, Nature Protocols[7].

1.3 Chronic liver diseases (CLD)

In the European Union, approximately 29 million people suffered from chronic liver conditions and more than 5500 liver transplants were performed in 2013[59].

In contrast to the loss of larger amounts of tissue, the regenerative process in chronic liver diseases (CLDs) is faced to repetitive tissue damages[39]. CLDs are defined by recurring events of tissue destruction and regeneration over a period of at least six months. CLDs are also called hepatitis. Over time, the regenerative capacity is impaired and a chronic wound healing response accrues[39]. CLDs are caused by several different etiologies.

Table 1: Etiologies of chronic liver diseases

Causes of hepatitis	Examples / manifestations
Viral	Hepatitis B (HBV) and Hepatitis C virus (HCV)
Non alcoholic fatty liver diseases	NAFLD (non-alcoholic fatty liver disease) NASH (non-alcoholic steatohepatitis)
Autoimmune	Autoimmune hepatitis Primary biliary cirrhosis (cholangitis) (PBC)
Toxins	Dugs, alcohol, intoxication
Parasites	-*Echinoccocus granulosus* -*Fasciola hepatica* -*Trypanosoma cruzi* - *Leishmania* -*Plasmodium spec.* - *Entamoeba histolytica*

Genetic disorders	-Wilson's disease (copper storage defects) -Hemochromatosis (iron overload) -Alpha 1-antitrypsin deficiency (alpha-1 antitrypsin (A1AT) accumulation in the liver)

All kinds of chronic hepatitis develop in fibrosis over time if they are not treated respectively cured. However, this process can take several years, to decades. For example, in the large majority the overall onset of fibroses in patients infected with hepatitis c virus (HCV) takes 10 to 15 years[60]. This very long timespan of disease is due to the high regenerative capacity of the liver. Nevertheless, the chronic inflammation of the tissue overcomes the regenerative potential over time. As a wound-healing response, extracellular matrix (ECM) proteins are deposit to the damaged tissue. The excessive accumulation of ECM as a response to liver injury defines liver fibrosis[61]. This ECM mostly consists of collagen, which is deposit by hepatic stellate cells (HSCs). The HSCs gain a myofibroblastic phenotype through response to hepatocellular damage[62]. Over time, this ECM forms scar tissue, which disturbs the hepatic blood flow. As a consequence the liver becomes hypoxic[10]. This can be the first step to liver failure.

The final phase of all progressive and chronic liver diseases is liver cirrhosis[63]. In the majority of patients, cirrhosis develops after 15-20 years of the onset of fibrosis[61]. It is characterized by the formation of regenerative nodules in liver parenchyma, encapsuled by fibrotic tissue[11]. In cirrhosis the hepatocellular function is impaired and blood flow is disturbed by fibrotic scar tissue. This can result in liver insufficiency and portal hypertension[64].

In healthy livers, the ECM amount is about 0.6 %, a cirrhotic liver can exhibit up to 50 % scar tissue[65].

Portal hypertension is the most important clinical consequence of cirrhosis[8]. Alongside portal hypertension also ascites, variceal bleeding, and hepatic encephalopathy are consequences of liver cirrhosis[63]. But also renal failure[61], pulmonary complications[66] and severe sepsis[67] are complications in cirrhotic patients.

Hepatocellular carcinoma (HCC) is a primary malignant tumor of liver cells and the second most cancer related cause of death in the world[68] and the fifth most common form of cancer worldwide[69]. HBV and HCV are high risk factors for HCC. Therefore it

is more prevalent in Asian and African countries, where the overall infection rates of HBV and HCV are much higher compared to the rest of the world. Anti angiogenic drugs can successful prolong survival in patients with HCC[70]. Anyway, partial hepatectomy is the treatment of choice in non-cirrhotic patients[71].
Even if there are animal models for the study of liver regeneration in CLDs and their long term consequences fibrosis / cirrhosis, the major animal model for the study of liver regeneration is partial hepatectomy[44].

Angiocrine factors and their role in liver regeneration

In the last years several angiocrine factors were discovered which play important roles in liver regeneration[30,72,73] and regeneration of other tissues e.g. lung[74] and heart[75,76]. Still the physiologic process, especially the trigger of liver regeneration is not understood. Furthermore the concept that signals from blood vessel can influence organs is not new by itself. It was shown before that those signals are important for liver[77] and pancreas[78] development. Anyhow, angiocrine signals display important parts of the puzzle of liver regeneration and more and more factors are identified[76]. Summarizing, angiocrine signals regulate organ morphogenesis, maintenance, and regeneration[79].

1.4 Macrophage migration inhibitory factor (MIF)

The macrophage migration inhibitory factor (MIF) also known as MMIF or glycosylation-inhibiting factor (GIF or GLIF), L-dopachrome isomerase, or phenylpyruvate tautomerase is a pleiotropic cytokine which is involved in innate immunity[80]. MIF does not possess a N-terminal signaling sequence and is secreted through a non-classical pathway via an ABCA1 transporter[81].
MIF upregulates adhesion molecules on endothelial cells and therefore leukocyte adhesion[82]. It was also shown to increase integrins (α5β3)[83]. In addition MIF is supposed to trigger rapid integrin activation and calcium signaling[84].
MIF also plays a protective role in liver fibrosis[85] and nonalcoholic steatohepatitis[86]. But, MIF is also involved in declining diseases. For example high plasma levels of MIF are associated with coronary heart disease and type 2 diabetes mellitus[87]. MIF is also associated with autoimmune diabetes[88]
Beside the role of MIF in several diseases, a possible contribution of MIF in liver regeneration is still uncharted.

1.5 Beta 1 Integrin (β1 integrin)

β1 integrin (or CD29) is a protein, which is encoded by the *ITGB1* gene in humans. Integrins are transmembrane heterodimers build up by non-covalently associated alpha and beta subunits[89]. Integrins can mediate cell-cell and cell-matrix (basement membrane) interactions. Therefore, integrins are connected to a so called IPP-complex consisting of the mediator proteins ILK, Pinch and Parvin (IPP-complex)[90]. This scaffold links integrins to the actin cytoskeleton[91].
Extracellular binding substrates for integrins are fibronectin, collagen, and laminin. Integrins become activated through conformational changes[92,93].
β1 integrin can build heterodimers with 10 different alpha subunits. The Most common for blood vessels are α3 and α5. Knockout mice for β1 integrin die before implantation[94].

Integrins positively influences cell proliferation[95] and survival[96]. In addition, they also play a role in mechanotransduction either as direct transducers of mechanical force or as intermediates in pathways of mechanotransduction[97]. Furthermore β1 integrin has been shown to sense shear stress on a cellular level[98]. It has also been shown that β1 integrin is required for lymph vessel expansion in the mouse embryo[99]. These are indications that β1 integrin could also play a role in liver regeneration. Indeed it was shown that β1 integrin knockout (KO) on hepatocytes impairs liver regeneration through decreased growth factor signaling[100].

1.6 Intracellular Adhesion Molecule 1 (ICAM-1)

ICAM-1 also known as CD54 is a cell surface glycoprotein, which mediates adhesion on endothelial cells but is also expressed on cells of the immune system. In humans, *the ICAM1* gene encodes for the ICAM-1 protein. ICAM-1 is highly glycosylated and has therefore a protein size between 76 and 114 kDa in mammalian cells[101].
ICAM-1 is supposed to be upregulated by the inflammatory cytokine MIF[102]. This interaction plays an important role in leukocyte adhesion because ICAM-1 acts as a ligand for the lymphocyte function associated antigen-1 (LFA)-1 (or CD11a)[103], which is expressed on macrophages and neutrophils. Thus, ICAM-1 plays a key regulatory role in the leukocyte adhesion cascade[104] to inflammatory tissues.

ICAM-1 is also required for normal liver regeneration after PHx, because ICAM-1 knockout mice display a lack in leukocyte recruitment to the liver tissue[105]. It was shown that leukocytes derived matrix metalloproteinase 9 (MMP9) cleaves hepatocyte growth factor (HGF) from the ECM[106]. This HGF is the main source of HGF in the first three hours of liver regeneration[52]. Therefore ICAM-1 contributes to liver regeneration.

1.7 VE-Cadherin

CDH5 is the human gene encodes for Cadherin 5, also known as Vascular endothelial cadherin (VE-caherin) or Cluster of differentiation 144 (CD144). Cadherins are calcium dependent adhesion molecules that form adherens junctions among cells. VE-cadherin is exclusively expressed on vascular endothelium and in contrast to other widely used Cre lines with endothelial promoters (e.g. Flk-1), it is not expressed on hematopoietic stem cells.

1.8 Lactate dehydrogenase (LDH)

Lactate dehydrogenase (LDH) is an enzyme that catalyzes the reaction from lactate to pyruvate. LDH appears in high levels in skeletal muscle, heart, kidney, brain and liver tissue. Due to high stability, LDH accumulates in pathological cell damage in the blood. Unfortunately LDH is not an organ specific blood marker because it is ubiquitous expressed. Nevertheless LDH is still used as a marker for cell death in clinical hemograms e.g. after myocardial infarction[107]. If LDH is enriched in blood after PHx it is very likely that it is caused by side effects of the PHx.

1.9 Aim of the thesis

The aim of this thesis was to investigate possible hemodynamic changes after PHx and a possible role of these changes in liver regeneration.

The underlying idea was that if PHx reduces the liver mass, the systemic blood circulation should not change. Therefore either the blood flow velocity should increase or the vascular bed should expand. Hemodynamics were characterized using partial hepatectomy and contrast enhanced ultrasound measurements. As a result, blood to liver mass ratio but not blood flow velocity increased after PHx. Afterwards mice livers were examined for protein and mRNA changes occurring simultaneously to the observed hemodynamic changes. Also proliferation rates and β1 integrin levels after PHx were examined using laser-scanning microscopy.

The hemodynamic changes after PHx were interpreted as mechanical stress to the endothelial cells. To clarify if hemodynamic changes mechanotransduce a cellular response to PHx, *ex vivo* liver perfusion and *in vitro* experiments were performed. *In vitro* both longitudinal stretching and shear stress experiments were performed. MIF and ICAM-1 were found upregulated as a result of mechanical force in different experimental setups. In addition, the interaction of the commonly occurring molecules MIF and ICAM-1 were tested in gain (recombinant protein) and loss of function (RNAi approach) experiments *in vitro*. To link the gained insights of MIF and β1 integrin with liver regeneration, respective knockout mice were challenged by PHx and afterwards examined.

2 Material and Methods

2.1 Chemicals

Chemicals without manufacturer declaration were purchased over the central chemical purchasing department (Zentrales Chemikalienlager) of the Heinrich Heine University (HHU) with a main focus on price. Therefore the manufacturer may vary but the purity and specifications were equal.

2.2 Mouse work

2.2.1 Animal experiments

Mice were kept at 22°C, air humidity of 55 % and 12 hour light/dark cycle with unlimited access to normal chow diet and water in the animal house (ZETT, Zentrale Einrichtung für Tierforschung und wissenschaftliche Tierschutzaufgaben) of the Heinrich Heine University Düsseldorf (HHU) and University Hospital Düsseldorf (UKD). All animal experiments were approved by the appropriate authority (LANUV, Recklinghausen, Germany) with the file numbers G205/11 (for PHx in wild type mice), G184/11 (for PHx in knockout mice) and O116/09 (for organ isolation of wild type mice).

2.2.2 Wild type mice

Adult male C57Bl/6JRj mice (Janvier Labs) between 12 and 15 weeks old were used for wild type studies. All knockout strains used in this study were generated on this genetic background or backcrossed to this background. Female mice were excluded from the study to avoid sexual differences and complications with estrogen receptor driven inducible knockout mice.

2.2.3 MIF knockout mice

Macrophage Migration Inhibitory Factor (MIF) knockout mice were kindly provided by Prof. Dr. Jürgen Bernhagen (RWTH Aachen / LMU München). Those mice were described previously[108] and are conventional knockouts for MIF.

2.2.4 Cdh5(PAC)-CreERT2 mice

Cdh5(PAC)-CreERT2 mice were kindly provided by Prof. Dr. Ralf H. Adams (MPI Münster). Those mice were described previously[109]. In those mice the Cre-recombinase just exists in cells which express Cdh5. Cdh5 (also called VE-cadherin) is exclusively expressed on vascular endothelium and in contrast to other widely used Cre lines with endothelial promoters (e.g. Flk-1), it is not expressed on hematopoietic stem cells.

2.2.5 C57BL/6J-TgH(IntloxP)RF mice

These mice carry a floxed β1 integrin gene and were kindly provided by Prof. Dr. Reinhard Fässler (MPI Martinsried). Those mice were described previously[94,110].

2.2.6 Inducible endothelial cell specific knockout of β1 integrin

To generate endothelial cell specific knockout of β1 integrin, the Cdh5(PAC)-CreERT2 mice were crossed with the C57BL/6J-TgH(IntloxP)RF mice.

2.2.7 Gene deletion in Cdh5(PAC)-CreERT2 x C57BL/6J-TgH(IntloxP)RF mice

To induce gene deletion of β1 integrin in the endothelial cells, mice received a total dosage of 10mg tamoxifen (CAS Number 10540-29-1, Sigma-Aldrich) solved in corn oil, via single 100µl intraperitoneal (i.p.) injections over five consecutive days with increasing dosage of tamoxifen (table 2). After the last injection, mice were kept for two weeks under normal conditions to induce the knockout.

Tamoxifen is a pro drug, which is metabolized to the active form 4-hydroxytamoxifen (4-OHT) by cytochromes P450. To solve the tamoxifen in corn oil a Sonoplus homogenizer UW 2200 (Bandelin) was used with two times 30-second pulses at 50 % power.

Table 2 Tamoxifen injection in mice. Injection amount of tamoxifen over five days

Day of injection	Tamoxifen dosage (mg)
1	1

2	1.5
3	2
4	2.5
5	3

2.2.8 Mouse genotyping

For mice genotyping the DNA was isolated from tail tip biopsies. The tissue was incubated in 100 µl lysis buffer (2 µl proteinase K (20 mg/ml, Qiagen), White-Flexi-Buffer (Promega)) for ≥ 6 hour at 56°C and 300 rpm. Subsequently proteinase enzyme activity was inactivated for 20min at 95°C. Supernatants were used for polymerase chain reaction (PCR).

For each mouse two different PCRs were performed. In one the presence or absence of the Cre-recombinase was checked and in the other PCR, it was checked if the floxed sequence within the β1 integrin gene was heterozygous or homozygous present. For each PCR a master mix (table 3) was prepared and 1 µl of the respective tail lysate was added to the master mix in a microreaction tube. PCR were performed on a TProfessional TRIO Thermocycler® (Biometra) or MyCycler™ Thermal Cycler System (Bio-Rad). Thermal profiles for the respective PCR is listed in table 5 and 6.

Table 3 Master mix composition for genotyping PCRs

Component	Volume (µl)
H_2O	12.8
$MgCl_2$	1.2
5x GoTaq Flexi buffer	4
dNTP Mix (10nM each)	0.4
Primer	0.4
Taq-polymerase	0.2
DNA (tail lysate)	1

Table 4 Primer sequences (5' - 3') for genotyping PCR

Primer	Sequence (5’ - 3’)
Cre-1 (fw)	GCCTGCATTACCGGTCGATGCAACGA
Cre-2 (rv)	GTGGCAGATGGCGCGGCAAGGTAAC
β1intL1 (fw)	GTGAAGTAGGTGAAAGGTAAC
β1intT56 (rv)	GGGTTGCCCTTCCCTCTAG

Table 5 Thermal profile for the Cre PCR

Step	**1**	**2**			**3**	**4**
Time (in s)	300	30	30	60	300	∞
Temperature (in °C)	94	94	58	72	72	10
Cycles	1	35			1	1

Table 6 Thermal profile for the β1 integrin loxP PCR

Step	**1**		**2**		**3**		**4**	
Time (in s)	180	30	30	30	30	30	30	∞
Temperature (in °C)	94	94	63	72	94	53	72	10
Cycles	1		10		35		1	

The PCR products of the respective primers (Cre-1 and Cre-2 for Cre; β1intT56 and β1intL1 for β1 integrin) and thermal profiles were analyzed on 1 % agarose gels in 1x TRIS-Acetate-EDTA-Buffer (TAE). A 100 bp ladder (Fermentas) was also loaded on the gels. 110 V were applied for 30min to the gels and images (of the gels) were taken subsequently using a Molecular Imager® ChemiDoc™ XRS Imaging System (Bio-Rad). Cre bands (approx. 700 bp) were either present or absent. Wild type mice did not show a Cre band. Homozygous bands (approx. 450 bp) Heterozygous (approx. 350 bp + approx. 450 bp) and wild type bands (approx. 350 bp) could be observed in the gels of β1 integrin loxP PCR.

2.2.9 Contrast ultrasound measurements (CEUS) in mice

Contrast ultrasound measurements were performed on a Vevo®2100 ultrasound system (FUJIFILM Visualsonics) at 18 MHz, equipped with a MS-250 transducer operating in a contrast specific imaging mode. A single bolus of 30 µl Vevo Micromarker™ Non-Targeted Contrast Agent (FUJIFILM Visualsonics) was injected intravenously via tail-vein catheter before each measurement, using an automated Vevo Infusion Pump (FUJIFILM Visualsonics). Liver mass was quantified using VevoCQ™ Software (FUJIFILM Visualsonics). To ensure that always the same area was examined, liver was measured just above the kidney. Anatomically the right liver lobe encloses the anterior tip of the right kidney and this lobe is not affected by the partial hepatectomy (PHx) surgery. Advantageously paired measurements in the same mice pre and post PHx were possible and considered in statistical analysis. The ultrasound system was located at the European Institute for Molecular Imaging (EIMI) Münster, Germany.

2.2.10 Partial Hepatectomy (PHx) in mice

To induce liver regeneration, partial removal of the organ mass was performed after the protocol from Mitchell and Willenbring (Nat. Protoc. 2008)[7]. To ensure anesthesia, the inhalant anesthetic reagent isoflurane is mixed to 2-3 % in 2 L/min O_2 and applied via a respiratory mask. When deep anesthesia is achieved 5 mg/kg of the analgetic agent Carprofen (a non steroidal anti inflammatory drug (NSAID)) is injected i.p. and the mice were placed on a warming pad to prevent hypothermia during surgery. Subsequent the abdominal fur is removed with a shearing machine and the abdominal skin is disinfected (Kodan, Schülke). A laparotomy is performed in two steps, whereas first the skin and second the muscle layer (peritoneum) is severed. The second incision is performed a bit shorter to secure optimal wound closure at the end of the surgery. To access the liver, the abdominal cavity is stretched with an alm retractor and hemostatic clamps. First the median and the left liver lobes are gently moved aside with a saline-moistened cotton tip to cut the falciform ligament (membrane) and the membrane between the caudate and the left liver lobe. To remove parts of the liver, first the left and then the median lobe is ligated with a 4-0 silk thread (Mersilene, Ethicon). Sufficient ligated lobes change their color from dark red to purple and can be cut just above the suture by using a micro-scissor. After potential bleedings are staunched, the abdominal cavity is flushed with a saline solution. After removing the

saline with medical swabs the peritoneum is closed with a 5-0 suture (Vicryl Plus, Ethicon). The skin is closed with wound clips (FST) and wiped with disinfectant. The mice is removed from anesthesia and placed under an infrared lamp to avoid hypothermia during recovery.
On the first two days post PHx, analgesia is maintained with 5 mg/kg Carprofen subcutaneous (s.c.) application.

2.2.11 *Ex vivo* liver perfusion

Hemoglobin free liver perfusion without recirculation of the perfusate was performed as described previously for rats[111] and adapted to mice by lower perfusion rates. Mice were narcotized via i.p. injections of a mixture of Xylazin 2 % (Rompun®, Bayer), and Ketamine 25 mg/ml (Ketanest®S, Pfizer). After mice did not show any reflexes, they were killed via cervical dislocation and the abdominal cavity was opened and the portal vein of the liver was cannulized. Livers were perfused with 37°C warm and oxygenated Krebs-Henseleit-Solution (KHS-buffer) at different perfusion rates over the portal vein. Perfusion rate was controlled constantly by the amount of outflow of the liver. To not disturb the experiment, ligations were applied before perfusion was started, but not tightened in conditions with PHx. PHx was performed after the perfusion rate stabilized at desired rates.

2.3 Biochemical methods

2.3.1 Organ isolation for RNA and Protein isolation

To isolate the livers from mice, they were narcotized with i.p injections of a mixture of Xylazin 2 % (Rompun®, Bayer), and Ketamine 25 mg/ml (Ketanest®S, Pfizer). Drugs were diluted 1:3 (Xylazin: Ketamine) to a concentration of 5 mg/mL Xylazin and 67.5 mg/ml ketamine. Mice were injected i.p. with 30-40 µl. The abdominal cavity of the narcotized animals was opened and blood was collected from the thoracic cavity after the vena cava inferior was cut. Blood was collected in EDTA tubes (Sarstedt) and kept on ice until the samples were centrifuged at 13000 rcf for 10min at 4°C. Thereby the blood plasma was separated from erythrocytes, platelets and leukocytes. The liver was cut out and every single lobe was weighted. In case for PHx also the scar tissue of the removed lobes was weighted. The upper part of the right lobe as well as one part of

the caudate lobe was fixed in 4 % PFA whereas the rest of the liver was frozen in liquid nitrogen for later analysis.

2.3.2 Immunostaining and imaging

Blood was scoured out of mice circulation and replaced with PBS using a peristaltic pump (ISM827B, ISMATEK) with physiologic perfusion[112] rate of 13 ml/min over the left heart ventricle. To fixate vessel dilation, after PBS, also 4 % PFA was perfused into the circulation. After removal of the liver it was fixed in 4 % PFA over night. Before cryo-sectioning, livers were equilibrated in 30 % sucrose and embedded in O.C.T. (optimal cutting temperature) (Sakura). Embedded liver lobes were cut to a sickness of 12 µm using a Microm HM 560 (Thermo Scientific) and Shandon MX 35 Premier+ blades (Thermo Scientific). Liver sections were transferred to Superfrost™ plus microscope slides (Thermo Scientific). Slides were washed before antibody staining two times for 5min with washing buffer (1xPBS^{++} + 0.2 % Triton X-100 (AppliChem)). Sections were blocked for 1 hour at room temperature in a moist chamber with blocking solution (PBS^{++} with 0.2 % Triton X-100, 3 % BSA (AppliChem) and 5 % normal donkey serum (Jackson ImmunoResearch). Subsequently slides were stained with primary antibodies (table 7) at 4°C over night in a moist chamber. After the incubation, slides were washed with washing buffer for three times 15-20min.

The corresponding secondary antibodies (table 8) were incubated for one hour at room temperature in a moist chamber. After that the slides were washed again with washing buffer for three times 15-20min.

Sections were mounted with Fluorshield™ histology mounting medium (Sigma-Aldrich) before used in microscopy.

Table 7 Primary Antibodies used for IHC

Antibody against (Company, Cat. No.)	Host species	Dilution
ICAM-1/CD54 (R&D, AF796)	Goat (gt) polyclonal	1:20
ICAM-1/CD54 (proteintech, 10020-1-AP)	Rabbit (rb) polyclonal	1:100
Integrin β1/CD29 (Merck-Millipore, MAB1997)	Rat (rt) monoclonal	1:200
Phospho-Histone H3 (PH3) (Merck-Millipore, 06-570)	Rabbit (rb) polyclonal	1:50
Laminin (Merck-Millipore, AB2034)	Rabbit (rb) polyclonal	1:200

Table 8 Secondary Antibodies used for IHC

Antibody (Company, Cat. No.)	Host species	Dilution
DAPI (Sigma-Aldrich, D9542)	-	1:1000
Anti gt IgG coupled to AF488 (life technologies, A-11055)	Donkey (dk)	1:500
Anti rb IgG coupled to Cy3 (Jackson, 711-165-152)	Donkey (dk)	1:500
Anti rb IgG coupled to AF488 (life technologies, A-11034)	Donkey (dk)	1:500
Anti rt IgG coupled to Cy3 (Jackson, 712-165-153)	Donkey (dk)	1:500

2.3.3 Proteome Profiler Array

The Proteome Profiler - Human Adipokine Array Kit (R&D / Biotechne) was used. Cell culture supernatant and cell lysates of stretched and unstretched human LSECs were

used as protein samples according to manufactures instructions. Both lysates and supernatants were pooled from three different experiments. Array membranes were incubated with ECL solution (Bio-Rad) and imaged on a Molecular Imager® ChemiDoc™ XRS Imaging System (Bio-Rad). Membranes of comparative conditions (e.g. stretched compared to unstretched) were images together to assure same image intensity.

2.3.4 MACS® Cell Separation

The MACS® cell separation method was used to separate LSECs from mice liver tissue. First a single cell suspension was prepared. Therefore the protocol, preparation of single-cell suspensions from mouse livers, from Miltenyi Biotec was used. In summary the livers were incubated in 37°C warm Krebs-Ringer-Buffer (KRB-buffer) containing DNAse I (30000 U/ml) and Collagenase IV (5000 U/ml). Subsequently the livers were grinded with a gentleMACS™ Dissociator and the program for liver single cell suspension. CD146 (LSEC) Micro Beads (Miltenyi Biotec) were used to isolate LSECs from the cell suspension on magnetic fields of QuadroMACS™ cell separator. PEP-buffer was used for cell sorting. CD146 is expressed on LSECs[113] and therefore recommended to isolate LSECs from mouse liver tissue.
Isolated LSECs were collected and lysed for western blots.

2.3.5 Laser scanning microscopy

Images were acquired using a LSM710 confocal microscope (Zeiss) with ZEN Imaging-Software (Zeiss). For quantifications same laser and microscope settings were used for the comparative images.

2.3.6 Sinusoid lumen quantification

Sinusoidal lumen area was quantified on images stained for ICAM-1 and DAPI in a blinded fashion, using Fiji's magic wand tool and an interactive graphic-tablet (DTU-1631, Wacom).

2.3.7 Image quantification

To quantify staining area, representing protein amount of different markers, Fiji (Fiji is just ImageJ – http//:pacific.mpi-cbg.de) a distribution of the open-source software ImageJ was used. FIJI is commonly used for biological image analysis[114]. The areas of the stained marker were measured using self-scripted macros underlying threshold method with predefined algorithms (for source code see supplements). The threshold was manually adjusted and randomly quality controlled for every staining. The result of each image was set in ratio to number of cells per image. Therefore another macro was used to count the stained nuclei per image (for source code see supplements).
Numbers of pH3 and TUNEL positive cells were counted manually. It was possible to distinguish between positive cells, which are positive (sinusoidal cells) or negative (Hepatocytes) for ICAM-1. ICAM-1 positive cells were called sinusoidal lining cells (SLCs). SLC are LSECs and macrophages and stellate cells.
Sometimes pH3 and DAPI stainings were fragmented, so that two or more small stains of pH3 could be observed next to each other (Figure 7E in the right lower corner). Therefore only nuclei were counted as proliferating cells when stainings of pH3 and DAPI overlapped (Figure 7D, F). In panel E only one of the two-pH3 positive dots overlapped with DAPI, so this area was counted as one proliferating cell.

2.3.8 TUNEL staining

TUNEL staining detects apoptotic DNA fragmentation with a red fluorescent label at the single-cell level. An In Situ Cell Death Detection Kit, TMR red (Roche Diagnostics) was used for the TUNEL staining on slides of livers from β1 integrin knockout or MIF knockout mice.
Compounds and solutions for TUNEL stainings were prepared in advance according to manufacturer's instructions. Slides were treated like in normal stainings, with additional incubation for 10min at 37°C with 200 µl of proteinase K (AppliChem, #A4392) diluted 1:500 in 10 mM Tris-HCL. After the normal washing, slides were put into permeabilization solution for 2min on ice under slow shaking. Afterwards 100 µl of the TUNEL staining was applied on the slides. The slides were incubated at 37°C for 60min. Afterwards slides were washed two times with PBS^{++} for 10min and one time with PBS^{++} with 0.2 % Triton X-100 for 20min. Slides were blocked for 1 hour with the same blocking solution used for other immunostainings.

2.3.9 Western blot

For protein lysates, mice livers were homogenized using a gentleMACS™ Dissociator (Miltenyi Biotec) with RIPA-Buffer added 1 % Y-30 (Sigma-Aldrich). Cells were lysed using a lysis buffer consisted of 50 mM HEPES pH7, 150 mM NaCl, 10 % Glycerol, 1 % Triton X-100, and complete cocktail of protease inhibitor (Roche Diagnostics). The cells were washed previously with PBS and incubated with the lysis buffer for at least 5min at 4°C. In normal cell culture dishes or stretching chambers, a cell scratcher could be used to lyse cells. In flow chambers slides a syringe with Luer connector was used to mechanical force to remove cells from the channel slide. Afterwards the samples were put into the cell disruptor for 5min, followed by a 10min centrifugation at 13000 rpm and a transfer of the supernatant to a new vial.

Protein content in lysates were determined using Pierce™ BCA Protein Assay Kit (Fisher Scientific). Same amounts of protein (10 µg) and Precision Plus Protein™ Dual Color Standard (Bio-Rad) were loaded on Mini-Protean® TGX™ Gels (Bio-Rad) and blotted on Trans-Blot® Turbo™ Transfer Packs (Bio-Rad) using the Trans-Blot® Turbo™ Transfer System (Bio-Rad).

The membranes were cut generously at kDa ranges of the examined proteins and then blocked with 0.5 % Tween 20 in PBS and 5 % BSA. Primary antibodies (table 9) were diluted in blocking solution and incubated at 4°C over night. Subsequently membranes were washed three times with 0.5 % Tween 20 in PBS and afterwards incubated for 1 hour with the secondary antibodies (table 10), followed by another three washing steps. The membranes were then incubated for 1min with Clarity Western ECL substrate (Bio-Rad) and imaged using a Molecular Imager® ChemiDoc™ XRS Imaging System (Bio-Rad). For housekeeping GAPDH was used in human samples and β-actin in mouse samples. Band intensities were quantified by using (Fiji is just) ImageJ.

Table 9 Primary Antibodies used for WB

Antibody	Dilution	Manufacturer	Cat. number	species reactivity
Goat anti-ICAM-1	1:500	R&D Systems	BBA17	human
Sheep anti-MIF	1:3200	R&D Systems	AF1978	human / mouse
Rabbit anti-GAPDH	1:5000	Abcam	ab9485	human
Mouse anti-β-actin	1:20000	Sigma-Aldrich	A2228	mouse
Goat anti-ICAM-1	1:2000	R&D Systems	AF796	mouse

Table 10 Secondary Antibodies used for WB, all conjugated with HRP

Antibody	Dilution	Manufacturer	Cat. number	species reactivity
Donkey anti-sheep - HRP	1:1000	R&D Systems	HAF016	sheep
Donkey anti-goat - HRP	1:5000	Jackson Immuno Research	705-035-003	goat
Donkey anti-mouse - HRP	1:5000	Jackson Immuno Research	715-035-150	mouse
Donkey anti-rabbit - HRP	1:5000	Jackson Immuno Research	711-035-152	rabbit

2.3.10 RNA isolation

The lysis and RNA isolation of the correlate sample was performed using the High Pure RNA Isolation Kit (Roche Diagnostics) for cells and the High Pure RNA Tissue Kit (Roche Diagnostics) for tissues. To expose the RNA, cells were scratched from the

culture dish using cell scrapers (Sarstedt or NUNC). Tissue samples were lysed using M Tubes and gentleMACS™ Dissociator (Miltenyi Biotec) and RNA program. Subsequently, the RNA concentration and purity was checked on a GENESYS BioMate 3 spectrophotometer (Thermo Scientific).

2.3.11 Complementary DNA (cDNA) synthesis from isolated RNA

The SuperScript II Reverse Transcriptase (Invitrogen) was used to synthesize the complementary DNA (cDNA) strand of the isolated RNA. The composition of the applied mix is shown in (table 11). The protocol was performed according to manufacturer's instructions.

Table 11 Master mix for cDNA synthesis

Component	Quantity
Oligo (dT)(450 µg/ml) (Eurofins MWG Operon)	1.11 µl
RNA	1.5 µg
dNTP Mix (10mM each) (Sigma-Aldrich, Cat.# D7295)	1 µl
H_2O	fill up to 12 µl
5x First Strand Buffer (Invitrogen, Cat. # 18064014)	4 µl
0.1 M DTT (Invitrogen, Cat. # 18064014)	2 µl
SuperScript II RT (200 units) (Invitrogen, Cat. # 18064014)	1 µl
ddH_2O	fill up to 20 µl

2.3.12 Quantitative real-time polymerase chain reaction (qPCR)

To determine expression levels for the examined genes a quantitative real-time polymerase chain reaction (qPCR) was carried out on LightCycler Nano Instruments (Roche Diagnostics) and the LightCycler Nano 1.1 software. If not other stated, β-2 microglobulin (B2M) was used as housekeeping gene. To analyze the obtained data,

the CT-Method was used[115]. Used primers (table 12), master mix composition (table 13) and thermal profile (table 14) are listed in the respective tables.

Table 12 Primer list used in qPCR

Target gene	Species	Forward sequence	Reverse sequence
Icam1	mouse	CGTGTATTCGTTTCCGGAGAGTG	TCAGTATCTCCTCCCCACGGA
Mif	mouse	GTGCCAGAGGGGTTTCTGT	AGGCCACACAGCTTACT
Itgb1	mouse	AATGCCAAGTGGGACACGGG	TGACTAAGATGCTGCTGCTGTG ACC
β2m	mouse	GAGCCCAAGACCGTCTACTG	GCTATTTCTTTCTGCGTGCAT
Lamc1	mouse	CTCCATCAACCTCACGCTG	CGGCTGGTGTGGAACTTG
ICAM1	human	ATGCCCAGACATCTGTGTCC	GGGGTCTCTATGCCCAACAA
MIF	human	AAGCTGCTGTGCGGCCT	TTGTTCCAGCCCACATTGG
ITGB1	human	CATCTGCGAGTGTGG	GGGGTAATTTGTCCC
B2M	human	GAGGCTATCCAGCGTACTCCA	CGGCAGGCATACTCATCTTTT

Table 13 qPCR Mix

Component	Quantity in µl
Roche DNA Green Master 2x (Roche Diagnostics)	5
Primer Mix (forward and reverse, 300 nM each)	2
H_2O	2
cDNA (0.75 µg)	1
Total	**10**

Table 14 qPCR- thermal profile

Step	Hold	Amplification			Melting
Time	600s	10s	10s	15s	0.1°C/s
Temperature	95°C	95°C	60°C	72°C	60°C to 95°C
Cycles	1	40			1

2.3.13 Blood Plasma measurements

Blood values in blood plasma of mice were measured on an automated analyzer for clinical chemistry Spotchem EZ SP4410 (Arkray). The blood plasma was diluted 1:10 with PBS and Liver-1 profile multi strips (Arkray, #77182) were used to measure six different blood markers for the liver (ASAT/GOT, ALAT/GPT, LDH, T-Pro, T-Bil, Alb).

2.3.14 MIF ELISA

Blood serum was diluted 1:10 in Reagent Diluent (DY995, Biotechne) and MIF levels were determined in Mouse MIF DuoSet ELISA (DY1978, R&D Systems) according to the manufacturer's guidelines. The optical density of the microplates were determined using an Infinite® 200 PRO microplate reader (TECAN).

2.4 In vitro studies

2.4.1 Cell Lines

Human microvascular sinusoidal endothelial-cells (hLSECs) (PELOBiotech) were cultivated in Microvascular Endothelial Cell Growth Medium Kit Enhanced (PELOBiotech) and used up to passage ≤7. Cells were grown on plastic or silicon dishes (stretch experiments) coated with Speed Coating Solution (PELOBiotech). Cells were cultured at 37°C and 5 % CO_2.

2.4.2 Cell stretching

For cell stretching experiments, cells were grown on STREX© stretch chambers (BioCat) coated with Speed Coating Solution (PELOBiotech). Unidirectional stretching was applied with a STREX© Mechanical Cell Strain Manual Stretcher for 30min or 1 hour.

2.4.3 Flow chamber assay

For flow experiments, hLSECs were grown on µ-Slides $I^{0.4}$ (Ibidi). 10^5 cells were seeded per slide according to manufactures guidelines (Application Note 3, Ibidi). Several slides could be connected using serial connectors (Ibidi) in one experiment. Liver sinusoidal shear stress is calculated to 3.7 dyn/cm^2 by the formula of Gross et. al[116,117]. All shear rates were applied by using the ibidi pump system (Ibidi) and matching perfusion sets (Ibidi) for the desired shear stress conditions. 3.7 dyn/cm^2 was used as normal culturing condition. Additionally static conditions (0 dyn/cm^2) and doubled shear stress conditions (7.4 dyn/cm^2) were examined. The higher shear stress rate was intended to reflect conditions after PHx. Therefore the shear stress was only enhanced for 30min to 1 hour after cultivating the cells at physiologic shear stress levels. The static conditions were not exposed to shear stress during the experiment except for media change. Even careful and slow change of culturing media can expose cells to shear stress.

2.4.4 Small interfering (siRNA) gene knockdown in human LSECs

To induce gene knockdown in human LSECs the small interfering RNA (siRNA) approach was used. Sequence suggestions (table 15) were made by Eurogentec

siRNA design service after giving the appropriate gene accession numbers. Lipofectamine® RNAiMAX Transfection Reagent (Thermo Fisher Scientific) was used as recommended by manufacturer to transfect cells with siRNA. After incubation for 48 hours, first the knockdown efficiency of each siRNA sequence was determined in pilot experiments. siRNA with knockdown efficiencies less than 50 % were replaced by other sequences. Three effective siRNAs were pooled and used in the experiments.

Table 15 siRNA sequences

Gene	Sequence	Sense	Antisense
MIF	1	CAGGGUCUACAUCAACUAU	AUAGUUGAUGUAGACCCUG
	2	UCAACUAUUACGACAUGAA	UUCAUGUCGUAAUAGUUGA
	3	CCGAUGUUCAUCGUAAACA	UGUUUACGAUGAACAUCGG
GC control	37 %	AGUAUAAUCGUAUGAUCCA	UGGAUCAUACGAUUAUACU
	47 %	ACACACGCUAUGUGAUACG	CGUAUCACAUAGCGUGUGU
	53 %	GUUAUGACGGUAGGCGAUG	CAUCGCCUACCGUCAUAAC

2.4.5 Recombinant human MIF on LSECs

Recombinant human MIF (289-MF, R&D Systems) was reconstituted in sterile PBS containing 0.2 % BSA and applied at a final concentration of 25 nM in starving medium, which contains no additives like FCS or growth factors. Just PBS with 0.2 % BSA was used in starving medium as control. Before MIF treatment, the cells were starved for 3 hours. Cells were incubated for one hour either with recombinant MIF or control mixture.

2.5 Buffers

2.5.1 Krebs-Henseleit-Buffer (KHB):

KHB is used in ex vivo perfsuion experiments and pre-heated to 37°C. It contains NaCl (115 mM), NaHCO3 (25 mM), KCl (5.5 mM), KH2PO4 (3 mM), Na2HPO4 (1.3 mM), MgCl2 (1.18 mM), CaCl2 (1.25 mM), NaH2PO4 (1.23 mM), NaH2SO4 (1.23 mM), Pyrovat (0.3 mM), lactate (2.1 mM) in H_2O.

2.5.2 Krebs-Ringer-Buffer (KRB):

154 mM NaCl, 5.6 mM KCl, 5.5 mM Glucose, 20.1 mM HEPES, 25 mM $NaHCO_3$, adjust to pH 7.4 with NaOH.

2.5.3 Phosphate-buffered saline (PBS):

KCl (5.4 mM), NaCl (0.27 M), KH_2PO_4 (3 mM), Na_2HPO_4 (1.3 mM) in H_2O.

2.5.4 Phosphate-buffered saline with Magnesium and Calcium (PBS++):

KCl (5.4 mM), NaCl (0.27 M), KH_2PO_4 (3 mM), Na_2HPO_4 (1.3 mM), $MgCl_2$ (5 mM,) $CaCl_2$ (9 mM) in H_2O.

2.5.5 PEP Buffer:

PEP-Buffer can be prepared by diluting MACS® BSA Stock Solution (Miltenyi Biotec) 1:20 with autoMACS® Rinsing Solution (Miltenyi Biotec). The final PEP buffer contains phosphate-buffered saline (PBS), pH 7.2, 0.5 % bovine serum albumin (BSA), and 2 mM EDTA. PEP buffer has to be stored at 2−8°C.

Note: If PEP buffer is prepared manually it has to be evacuated with a vacuum pump for 10min to avoid air bubbles that could occlude the MACS® separation column.

2.6 Statistical analysis

Statistical significance was determined using GraphPad Prism® 6. If not otherwise stated, quantified data are presented as means ± standard deviation (SD). Respective statistical tests are mentioned in figure legends. Differences with p-values ≤ 0.05 were considered significant.

3 Results

The hypothesis that hemodynamic changes occur after PHx due to reduced organ mass, had already formulated at the start of the thesis[52], nonetheless, no experimental data was provided at this time point.

The underlying working hypothesis predicts that under normal conditions, blood from abdominal organs flows through the liver to the heart (Figure 4A). After PHx, the liver mass is reduced by two third but more or less the same amount of blood pervades the smaller liver. Therefore hemodynamic changes must occur (Figure 4B). During liver regeneration the tissue recovers and the hemodynamic situation relaxes (Figure 4C). After complete restoration of the liver mass, the hemodynamic situation should be similar like before (Figure 4D).

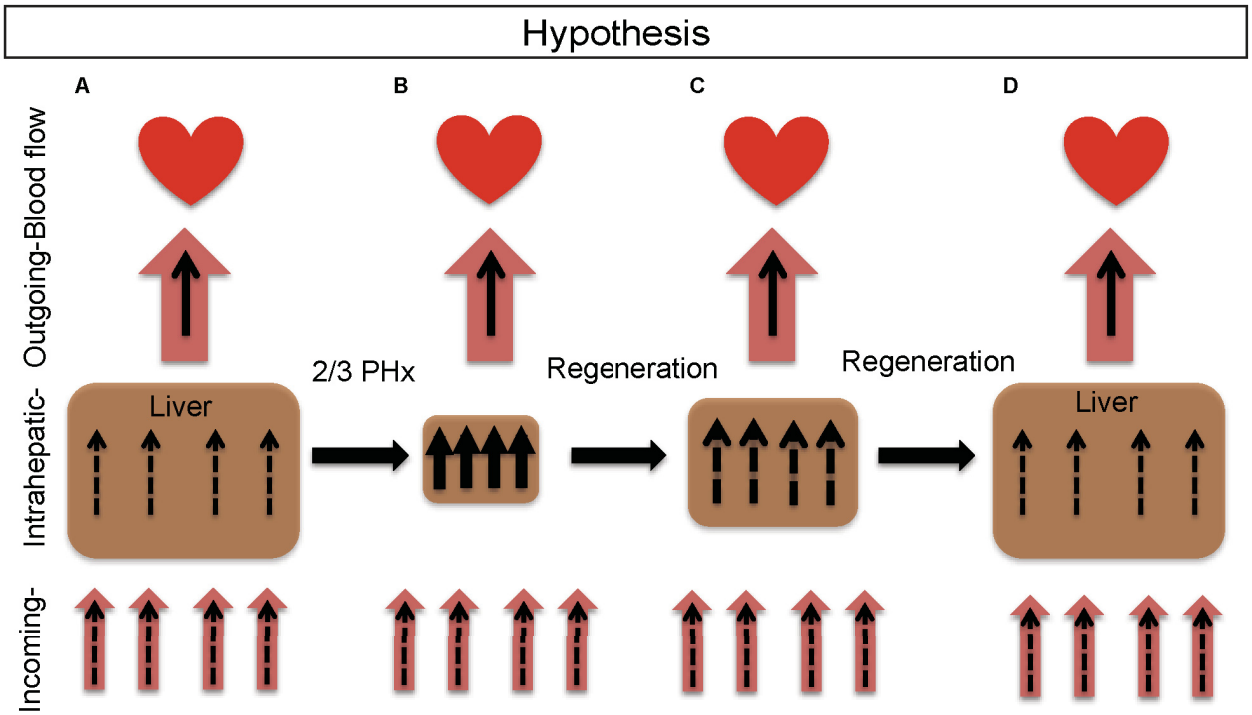

Figure 4: Working hypothesis. A) Blood flows through the liver to the heart. B) After PHx, the organ mass is reduced and intrahepatic blood flow must be changed. C) During organ mass regeneration the intrahepatic hemodynamic situation relaxes. D) After the organ mass is fully restored, the intrahepatic blood flow is completely restored.

3.1.1 Hemodynamic changes in the liver after PHx

To address the question if hemodynamic changes after PHx occur, contrast enhanced ultrasound (CEUS) measurements in C57Bl/6JRj (C57Bl/6J) mice were performed before and within one hour after PHx. The relative intrahepatic blood volume (normalized to liver tissue) doubled significantly after PHx (Figure 5B) whereas the relative blood flow was not significantly induced upon PHx (Figure 5C).

Liver sections stained for ICAM-1 as a blood vessel marker and DAPI showed significant dilated sinusoids (Figure 5D, E) simultaneously to the increased blood volume (Figure 5B). The vessel dilation increased by twofold. These results indicated that hemodynamic changes in the liver indeed occur after PHx.

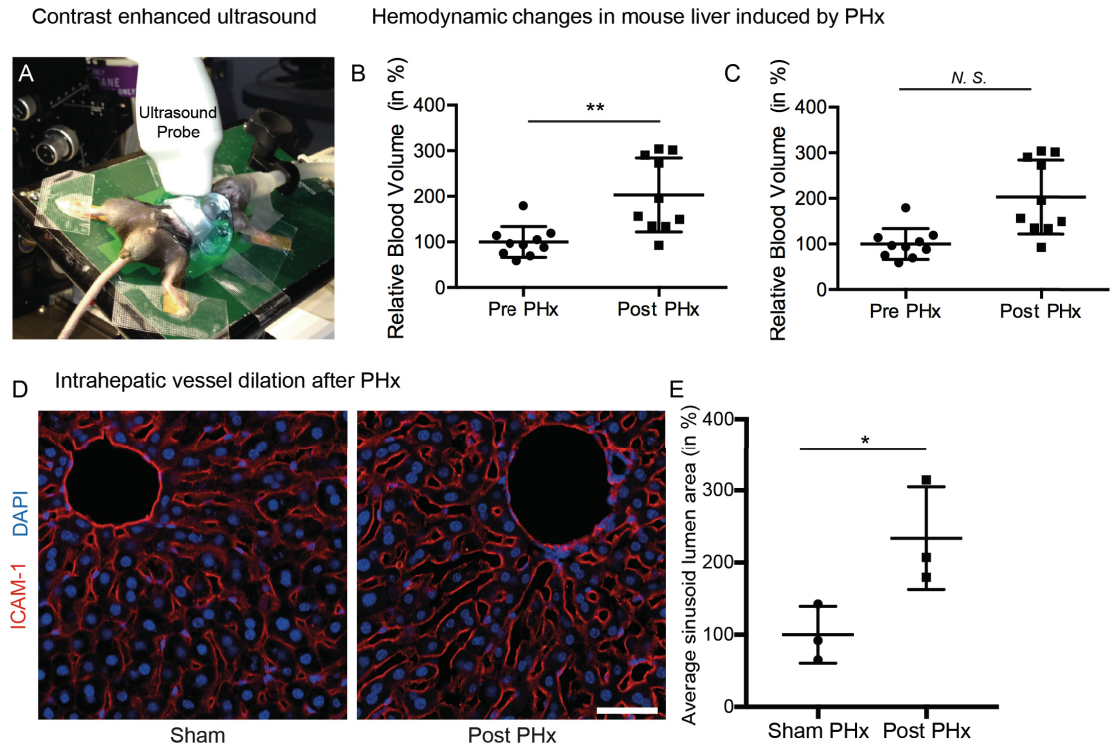

Figure 5: Hemodynamic changes in the liver after PHx lead to intrahepatic vessel dilation and LSEC stretching. A) Overview of ultrasound measurements in C57Bl/6J mice pre and post partial hepatectomy (PHx), B-C) Quantification of (B) blood volume and (C) blood flow velocity in right liver lobes normalized to measurement area (n=10 animals, used for repeated measurements pre and post PHx). (Pre PHx set to 100 %) p-values ≤ 0.05 considered as statistically significant in Student‘s t-test. D) LSM images of right liver lobe sections, stained

for ICAM-1 (red) and DAPI (blue). Scale bar = 20 µm (E) Quantification of sinusoid lumen area in LSM images (n=3 animals per condition) p values ≤ 0.05 considered as statistically significant in Student‘s t-test. All values are mean values ± standard deviation (s. d.).

3.1.2 β1 integrin expression after PHx

Whereas the vessel dilation (shown in Figure 5D, E) was a fast response to PHx (within one hour), changes in components of the basement membrane occurred only days later. For example β1 integrin mRNA expression (Figure 6J) and protein expression (Figure 6J) increased in the first two days after PHx. β1 integrin is expressed stronger than other components of the basement membrane (Figure 6B) in quiescent liver tissue. Here it is remarkable that the staining for β1 integrin (Figure 6B, E, H) visibly overlaps with the staining for ICAM-1 (Figure 6A, D, G). While hepatocytes are known to express β1 integrin[118,119], the expression on intrahepatic vessels was much stronger represented in these experiments. Both mRNA and protein level increased significantly two days after PHx (Figure 6J, K) and mRNA alone already increased significantly one day after PHx (Figure 6J). The mRNA levels of β1 integrin increased twofold after one day and threefold after two days of regeneration (Figure 6J). The protein content of β1 integrin increased twofold after two days of regeneration compared to sham animals (Figure 6K). This increase in β1 integrin protein represented in staining intensity can be observed in the merged images of β1 integrin and ICAM-1 in Figure 6. In the sham treated condition, ICAM-1 (red) was more present than β1 integrin (green). This balance results in a more red or orange color of the blood vessels (Figure 6C). During regeneration the β1 integrin (green) intensity increased and the images displayed more yellow vessels at one day after PHx (Figure 6F) and even more yellow/green vessels at two days after PHx (Figure 6I). These results indicate that β1 integrin expression is induced stronger on vasculature cells after PHx.

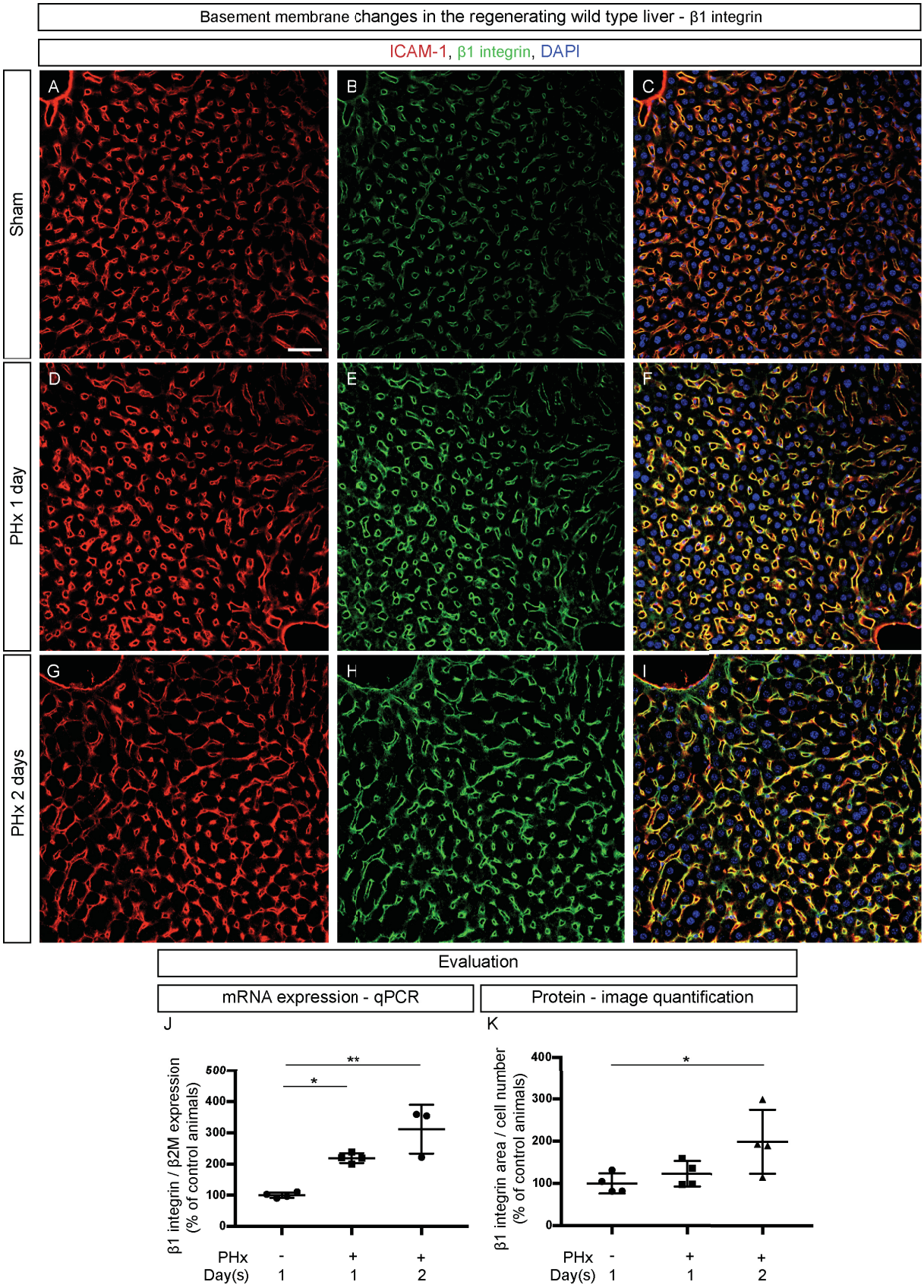

Figure 6: Expression of the mechanosensor β1 integrin increases in wild type mice livers after PHx. Livers of wild type (wt) mice either PHx treated or sham treated (control) were examined for β1 integrin expression determined by Immunostaining and qPCR. ICAM-1

was used as a vessel marker in the liver (red) and DAPI was used to stain the nuclei (blue). Scale bar = 50 µm. (A-C) Images show expression of ICAM-1 and β1 integrin in sham operated mice (A-C), one day after PHx. (D-F) and two days after PHx (G-I) Expression of ICAM-1 and β1 integrin in mice two days after PHx. (J) qPCR: Quantification of β1 integrin expression one day and two days after PHx compared to control mice. n ≥ 3 animals per condition for mRNA analysis. (K) Quantification of β1 integrin area in LSM images one day and two days after PHx compared to control mice. All values are mean values ± s.d. One-way ANOVA followed by Dunnetts's multiple comparisons test was used for statistical evaluation, p values ≤ 0.05 *, p ≤ 0.01 **, n ≥ 4 animals per condition.

3.1.3 Cell proliferation in wild type mice (C57Bl/6J) after PHx

Liver regeneration (and regeneration of tissues in general) depends on proliferation of existing cells. To solve the question, which cell type proliferates and when the proliferation takes place, regenerating liver tissue from wild type mice (C57Bl/6J) after PHx was examined. The phosphorylated Histone H3 (pH3) was used as a cell proliferation marker[120].

Liver tissue that underwent PHx was compared to sham treated tissues. Co-stainings of pH3 (proliferating cells), ICAM-1 (sinusoidal vessels) and DAPI (nuclei) were used to evaluate cell proliferation rates and to distinguish between parenchymal cells (hepatocytes) and sinusoidal lining cells (SLCs). Examples of positive counted proliferating nuclei are indicated with white arrows (Figure 7 A-C). The positive cells for pH3 were normalized to total nuclei in the corresponding images.

No significant changes in proliferation of hepatocytes (Hep), SLCs or total cells occurred after one day of regeneration compared to sham animals (Figure 7G, H, I). The most proliferating cells (pH3 positive) were found after two days of regeneration regardless of the cell type (Figure 7G, H, I). The proliferation rates of SLCs increased about fourfold on day two after PHx, but just about 50 % after one day of regeneration (Figure 7I). Hepatocyte proliferation one day after PHx was increased by about three times, but at two days after PHx it was about 40 fold increased (Figure 7H). Overall cell proliferation in liver sections were increased by about 12 fold at two days after PHx (Figure 7G). Despite the overall increase in proliferating cells after one day, there was also a significant upregulation between one day and two days after PHx (Figure 7G, H, I). This indicates the escalating increase in proliferation at this time point.

Comparing the proliferation rates of SLCs and hepatocytes indicates a much higher proliferation of hepatocytes compared to other cell types in the liver at day two after PHx. These results are in line with previous findings that report a maximum in cell proliferation at two days after PHx[30,51,72].

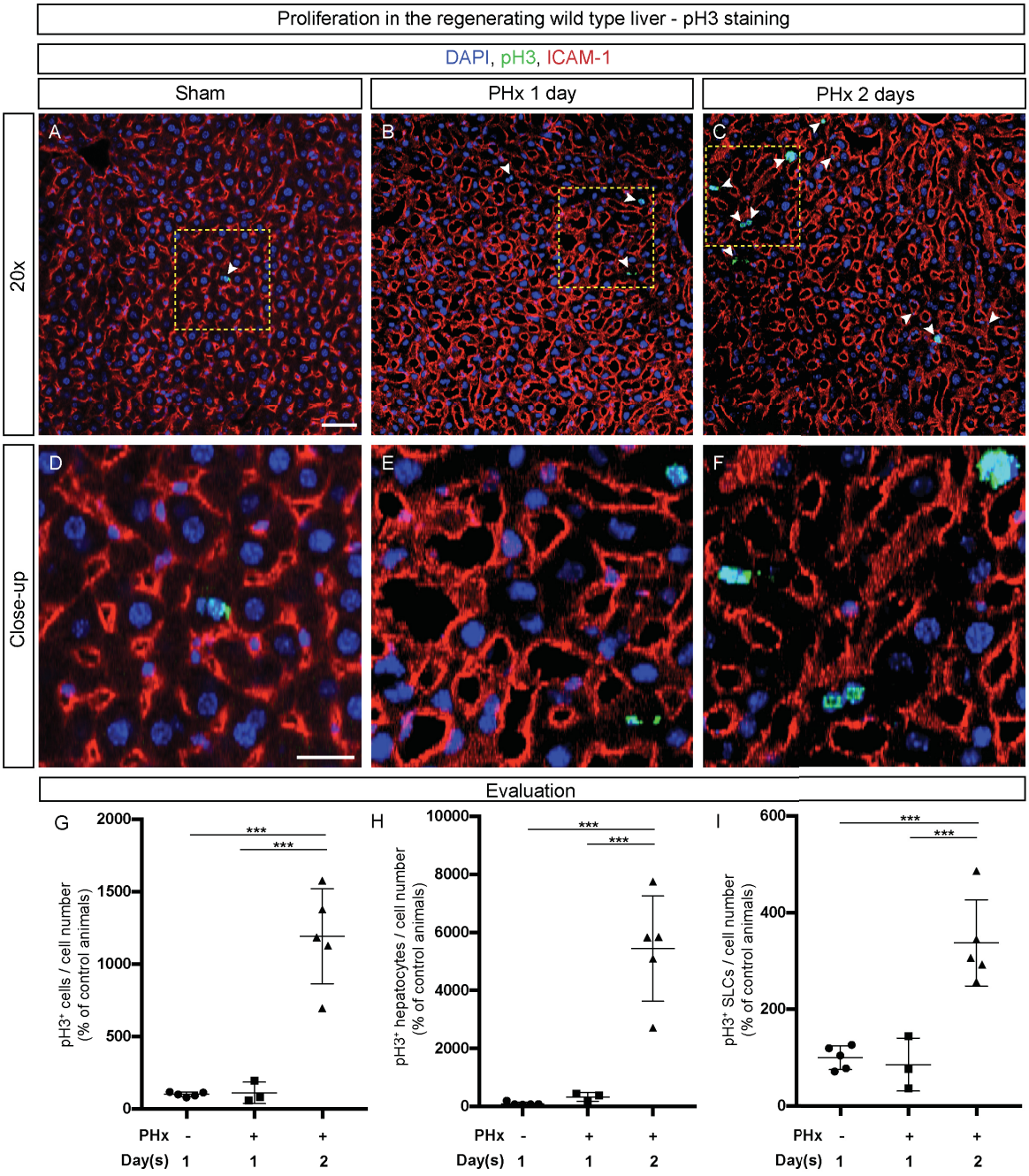

Figure 7: Correlation of β1 integrin expression and liver cell proliferation. Proliferation of liver cells in wt livers at different time points after 2/3 PHx in comparison to proliferation in livers of sham operated (control) mice determined by pH3 staining. ICAM-1 was used as a vessel marker in the liver (red) and DAPI was used to stain the nuclei (blue). Scale bar A-C = 50 µm,

scale bar D-F = 25 µm. White arrows point at all counted pH3 positive cells in pictures A-C). A) Proliferation in the liver of a sham operated mice. B) Proliferation in the liver of a mice one day after PHx. C) Proliferation in the liver of a mice two days after PHx. D-F) Close-ups of the pictures A-C) (yellow square). G) pH3 positive cells in relation to total cell number at the different time points after PHx. H) pH3 positive hepatocytes in relation to total cell number at the different time points after PHx. I) pH3 positive SLCs in relation to total cell number at the different time points after PHx. In all calculations control animals were set to 100%. All values are mean values ± s.d. One-way ANOVA was used for statistical evaluation, $p \leq 0.05$ *, $p \leq 0.01$ **, $p \leq 0.001$ *** $n \geq 4$ animals per condition.

3.1.4 Cell proliferation in endothelial cell specific β1 integrin knockout mice after PHx

After the proliferation rates of wild type mice were investigated, heterozygous and homozygous endothelial cell specific knockout mice for β1 integrin were examined in the same experimental setup. Sham animals were compared to animals two days after PHx. At this time point wild type mice showed their maximum in proliferating cells (Figure 7G).

The heterozygous knockout mice showed a threefold increase in pH3 positive cells two days after PHx compared to sham animals (Figure 8E). This increase was much lower compared to the increase in wild type mice (Figure 7G) but still significant. The value for wild type mice was about 12 fold at the same time point. This result alone indicated a delayed or even inhibited liver regeneration in endothelial specific β1 integrin KO mice.

In contrast to wild type and heterozygous mice, the homozygous KO did not show a significant increase in proliferating cells (Figure 8 E).

In addition to proliferating cells also lactate dehydrogenase (LDH) levels in blood plasma was measured. LDH is an enzyme that catalyzes the reaction from pyruvate to lactate and is present in almost all cell types. Due to this fact, LDH is often used as a marker for cell death in clinical applications[107].

Neither heterozygous, EC specific KO mice after PHx, nor sham treated homozygous EC specific KO mice showed increased levels of LDH (Figure 8F). In contrast, homozygous EC specific KO mice for β1 integrin showed a significant increase (about twofold) of LDH in blood plasma. This increase is about twofold and highly significant (Figure 8F).

The reduced proliferation in heterozygous β1 integrin knockout mice and the almost completely prevented proliferation in homozygous β1 integrin in addition to the increased blood plasma levels of LDH indicated an important role of endothelial β1 integrin for liver regeneration.

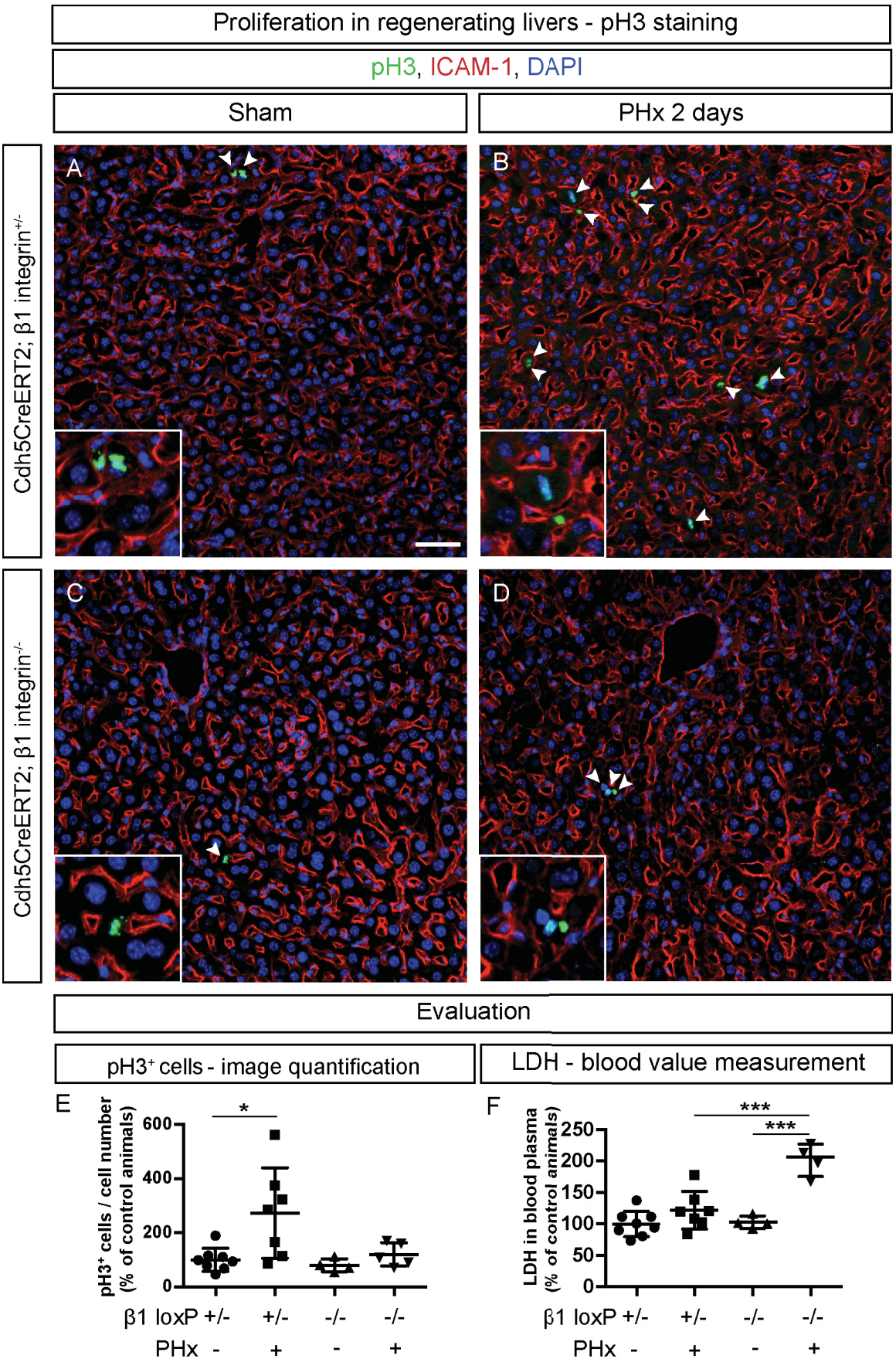

Figure 8: Liver regeneration after PHx is impaired in endothelial specific β1 integrin knockout mice. Proliferation of liver cells in livers of heterozygous and homozygous β1

integrin knockout mice two days after 2/3 PHx in comparison to proliferation in sham operated (control) mice determined by pH3 staining. ICAM-1 was used as a vessel marker in the liver (red) and DAPI was used to stain the nuclei (blue). Scale bar A-D = 50 µm, white arrows point at all counted pH3 positive cells in pictures (A-D). (A) Proliferation in the liver of a sham operated heterozygous β1 integrin knockout mouse. (B) Proliferation in the liver of a heterozygous β1 integrin knockout mouse two days after PHx (C) Proliferation in the liver of a sham operated homozygous β1 integrin knockout mouse. (D) Proliferation in the liver of a homozygous β1 integrin knockout mouse two days after PHx (E) Scatter plot of pH3 positive cells in relation to total cell number in heterozygous and homozygous β1 integrin knockout mice. Sham operated and two days after PHx. (F) LDH values measured in blood plasma of heterozygous and homozygous β1 integrin knockout mice. Sham operated and two days after PHx. Heterozygous sham operated β1 integrin knockout mice were set to 100 %. All values are mean values ± s.d. Two-way ANOVA was used for statistical evaluation, $p \leq 0.05$ *, $p \leq 0.01$ **, $p \leq 0.001$ *** $n \geq 4$ animals per condition.

3.1.5 Cell death after PHx in endothelial cell specific β1 integrin knockout mice

Homozygous EC specific KO mice for β1 integrin showed a strongly reduced proliferation (Figure 8E) and elevated levels of the cell death marker LDH in blood plasma (Figure 8F) at time points at which wild type mice showed massive cell proliferation after PHx. This finding raised the question if beside reduced proliferation also increased tissue damage is present. To determine this, TUNEL (Terminal deoxynucleotidyl transferase-mediated dUTP-biotin nick end labeling) stainings were performed to quantify cells undergoing programmed cell death (apoptosis). Interestingly TUNEL positive cells could only be observed in the liver periphery (Figure 9A-C). There was a huge heterogeneity between the examined mice, which prevented significant results. Due to heterogeneity in this group no significance could be detected. This feature is similar to the embryonic lethal phenotype of endothelial specific (not inducible) KO of β1 integrin (J. Axnick, Dissertation 2016).

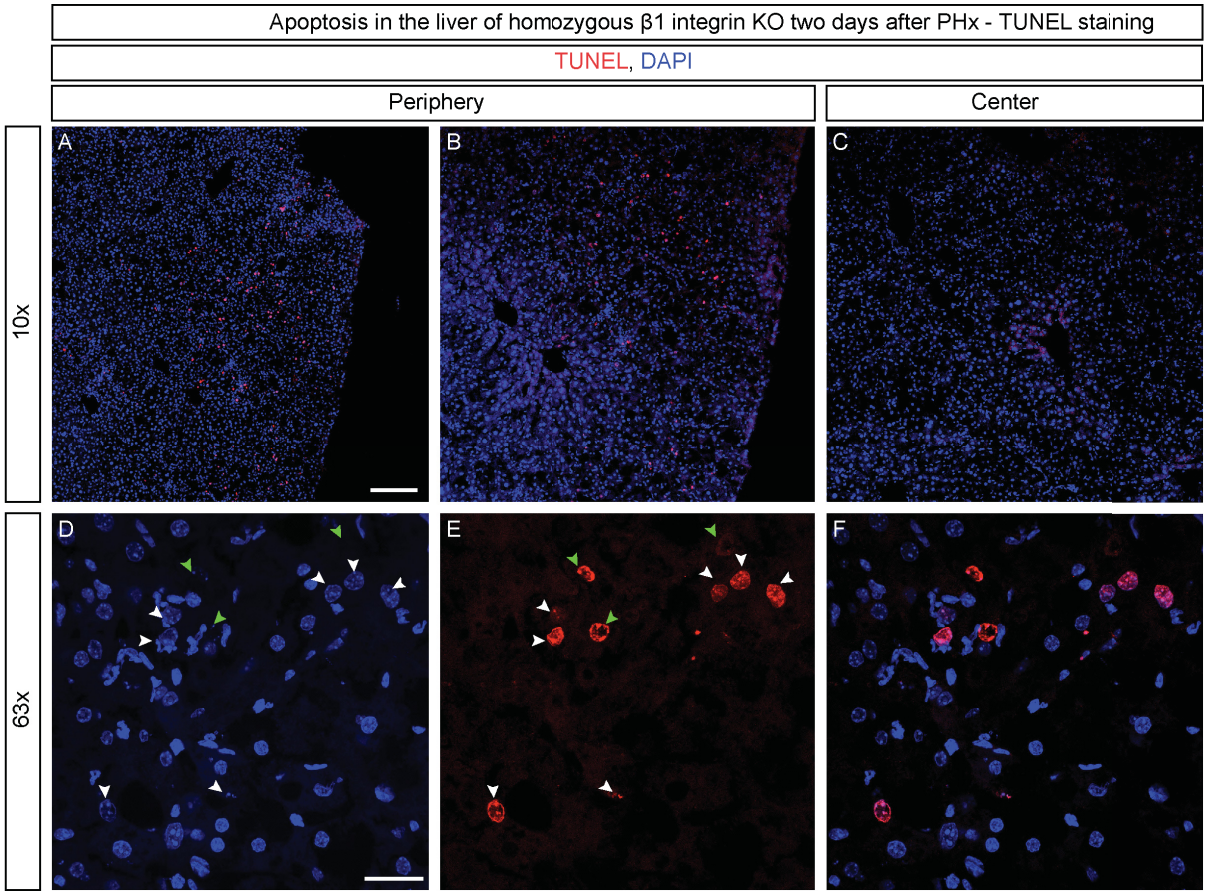

Figure 9: Apoptotic cells in liver periphery of homozygous β1 integrin ablation after PHx. TUNEL positive cells in periphery of homozygous β1 integrin ablation determind by TUNEL staining. (A-C) Shows an overview of TUNEL staining in liver sections. (A) and (B) show staining in the periphery and (C) in the center of a liver section. (D-F) High magnification images of TUNEL staining. (D) Depicts the DAPI channel, (E) the TUNEL staining and (F) a merge of both channels. White arrows point at cells stained with TUNEL which show an intact nucleus and green arrows point at cells stained with TUNEL which show a degraded nucleus. Scale bars: A=100 µm, D=25 µm.

3.1.6 MIF is released from LSECs after exposure to mechanical forces

To investigate if the proteome profile for secreted proteins of LSECs is changed after exposure to expose to mechanical stress, cell culture supernatants of stretched human LSECs (hLSECs) were applied to a proteome profiler array. Among several proteins with increased abundance in the supernatant of stretched compared to unstretched hLSECs, the macrophage migration inhibitory factor (MIF) was strongly upregulated (Figure 10A-C). Next, it was assessed if MIF levels are also affected in mice after PHx *in vivo* MIF levels in MACS sorted CD146 positive liver cell fractions from mice livers

(assumed to be murine LSECs, (mLSECs)) were examined in western blots (Figure 10D). Of note, MIF protein but not β-actin (housekeeping control) was significantly down regulated in mLSECs 30min after PHx compared to sham control, (Figure 10D, E). In sum, these experiments indicate that MIF is secreted upon stretching of LSECs *in vitro* and potentially *in vivo*.

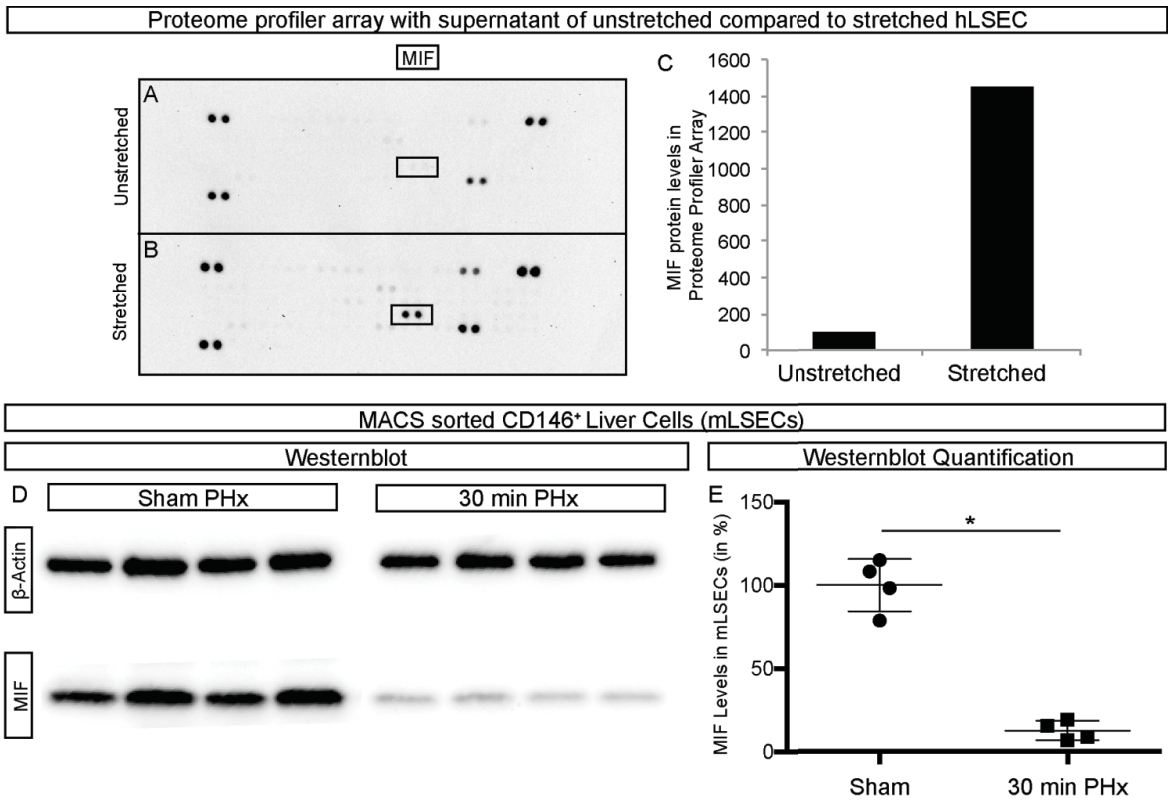

Figure 10: MIF is secreted from LSECs after mechanical stimuli. Proteome profiler array show a strong enrichment of MIF protein in cell culture supernatant of (60min) stretched (B) compared to unstretched (A) LSECs. Protein dots for MIF are indicated by black boxes on array nitrocellulose membranes in panel (A) and (B). Cell culture supernatants from three individual experiments were collected on different dates and frozen. After thawing, supernatants were pooled and incubated on array membranes. Dot intensity for MIF was quantified (C) using an automated imaging script in FIJI. (D, E) Western blots of MACS® sorted CD146 positive cells from mice livers (murine LSECs) underwent PHx or sham surgery (D). (E) Quantification of western blots of panel (E). Values are mean values ± s.d., p values ≤ 0.05 considered as statistically significant in Student‘s t-test (n = 4 animals per condition).

3.1.7 MIF protein is increased in blood plasma of mice after PHx

Since the previous experiments had indicated that MIF is secreted upon mechanical stress mimicking increased hepatic blood volume after PHx, it was now investigated, if MIF blood concentration was increased after PHx *in vivo*. In wild type mice MIF was significantly increased in blood plasma 30min after PHx (Figure 11A). Also endothelial specific heterozygous knockout mice for β1 integrin showed a significant upregulation of MIF in blood plasma after PHx compared to sham mice with the same genotype (Figure 11B). In contrast to those mice, homozygous endothelial specific β1 integrin knockout mice did not show increased levels of MIF after PHx compared to sham animals.

The increase of MIF protein in plasma of wild type and endothelial specific, heterozygous β1 integrin knockout mice correlates with the decreased MIF levels in mLSECs shortly after PHx (Figure 10E).

Importantly, the finding that MIF levels were not increased in blood plasma of endothelial specific homozygous β1 integrin knockout mice indicates that β1 integrin on LSECs is crucial for the secretion of MIF from LSECs. Similarly, these findings indicate (but do not fully prove) that LSECs are the major cell type responsible for increased circulating MIF levels after PHx.

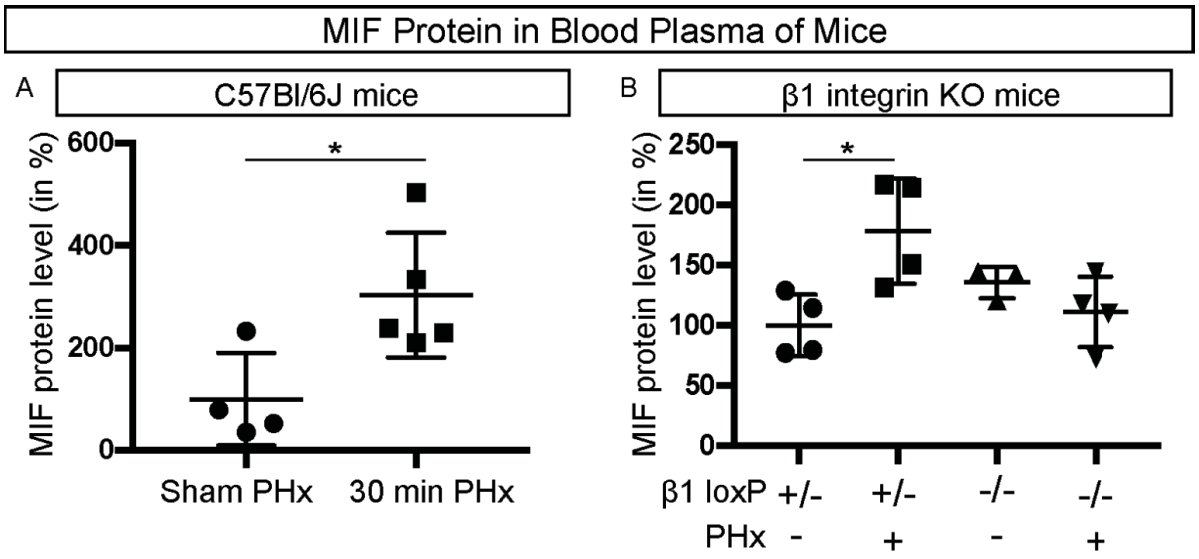

Figure 11: MIF is increased in blood plasma of mice after PHx. (A) MIF levels in blood serum of C57Bl/6J mice shortly after PHx. (B) MIF levels in blood serum of endothelial specific β1 integrin knockout mice shortly after PHx. All values are mean values ± s.d. Student‘s t-test was used in (A) and one-way ANOVA followed by Tukey’s multiple comparison test in (B) was used for statistical evaluation, $p \leq 0.05$ *, $n \geq 3$ animals per condition.

3.1.8 MIF and ICAM-1 expression increases in mice livers shortly after PHx

Established angiocrine signals, important for liver regeneration[30,72,73], usually play a role after one or more days of regeneration but the observed vessel dilation (Figure 5) occurred much faster. This raised the question if there are changes in the liver at this early time point. Within the first hour after PHx both, ICAM-1 and MIF protein content increased in the mouse liver samples (Figure 12A). The mRNA levels for MIF (Figure 12B) and ICAM-1 (Figure 12C) increased significantly compared to sham treated mice (0min of regeneration) in lysates of liver tissue already 30min after PHx. Remarkable, both MIF and ICAM-1 mRNA levels were down-regulated already 60 min after PHx again (Figure 12B, C). The protein levels of both MIF and ICAM-1 were upregulated after 30min as well (Figure 12D, E). Unlike the mRNA levels, protein levels of MIF and ICAM-1 remained upregulated after 60min (Figure 12D, E). These results indicate that MIF and ICAM-1 expression is significantly increased already 30min after PHx, when other canonical angiogenic signals such as Id-1 or Ang2 are not yet upregulated.

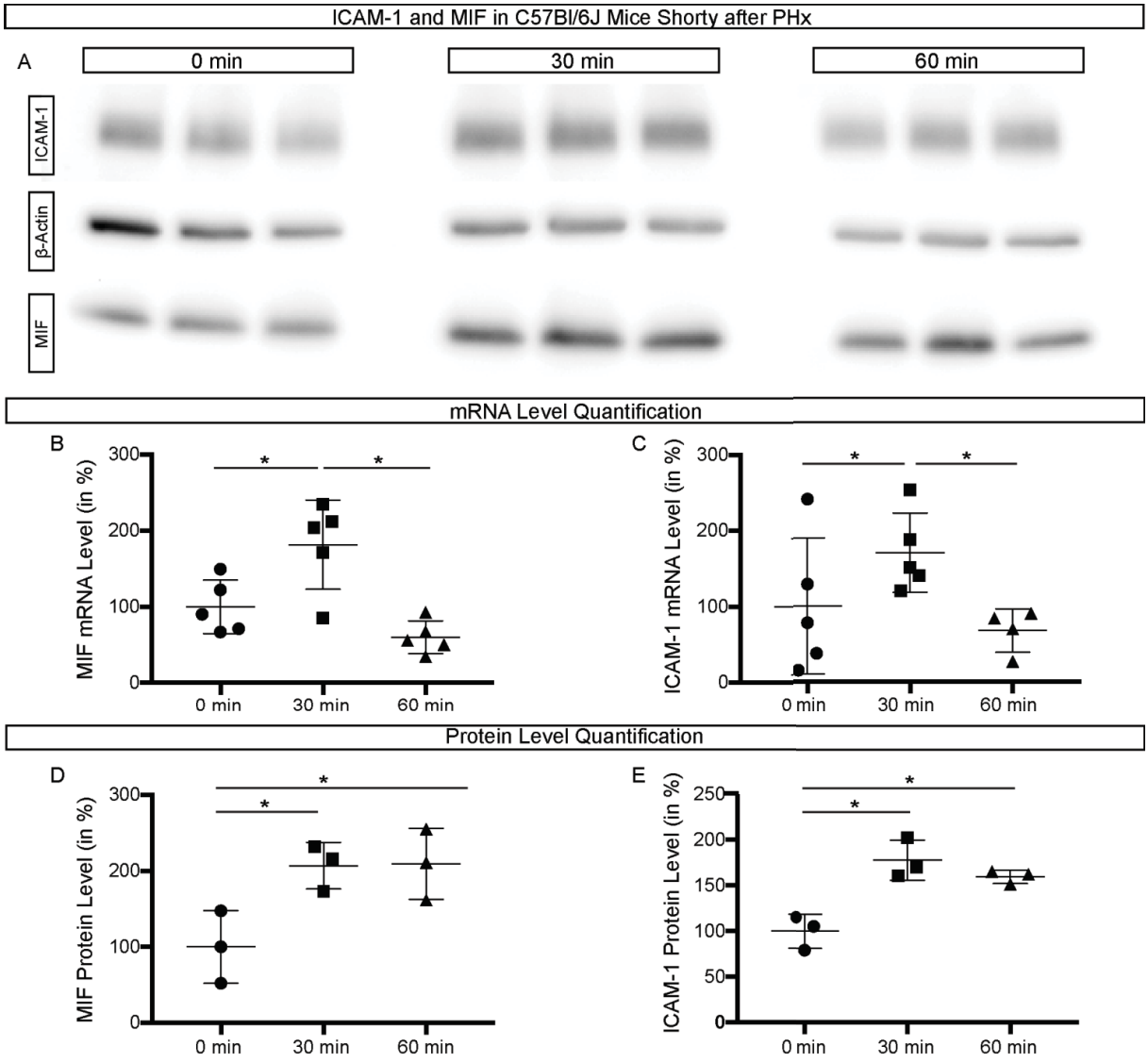

Figure 12: MIF and ICAM-1 expression increases shortly after PHx. (A) Western blots of C57Bl/6J mice liver lysates on different time points after PHx, stained with antibodies against ICAM-1, MIF and β-actin. (B, C) Quantification of mRNA levels for (B) MIF and (C) ICAM-1 in whole liver lysates of C57Bl/6J mice. Expression levels of 0min set to 100%, β2M was used as housekeeping gene. (D, E) Quantification of western blots shown in (A) for MIF (D) and ICAM-1 (E). (n ≥ 3 animals per condition) p values ≤ 0.05 considered as statistically significant in ordinary one-way ANOVA, followed by Dunnetts's multiple comparisons test. All values are mean values ± s.d.

3.1.9 MIF and ICAM-1 expression correlates with perfusion rate of the liver

To find out whether the early changes after PHx observed in Figure 12 are attributable to the hemodynamic changes after PHx (Figure 5), *ex vivo* liver perfusion experiments

were performed (Figure 13A). In this experimental setup it is possible to manipulate the perfusion rate of the liver (perfused with pre-warmed and oxygenated buffer). In addition PHx can be simulated by ligation of liver lobes. If similar changes like in the *in vivo* situation would occur, these effects could be justified due to mechanical perfusion effects, independent of i.e. hormones secreted from other tissues.

The liver is perfused by about 25 % of the left cardiac output[10]. This output is between 12 and 16 ml per min in mice[121]. To not overestimate any possible side effects, the perfusion rate of the control condition was set to 4 ml/min. After one hour of *ex vivo* liver perfusion, protein contents of MIF and ICAM-1 were examined. In simulated PHx conditions, ICAM-1 but not MIF protein levels were significantly upregulated when the flow rate was kept at 4 ml/min (Figure 13B, C, D).

Contrast enhanced ultrasound measurements before and after PHx indicated a duplication of blood to liver ratio (Figure 5). A transfer of this result to the *ex vivo* perfusion setup without PHx, in particular 8 ml/min instead of 4 ml/ml perfusion rate, alone was also capable to increase ICAM-1 protein levels significantly (Figure 13D). In addition, under this condition, also MIF protein was significantly upregulated (Figure 13C).

These results indicate that the protein upregulation is due to increased mechanical forces after liver ligation in the *ex vivo* setup. Most likely this finding is also applicable to the *in vivo* situation after PHx (Figure 12).

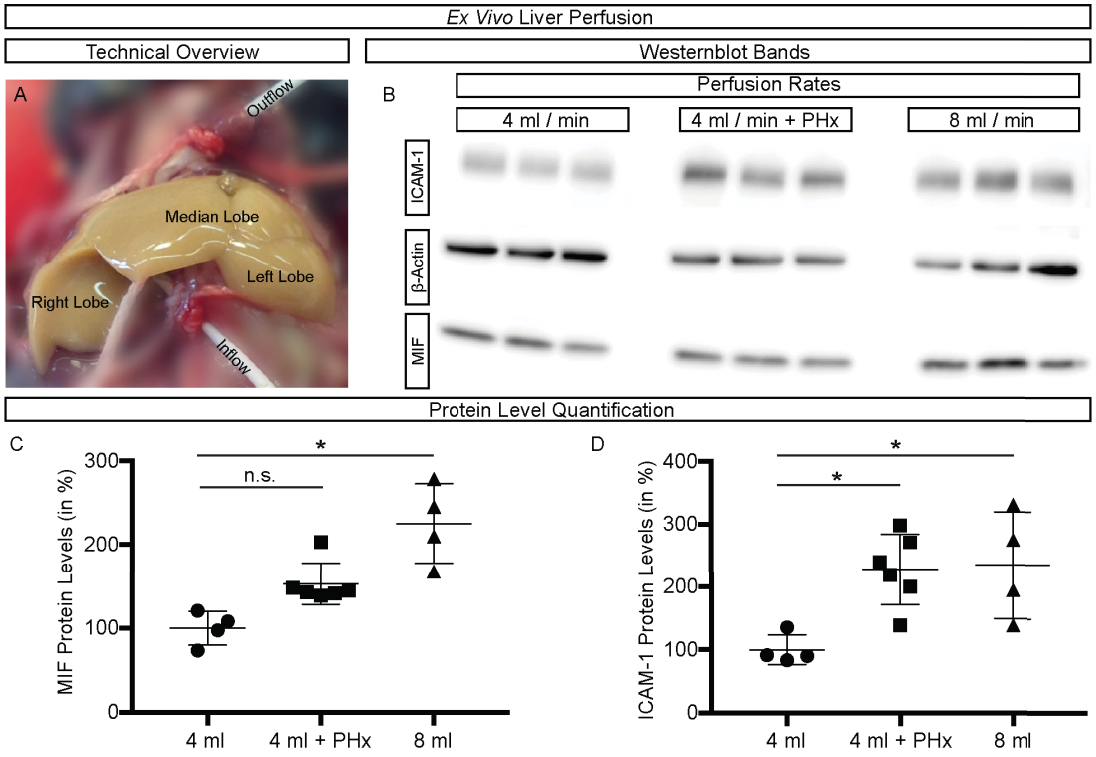

Figure 13: MIF and ICAM-1 is upregulated by increased *ex vivo* perfusion in mice livers. (A) Overview of ex vivo perfused mice liver. (B) Western blots of *ex vivo* perfused C57Bl/6J mice livers with different perfusion rates and with or without PHx, stained with antibodies against ICAM-1, MIF and β-actin. (C, D) Quantification of western blots of whole liver lysates afer *ex vivo* perfusion. P values ≤ 0.05 considered as statistically significant in ordinary one-way ANOVA, followed by Dunnetts's multiple comparisons test. All values are mean values ± s.d., n ≥ 4 animals per condition.

3.1.10 Mechanotransduction increases MIF and ICAM-1 expression in hLSECs *in vitro*

The results of increased blood to liver ratio (Figure 5B) and subsequent vessel dilation (Figure 5E) after PHx *in vivo* indicate a stretching of the sinusoidal vessels and therefore the LSECs. This stretching inevitably induces mechanical stress to the endothelium. To determine if this mechanotransduction has an effect on LSECs, and subsequently on MIF and ICAM-1 expression, human liver sinusoidal endothelial cells were either seeded on silicon stretching chambers (Figure 14A, B) or in flow chambers (Figure 14C) and exposed to the respective mechanical stress. These different experimental setups were necessary because in the *in vivo* situation both mechanical

forces stretching and increased shear stress (due to increased blood flow) can play a role.

In the stretching chambers, LSECs were exposed to different time spans of cell stretching and mRNA expression was analyzed afterwards. Stretching for 60min of LSECs led to significant increase in ICAM-1 (Figure 14E) and MIF (Figure 14D) mRNA levels.

ICAM-1 is known to be upregulated by increased shear stress[122,123]. Those findings could be confirmed in this study. ICAM-1 mRNA expression was upregulated in flow conditions of 3.7 dyn/cm^2 compared to static flow conditions of 0 dyn/cm^2. ICAM-1 was also upregulated in higher shear stress conditions of 7.4 dyn/cm^2 (Figure 14G). The 3.7 dyn/cm^2 condition reflects the normal physiologic condition in the liver[117]. The 7.4 dyn/cm^2 shear stress condition shall reflect the doubled ratio of blood volume to liver tissue after PHx (Figure 5B). Cells in all conditions were incubated for at least 48 hours. Both flow conditions were incubated at 3.7 dyn/cm^2. In the increased flow condition, shear stress was increased to 7.4 dyn/cm^2 for 30min. There was no difference in MIF mRNA expression between static (0 dyn/cm^2) and physiologic (3.7 dyn/cm^2) shear stress condition, but further increasing shear stress (7.4 dyn/cm^2) induced upregulated levels of MIF mRNA compared to static control (Figure 13F).

These results of increased MIF and ICAM-1 expression after exposure to mechanical forces fall into line with the previous results of increased MIF and ICAM-1 expressions (and MIF secretion) after *in vivo* PHx and increased perfusion in the *ex vivo* setup.

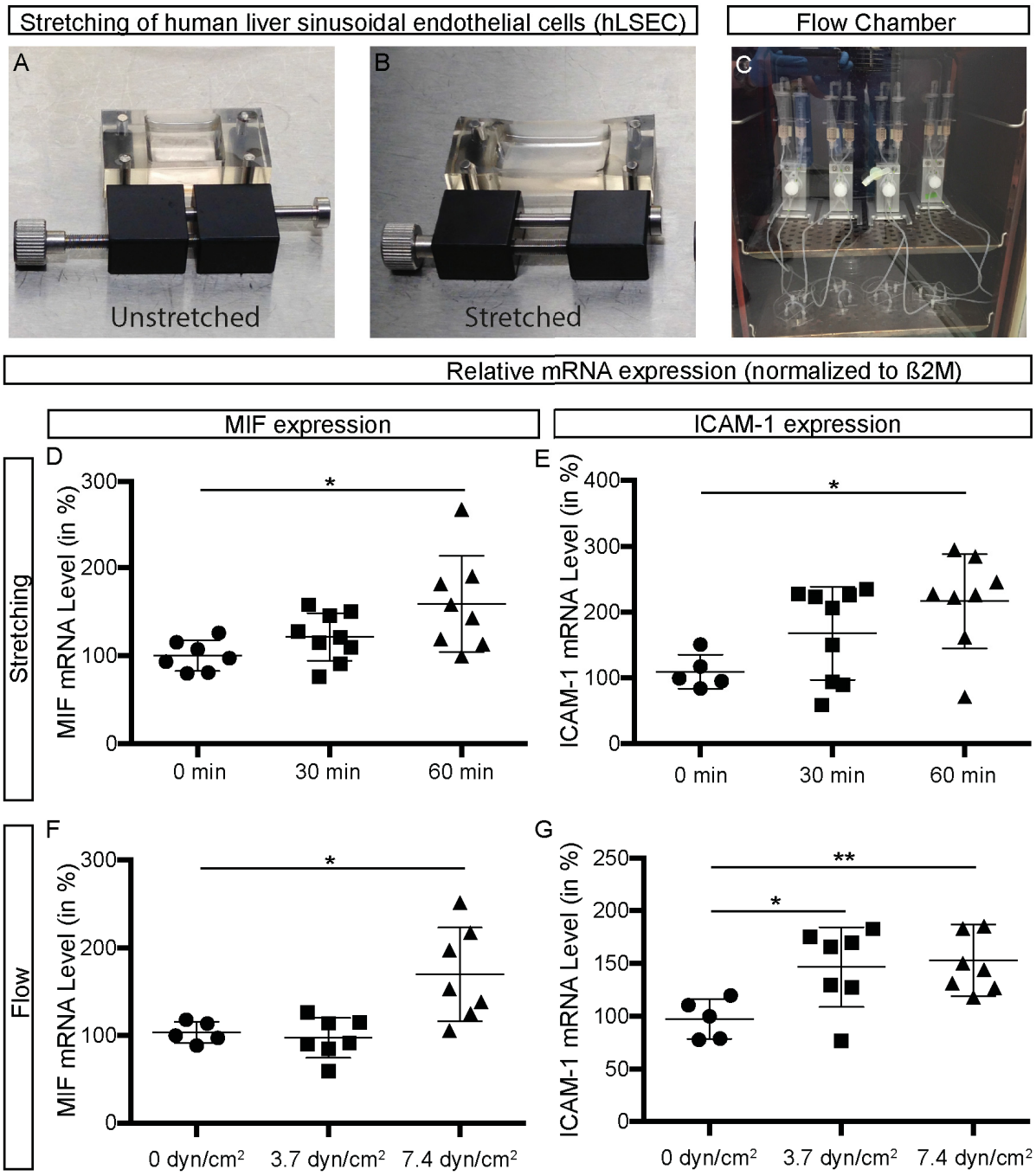

Figure 14: Mechanotransduction increases MIF and ICAM-1 expression *in vitro*. Experimental setup of stretching chambers in unstretched (A) and stretched (B) conditions. Experimental setup of flow chambers (C). Relative mRNA expression (normalized to β2M) in hLSECs in stretching chambers at different time points of stretching for MIF (D) and ICAM-1 (E). n ≥ 5 stretching chambers. p values ≤ 0.05 considered as statistically significant in ordinary one-way ANOVA, followed by Tukey's multiple comparisons test. All values are mean values ± s.d. Relative mRNA expression (normalized to β2M) in hLSECs at different shear stress rates in flow chambers for MIF (F) and ICAM-1 (G). Cells were cultivated for 3 days under flow at 3.7 dyn/cm^2 with 30min of increased shear stress (7.4 dyn/cm^2) compared to a static control and cells that only experienced a shear stress of 3.7 dyn/cm^2. N ≥ 4 flow chambers. P values

≤ 0.05 considered as statistically significant in ordinary one-way ANOVA, followed by Tukey's multiple comparisons test. P < 0.05 *, p < 0.01 **, n ≥ 5 animals per condition.

3.1.11 MIF is upstream of ICAM-1 *in vitro*

In literature evidence can be found that MIF can upregulate ICAM-1 during physiologic events like artherosclerosis[124] and this pathway was found in monocytes[102] and also endothelial cells[125].

To test the hypothesis that MIF can regulate ICAM-1 expression in LSECs, RNA interfering experiments were performed *in vitro*. Therefore small interfering RNA against MIF were transfected into human liver sinusoidal endothelial cells (hLSECs). After testing the knockdown efficiency of MIF, the effect on ICAM-1 expression was measured. It could be observed that MIF specific knockdown alone leads to a reduction in ICAM-1 mRNA level expression (Figure 15A). In addition to this loss of function approach, a gain of function approach was performed with incubation of recombinant human MIF on the hLSECs. Recombinant human MIF was able to increase ICAM-1 mRNA expression levels significantly on hLSECs (Figure 15B).

This regulation was also tested on protein level. Therefore western blots of cell lysates were performed (Figure 15C). First the effect of siRNA, specific against MIF, was tested on the MIF protein expression. This manipulation resulted in a significant reduced MIF protein expression on LSECs (Figure 15D). This result proves the efficiency of the siRNA. More interestingly was the effect of siRNA knockdown of MIF on the ICAM-1 protein expression in LSECs. In addition to the decreased mRNA expression of ICAM-1 (shown in Figure 15A), also the protein level of ICAM-1 was significantly reduced, compared to control conditions (Figure 15E).

This result underlines the importance of MIF because the overall ICAM-1 upregulation is at least partially attributable to MIF after LSEC were exposed to mechanical stress.

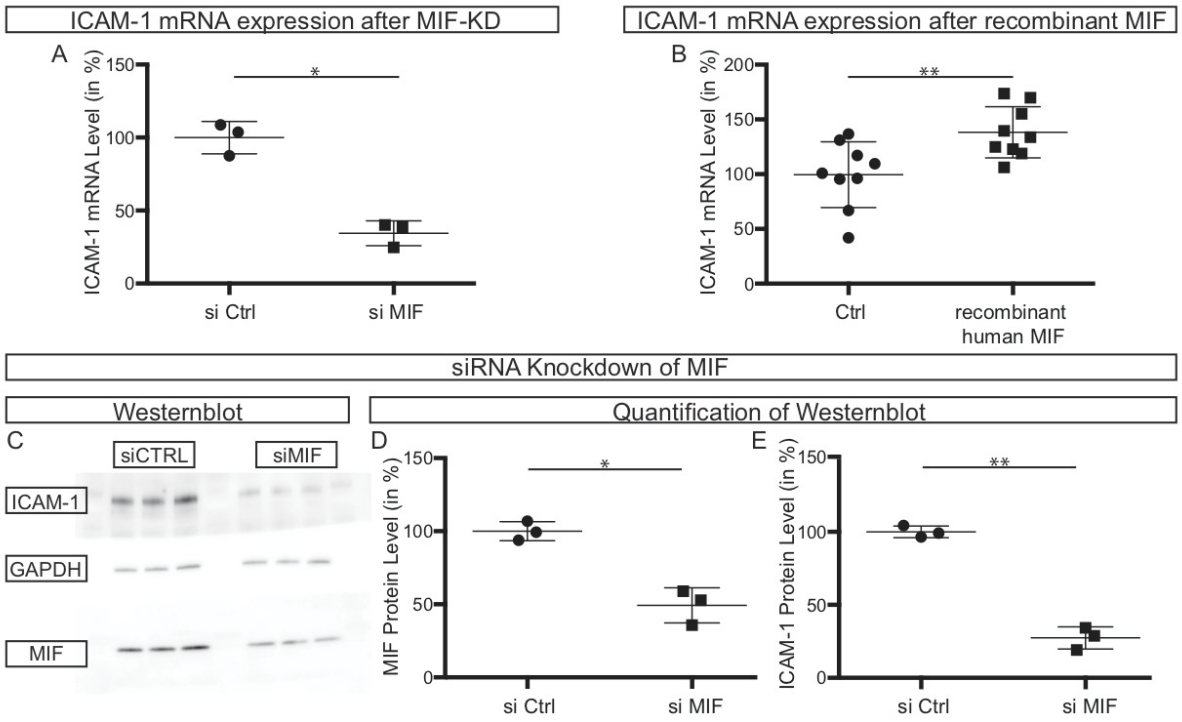

Figure 15: MIF is upstream of ICAM-1 expression in human LSECs *in vitro*. (A) ICAM-1 mRNA expression (normalized to β2M) in human LSECs after siRNA knockdown of MIF. (B) Analyses of ICAM-1 mRNA expression using qPCR in human LSECs after treatment with recombinant human MIF. (C-E) Western blot analysis of human LSECs after siRNA knockdown of MIF. Quantification of protein levels (normalized to GAPDH) for MIF (D) and ICAM-1 (E). P values ≤ 0.05 considered as statistically significant in Student's t-test, $p < 0.05$ *, $p < 0.01$ **, $n \geq 3$ animals per condition.

3.1.12 MIF is required for ICAM-1 expression and liver regeneration after PHx

The previous results indicate a possible role of MIF during liver regeneration after PHx. To test this issue, MIF conventional knockout mice (KO) were examined. First ICAM-1 levels of MIF KO mice were compared to control mice. As expected, no MIF protein could be detected in western blots of MIF KO mice (Figure 16A).

Interestingly, MIF KO mice showed reduced levels of ICAM-1 protein (compared to control mice) in whole liver lysates even without PHx (Figure 16A, B). This result supports the *in vitro* data that MIF is upstream of ICAM-1 (Figure 15). In addition, MIF is apparently needed for normal ICAM-1 expression. MIF KO mice also show reduced

ICAM-1 levels after PHx (data not shown). To clarify the role of MIF in liver regeneration, ICAM-1 levels are not sufficient.

Therefore MIF KO mice underwent PHx and cell proliferation and apoptosis were analyzed at two days after PHx. At this time point the wild type mice showed a maximum in pH3 positive cells (Figure 7) unlike β1 integrin homozygous knockout mice (Figure 8E). MIF KO mice demonstrated a strong tendency of less proliferating pH3 positive cells (Figure 16D) and had significantly more apoptotic (TUNEL positive) cells in liver sections (Figure 16C).

The results of MIF KO mice indicate that MIF plays an important role for liver regeneration after PHx, which might be partially mediated by a concomitant increase in ICAM-1.

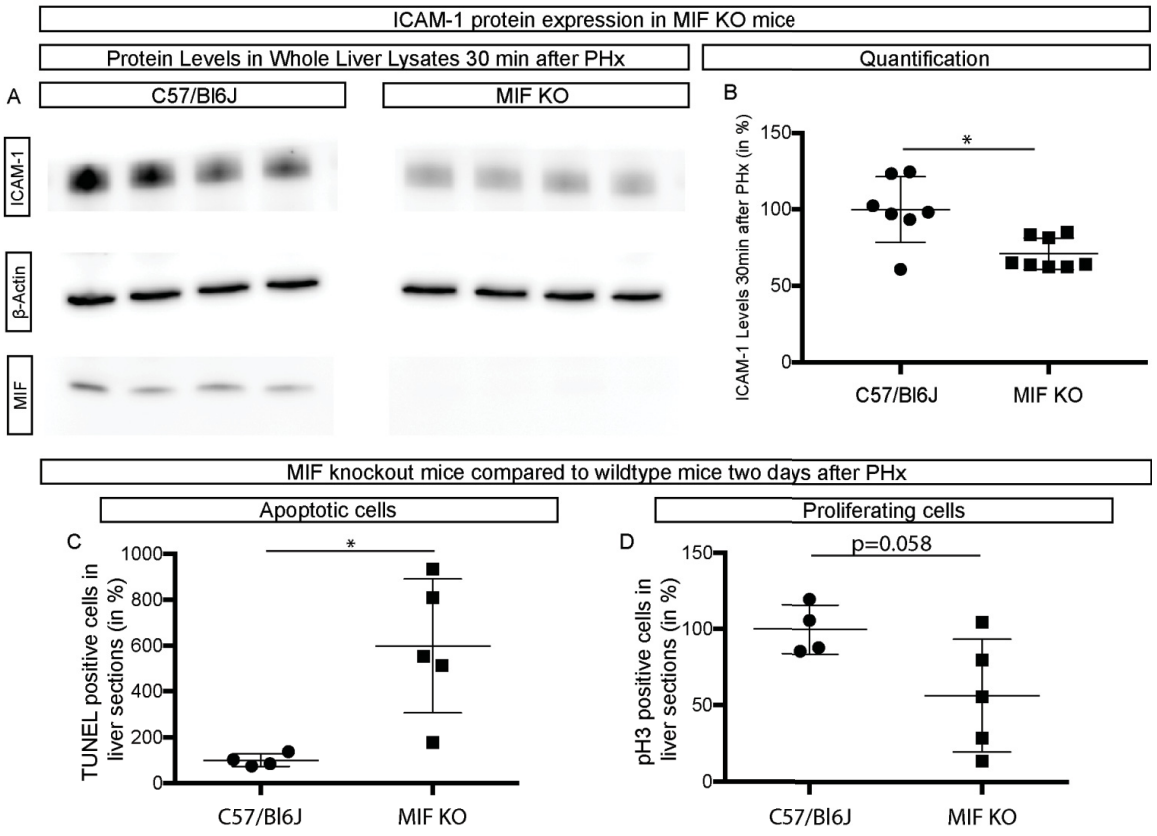

Figure 16: MIF is required for normal ICAM-1 expression and liver regeneration after PHx. (A) Westernblots of C57Bl/6J and MIF-knockout mice liver lysates after PHx, stained with antibodies against ICAM-1, MIF and β-actin. (B) Quantification of westernblots shown in (A) (n ≥ 4 animals per condition) p values ≤ 0.05 considered as statistically significant in Student‘s t-test. (C, D) Quantification of pH3 positive (C) and TUNEL positive (D) cells in mice liver

sections of C57Bl/6J mice compared to MIF knockout mice. (n ≥ 4 animals per condition) p values ≤ 0.05 considered as statistically significant in Student‘s t-test.

4 Discussion

4.1.1 Relevance of the work

Many patients are suffering from chronic liver diseases with severe decreased life quality over decades[126]. In the USA, 150000 patients are supposed to die from chronical viral hepatitis (HBV and HCV) in the next 10 years and around 3.5 to 5.3 million patients are infected with chronic viral hepatitis[127]. Additionally, there are many other etiologies for chronic liver diseases (CLD) (Table 1). 29 million people suffer from CLDs of different etiologies in the European Union[59]. It can take several decades from the onset of CLDs to fulminant hepatic failure. This delay is due to the regenerative capacity of the liver. Unfortunately the underlying processes are not completely understood. This fact and the notion that development of these diseases takes many years may be a reason why many potential antifibrotic drugs work *in vitro* and in animal models but could not be validated in clinical trials[39]. Importantly, no cure for fibrosis and cirrhosis is available. If fulminant liver failure occurs in the end stage of CLDs a liver transplant is inevitable. Fortunately liver transplants are not exclusively dependent on deceased organ donors. Because of the regenerative potential of the liver also living donor transplants are possible[128]. Thereby only a portion of the liver is removed from the donor and transplanted in the recipient. The pieces increase in size in both donor and recipient to fulfill the physiologic functions. Interestingly the final liver mass is adapted to the physiologic demands in both individuals. This effect is still not understood.

Because of the overall prevalence of liver diseases and the increasing demand for liver transplants, liver regeneration is extensively studied all over the world.

In theory, understanding the molecular pathways regulating liver regeneration might help in the future to find new cures for cirrhosis and terminal liver failure.

Earlier research identified many angiocrine factors for liver regeneration[30,72,76]. The concept of blood vessel derived signals that are important for organ growth is not novel[77,78], but had not been looked at in the context of liver regeneration. Earlier research of liver regeneration before this mental effort mainly focused on the liver parenchymal cells (hepatocytes)[44]. The idea of possible hemodynamic changes after PHx was present in literature but not experimentally addressed[52]. Until now it was

speculated that the portal blood flow in the liver after PHx increases by three fold[52] but experimental data were not provided so far.

Nevertheless hemodynamic changes in the liver would be expected to be the very first event after partial hepatectomy. More precise, the hemodynamics should change already when the liver lobes are ligated before removed. Therefore, while previous efforts looked mainly on later effects after PHx, in this thesis, also early effects were investigated on a molecular level.

4.1.2 Hemodynamic changes after PHx

The aim of this thesis was to investigate possible hemodynamic changes after PHx and a possible role of these changes in liver regeneration.

Theoretically there are two options how hemodynamics could change after PHx. Either the blood flow velocity in the liver increases, namely the blood just flows faster through the liver, or the liver vessels compensate the physiological changes by dilation of the vascular bed (vasodilation).

The first experimental results from CEUS displayed a significant increase in blood to liver ratio shortly after PHx (Figure 5B). This indicates that the liver contains more blood after PHx. The blood speed velocity showed only a slight non-significant tendency to be increased (Figure 5C). Combining these results it can be concluded that there is more blood in the liver but it does not flow faster through the tissue.

These CEUS data do not inform about the tissue integrity after PHx: to a certain extent it would be possible that the increased blood amount results in tissue hemorrhages, i.e. inbleeding into the liver parenchyma. This could be excluded, since LSM images of fixed livers showed intact liver tissue and dilated liver vessels (Figure 5F). This is might be possible due to the anatomic feature of the hepatic perisinusoidal space (space of Disse). This space could serve as a biological buffer zone where blood vessels expand when more blood enters the liver after PHx.

Since vasodilation is often triggered under influence of nitric oxide (NO), it is possible that changes in NO play a role in the vasodilation identified after PHx, nonetheless the fact that blood amount in the liver is increased, points to a mechano-physical effect on the vascular structure.

4.1.3 β1 integrin expression after PHx

The aim of the thesis was to clarify if the hemodynamic changes after PHx contribute to liver regeneration. Since hemodynamic changes occur very fast after PHx, whereas liver regeneration, i.e. hepatocyte proliferation is only noticeable after several hours to days after PHx. Both early (30min after PHx) and late (i.e. 2 days after PHx) time points were routinely assessed in this thesis. Earlier investigations had demonstrated that laminin, an ECM protein, is upregulated two days after PHx (diploma thesis T. Buschmann). The presence of laminin alters cellular signaling at least in part through β1 integrin, a transmembrane protein involved in the mediation of cell-cell and cell-matrix (extracellular matrix) interactions. Notably, β1 integrin was significantly upregulated at two days after PHx (Figure 6K). Of note, this fact at that time did not prove that β1 integrin plays a critical role in liver regeneration; moreover, integrins are activated by conformational changes[92,93], therefore an increase in signaling could occur independent of increased protein amounts already at earlier time points.

β1 integrin is expressed on hepatocytes[129], nonetheless, the protein increase after PHx appears to be mainly in SLCs (sinusoidal lining cells), which might include endothelial cells, but also Kupffer cells and HSCs (all expressing ICAM-1, Figure 7B, E, H).

It is currently unclear, why β1 integrin protein expression is increased two days after PHx, since in this thesis it was demonstrated, that β1 integrin already alters important molecular events early after PHx, when β1 integrin protein levels are still unchanged (see below). One possible explanation for the late increase in β1 integrin protein could be that the liver capillaries gain more ECM during regeneration, which has been proposed to be necessary for full angiogenesis during liver regeneration[10].

4.1.4 Liver regeneration after PHx

The upregulated protein expression of β1 integrin (Figure 6) correlates with maximal cell proliferation in regenerating livers (Figure 7G-I). The hepatocyte proliferation in mice livers peaks around 48 hours after PHx in literature[30,51]. In this thesis, the examined livers also showed a strong increase in pH3 positive cells as an accepted marker for proliferation[30] at this time point (Figure 7H). At the same time point also SLCs showed strong proliferation. In an earlier publication, the maximum proliferation of LSECs was found to be from day 4 to 8 after PHx, with no increase on day two[30]. In this study, proliferation on SLCs (all ICAM-1 positive cells) including LSECs was already significantly upregulated at two days after PHx. These results could indicate

that non-LSEC SLCs are proliferating earlier than LSECs, although that remains to be tested.

4.1.5 Liver regeneration in endothelial specific β1 integrin knockout mice

To test if β1 integrin plays a role in liver regeneration, endothelial specific inducible knockout mice for β1 integrin were examined after PHx. Both, heterozygous and homozygous knockout mice for β1 integrin showed a decrease in proliferating cells (pH3 positive cells) compared to wild type mice (Figure7). In heterozygous knockouts there was still a significant increase in proliferation two days after PHx (Figure 8E). This was not true for homozygous knockout mice (Figure 8E). Importantly, endothelial specific knockout mice for β1 integrin showed increased levels of LDH in blood plasma (Figure 8F), which might be explained by increased apoptosis in periphery of the liver (Figure 9), similar to what has been demonstrated in conventional endothelial β1 integrin KO embryos (Jennifer Axnick, Dissertation in the Lammert laboratory 2016).
These results indicate that endothelial β1 integrin plays a role in liver regeneration and in addition, it is needed to prevent excessive liver damage after PHx. β1 integrin is known as a mechanotransducing molecule[130]. Therefore it is likely that in the knockout mice, the endothelium cannot sense the altered mechanical forces due to hemodynamic changes after PHx.
Signaling of integrins is important for liver maintenance. For example knockout of the integrin signaling mediating kinase, ILK (integrin linked kinase), which is normally linked to either β1 – or β3 integrin[131] leads to increased liver size even without PHx[132]. β1 integrin also participates in vascular remodeling in other tissues, for example in neurovascular remodeling after stroke[133].

4.1.6 MIF levels in LSECs exposed to mechanical force

To identify possible new angiocrine factors that occur in the blood corresponding to the hemodynamic changes after PHx, proteome profiler arrays were performed. To simulate the *in vivo* setting after PHx, human liver sinusoidal endothelial cells (LSECs) were stretched in silicon stretch chamber devices. The LSECs build up the vessel walls of liver sinusoids. Since the sinusoids are dilated after PHx, the LSECs must be stretched during this process.

After PHx, interestingly the macrophage migration inhibitory factor (MIF) was found to be increased in the supernatant of stretched, compared to unstretched LSECs (Figure 10A, B).

The fact that MIF was upregulated in the supernatant indicates that the protein is secreted. Potentially, MIF in the supernatant could be derived from dying respectively dead cells. In contrast, only single detached cells were observed after the stretching, indicating that this is highly unlikely. Nontheless, this aspect is a possible technical limitation of this *in vitro* method.

Therefore MIF secretion was investigated in the *in vivo* setting.

LSECs from livers of mice, which underwent PHx or sham surgeries, were isolated to consider this aspect (Figure 10D). Perhaps unexpected, LSECs of mouse livers 30min after PHx displayed dramatically lower MIF levels compared to LSECs from sham animals, whereas the housekeeping protein β-actin was not changed (Figure 10D, E). This indicates either lower expression, degradation or secretion of MIF.

Combining the results of MIF expression of *in vitro* and *in vivo* experiments with LSECs, these experiments strongly point to the notion that MIF is secreted upon mechanical stimulus by cell stretching.

4.1.7 MIF levels in blood plasma after PHx

To finally determine if MIF is secreted *in vivo*, MIF levels in blood plasma of the same mice which were used for LSEC isolation (Figure 10) were examined 30min after PHx. In wild type mice, MIF increases in blood plasma 30min after PHx, at the exact time, that MIF protein levels fall in LSECs from the same mice (Figure 11A). This is also true for endothelial specific heterozygous knockout mice but not for homozygous mice of β1 integrin (Figure 11B).

The facts that MIF is significantly lower in LSECs but significantly higher in blood serum at the same time point again indicate that the plasma increase of MIF *in vivo* after PHx is at least in parts due to secretion from LSECs.

Importantly, the fact that MIF is not increased in the plasma of the homozygous endothelial specific β1 integrin knockout mice under the influence of increased mechanical force strongly indicates that β1 integrin is necessary for normal MIF secretion from endothelial cells. MIF was earlier reported to be secreted through a non-classical pathway via an ABCA1 transporter[81]. Therefore it is possible that β1 integrin

is necessary for mechanotransduction of the hemodynamic changes after PHx, which alters intracellular pathways ending in MIF secretion.

MIF is an inflammatory cytokine, which is normally involved in immune response, but it was shown that MIF also plays a role in reperfusion injury in several organs like heart, liver, intestine or brain[134]. Reperfusion injury is a dangerous complication in liver transplantation[135]. MIF is also thought to prevent liver fibrosis[85] and fatty liver disease[86]. In addition MIF is supposed to upregulate ICAM-1, a previously described important factor for liver regeneration[105]. Therefore, the role of MIF was further investigated in the context of liver regeneration.

4.1.8 MIF and ICAM-1 expression after PHx

To proof if PHx has an influence of the MIF and ICAM-1 expression, wild type mice livers were examined for mRNA and protein levels.

Astonishingly mRNA and protein levels of MIF (Figure 12B, D) and ICAM-1 (Figure 12C, E) were significantly upregulated already 30min after PHx. The mRNA levels for both genes were decreased 30min later/60min after PHx (Figure12 B, C). This indicates very quick molecular changes existing after PHx. It was assumed that the increased blood to liver ratio caused these upregulations because they correspond in time.

4.1.9 MIF and ICAM-1 in *ex vivo* liver perfusion

To clarify the question if the upregulation of MIF and ICAM-1 is due to the hemodynamic changes, *ex vivo* liver perfusion experiments were performed (Figure 13). Normally, the perfusion rate and pressure is monitored to be constant during the experiments in this method[119]. We adapted this technique to manipulate the perfusion rate of mice livers. Thereby the *in vivo* situation after PHx could be mimicked, either by ligation of the same liver lobes like in the PHx or by just increasing the perfusion rate to same amounts like it increases after PHx in vivo (twofold, Figure 5B).

The ligation of liver tissue in the *ex vivo* experiments were sufficient to increase ICAM-1 (Figure 13D) protein but MIF (Figure 13C) was not significantly upregulated. When the experimental perfusion rate was doubled (8ml per min) both proteins, ICAM-1 (Figure 13D) and MIF (Figure 13C) were significantly upregulated.

Therefore, the expression of both proteins in mice livers after PHx correlates with the perfusion rate in *ex vivo* perfusion.

Because in this experimental setup the livers were perfused with a pre-warmed isotonic buffer instead of blood, a contribution of unknown factors in the blood, i.e. hormones secreted by other organs, can be excluded, strongly arguing for a direct role of mechanical forces in ICAM-1 and MIF upregulation.

In sum, the mechanical forces acting on the blood vessels either by reducing the liver size or by increasing the perfusion rate led to an increase in the expression of MIF and ICAM-1 protein in *ex vivo* liver perfusion experiments.

4.1.10 MIF and ICAM-1 expression after mechanotransduction *in vitro*

The next question was, if mechanical stress, can upregulate MIF and ICAM-1 expression in human LSECs.

Therefore mechanical stress was applied to human cells in two individual *in vitro* methods.

The hemodynamic changes after PHx leads to vessel dilation and therefore to stretching of LSECs. In addition to stretching, also shear stress is a mechanical force. To test the influence of increased shear stress, LSECs were seeded in flow chambers (Figure 14C) where different shear stress rates could be applied by altering the flow speed/higher perfusion rates. Shear stress is a slightly different mechano-physical force compared to stretching. Theoretically it should occur at the very beginning of vessel dilation after PHx *in vivo*.

In the shear stress experiments, two different shear rates (dyn/cm^2) were compared to static cultured cells. The first shear rate was the calculated shear rate for liver sinusoids (3.7 dyn/cm^2) under normal physiologic conditions; the second shear rate was doubled (7.4 dyn/cm^2). Of note, the shear stress immediately after PHx acting on LSECs has not been determined so far.

Both stretching and increased shear stress (flow) led to upregulation of both ICAM-1 and MIF mRNA (Figure 14D, E). ICAM-1 is known to be shear stress dependent. But interestingly ICAM-1 was only upregulated in normal shear rates compared to static controls (Figure 14G). No increase between physiologic and increased shear stress rates was observed for ICAM-1. MIF was upregulated contrarily. For MIF there was no change between static and physiologic conditions but it was upregulated in increased flow conditions (Figure 14F). Summarizing, both MIF and ICAM-1 are increased by

mechanotransduction. The result that MIF mRNA is only increased in higher shear rates could be an additional hint that MIF is secreted, as after MIF secretion new MIF have to be synthesized by the cells.

4.1.11 MIF and ICAM-1 interactions *in vitro*

These novel *in vitro* results raised the question if MIF is upstream of ICAM-1 in human LSECs.

To address this question gain of function (GOF) and loss of function (LOF) approaches were carried out.

First LOF experiments were performed using RNAi. LSECs were transfected with siRNA against MIF. As a result beside MIF, also ICAM-1 mRNA levels were significantly down regulated (Figure 15A). As a GOF approach, LSECs were incubated with recombinant human MIF. ICAM-1 mRNA levels were increased in this setting (Figure 15B). The LOF approach also worked on protein levels. After transfection with siRNA against MIF, both MIF (Figure 15D) and ICAM-1 (Figure 15E) protein levels were decreased.

Protein levels for the GOF approach could not be examined due to scarcity of high quality recombinant MIF protein.

Nevertheless, combining the results of GOF and LOF approaches suggest that MIF is upstream of ICAM-1 expression on LSECs.

These results of increased MIF and ICAM-1 expression after exposure to mechanical forces *in vitro* fall into line with the previous results of increased MIF and ICAM-1 expressions after *in vivo* PHx and increased perfusion in the *ex vivo* setup. In all three setups, LSECs are exposed to mechanical stress and upregulate MIF and ICAM-1.

4.1.12 Role of MIF in liver regeneration

Afterwards a possible regulation of ICAM-1 via MIF *in vivo* was examined. Therefore protein levels of MIF knockout mice were analyzed (Figure 16A, B). Strikingly, conventional knockout mice for MIF showed significantly reduced ICAM-1 levels in the liver even without PHx (Figure 16B).

ICAM-1 is known to be an important factor for liver regeneration[105]. For this reason the regeneration in MIF knockout mice was also analyzed. Since two days after PHx hepatocytes proliferate in wild type, but not in homozygous, endothelial specific

inducible β1 integrin knockout mice, this time point was chosen for analysis of proliferation in MIF KO mice. MIF knockout mice showed a near significant reduction in proliferation cells in livers at two days after PHx ($p=0.058$, Figure 16D). Conversely, there was also a significant increase in apoptotic cells in MIF KO liver sections (Figure 16C).
In sum, this experiment strikingly reveals an important role for MIF in liver regeneration after PHx.

4.1.13 Conclusion

Summarizing all results of this thesis, the following model can be generated. PHx leads to vessel dilation and therefore to mechanotransduction on endothelial cells. Next β1 integrin is needed as a mechano-sensor to sense the mechanical forces. MIF is secreted as a result of the mechanical force if mechanotransduction via β1 integrin takes place. As a consequence ICAM-1 is upregulated. It is known that ICAM-1 is necessary for leukocytes recruitment, which is another critical event during liver regeneration.
The current thesis increases and develops our understanding of molecular events during liver regeneration. It provides evidence for the first time that the vasodilation/shear stress-β1 integrin-MIF cascade plays an important role in liver regeneration.

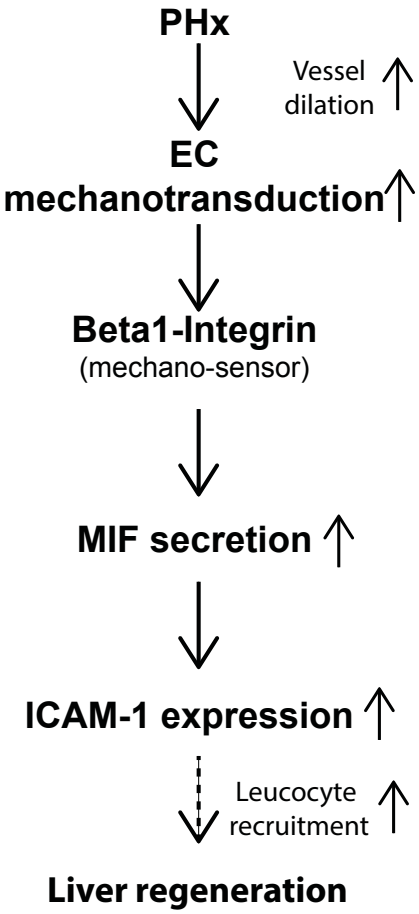

Figure 17: Model. Partial hepatectomy leads to intrahepatic vessel dilation and therefore to endothelial cell stretching. This stretching is mechanotransduced and sensed by β1 integrin. As a result MIF is secreted and ICAM-1 is upregulated. This increase results in leukocyte recruitment to the liver vessels and hepatocyte growth factor (HGF) is cleaved from the basement membrane. This release of HGF is the first trigger of liver regeneration.

Outlook

The concept that liver regeneration is triggered by mechanical forces acting on endothelial cells prior to parenchymal responses has the potential to be highly relevant also for other tissues and should be considered in the general research on regeneration.

Furthermore, it will be highly informative which role the hemodynamics play in liver fibrosis, portal hypertension or liver transplants. While liver transplants are performed with high success rates today, the optimal hemodynamics for organ acceptance are still unknown[136]. Therefore, hemodynamic changes after split liver transplantation could be relevant and should be investigated.

To gain more insights into these questions, Laser Doppler velocimetry experiments in mice may be performed in single liver vessels. These experiments could give insights in the exact shear stress rates in the liver vessels. Proof of principle experiments were already performed during this thesis at the EIMI.

In addition, it would be interesting to examine the intercellular intermediate steps between sensing of the mechanical forces, and the upregulation of MIF.

To prove the critical role of endothelial MIF production in liver regeneration, endothelial-specific MIF KO mice should be generated and phenotyped.

To get a more comprehensive understanding of liver regeneration, other sinusoidal cell types like HSCs or Kupffer cells should be considered as key players in liver regeneration. Since they are also exposed to the increased mechanical stress after PHx, they could also play a relevant (positive or negative) role in liver regeneration after PHx.

Since MIF participates in liver regeneration and regulates ICAM-1 expression, increasing local MIF levels could be helpful for treating diseases where liver regeneration is not sufficient.

The aspect if long-term increased hemodynamics (as found in patients with hypertension) correlates with bigger livers in the human setting, is already under examination in ongoing collaborations between the Institute of Metabolic Physiology and the German Diabetes Center (DDZ).

Index of figures

Index of tables

Abbreviations

A1AT: Alpha 1-antitrypsin

AF: Alexa Fluor®

AL(A)T: Alanine transaminase or alanine aminotransferase

Alb: Albumin

ANOVA: Analysis of variance

Approx.: Approximately

AS(A)T: Alanine transaminase or aspartate aminotransferase

B2M: β_2-microglobulin

bp: base pair

BM: Basement membrane

CD: Cluster of Differentiation

CEUS: Contrast enhanced ultrasound

CLD: Chronic Liver Disease

Ctrl: Control

DAPI: 4'6-Diamidine-2'-phenylindole dihydrochloride

DNA: Deoxyribonucleic acid

ECM: Extracellular matrix

EDTA: Ethylenediaminetetraacetic acid

e.g.: *Exempli gratia*

EIMI: European Institute of Molecular Imaging

ELISA: Enzyme-linked immunosorbent assay

Flk-1: Fetal liver kinase-1 / VEGFR2

fw: Forward

GAPDH: Glyceraldehyde 3-phosphate dehydrogenase

GOF: Gain of Function

GOT: Glutamic oxaloacetic transaminase

GPT: Glutamate-pyruvate transaminase or glutamic-pyruvic transaminase

Gt: Goat

HBV: Hepatitis B Virus

HCC: Hepatocellular Carcinoma

HCV: Hepatitis C Virus

HEP: Hepatocyte

HGF: Hepatocyte growth factor

HHU: Heinrich-Heine-University Düsseldorf

hLSEC: Human Liver Sinusoidal (Microvascular) Endothelial Cell

HSC: Hepatic stellate cell

ICAM-1: Intracellular adhesion molecule-1

i.e.: *Id est*

IHC: Immunohistochemistry

ILK: Integrin-linked kinase

i.p.: Intraperitoneal

KC: Kupffer cell

KHS: Krebs Henseleit Solution

KO: Knockout

KRB: Krebs-Ringer-buffer

LDH: Lactate dehydrogenase

LDLT: Living donor liver transplant

LFA-1: Lymphocyte function-associated Antigen-1

LOF: Loss of Function

LSEC: Liver sinusoidal endothelial cell

LSM: Laser Scanning Microscopy

LYVE-1: Lymphatic Vascular Endothelial Hyaluronan Receptor-1

MHz: Megahertz

MIF: Macrophage Migration Inhibitory Factor

mLSEC: Murine Liver sinusoidal endothelial cell

MMP: Matrix Metalloproteinase

mRNA: Messenger RNA

ms: Mouse

NAFLD: Non-alcoholic fatty liver disease

NASH: Non-alcoholic steatohepatitis

NO: Nitric oxide

P: Passage (of cells)

PBC: Primary biliary cirrhosis (cholangitis)

PBS: Phosphate Buffered Saline

PBS^{++}: Phosphate Buffered Saline with Mg^{2+} and Ca^{2+}

PCR: Polymerase Chain Reaction

PECAM-1: Platelet endothelial cell adhesion molecule-1

PFA: Paraformaldehyde

pH3: Phospho-Histone H3

PHx: Partial Hepatectomy

Rb: Rabbit

rcf: Relative centrifugal field

RNA: Ribonucleic acid

RNAi: RNA interference

Rt: Rat

rv: Reverse

RWTH: Rheinisch-Westfälische Technische Hochschule

s.c.: Subcutaneous

s.d.: Standard deviation

Sh: Sheep

si(RNA): Small interfering (RNA)

SLC: Sinusoidal lining cell

T2DM: Type 2 Diabetes Mellitus

TAE: TRIS-Acetate-EDTA

T-Bil: Total Bilirubin

T-Pro: Total protein

TRIS: Tris(hydroxymethyl)aminomethane

TUNEL: Terminal deoxynucleotidyl transferase-mediated dUTP-biotin nick end labeling

taq-polymerase: Polymerase derived from *thermus aquaticus*

UKD: University Hospital Düsseldorf

V: Volt

VE-Cadherin: Vascular endothelial cadherin

VEGFR-2: Vascular endothelial growth factor receptor-2

VEGFR-3: Vascular endothelial growth factor receptor-3

vs.: Versus

qRT-PCR: quantitative Reverse Transcriptase - Polymerase Chain Reaction

WB: Western blot

wt: Wild type

Contributions

Eckhard Lammert supervised Tobias Buschmann during the thesis.

Tobias Buschmann performed most of the experiments and crucially contributed in figure assembling.

Jennifer Axnick was involved in learning PHx and performed preliminary surgeries and worked on liver development as a partner project in the SBF 974.

Isabelle Hermanski was supervised by Tobias Buschmann and Eckhard Lammert for her Master Thesis and worked on liver tissues after PHx from wild type and β1 integrin knockout mice performed by Tobias Buschmann. Isabelle Hermanski focused on ECM changes after PHx and cell proliferation.

Paul Schauerte was supervised by Tobias Buschmann and Eckhard Lammert for his Bachelor and Master Thesis. He worked on *in vitro* experiments with human LSECs, focused on MIF in shear stress assays (stretching- and flow-chamber). Flow-chambers were established by Tobias Buschmann.

Nicole Eichhorst and Tobias Buschmann planned, designed and performed *ex vivo* liver perfusions for mice. Tobias Buschmann analyzed the liver tissues after *ex vivo* perfusion. Experiments were designed by Eckhard Lammert and Tobias Buschmann.

Richard Holtmeier and Tobias Buschmann performed CEUS. Richard Holtmeier operated the ultrasound system and Tobias Buschmann performed PHx. Experiments were designed by Eckhard Lammert and Tobias Buschmann. CEUS measurements were performed at the European Institute of Molecular Imaging (Münster).

The collaboration with Prof. Bernhagen and Prof. Trautwein enabled access to MIF knockout mice. PHx of MIF knockout mice were performed by Tobias Buschmann at RWTH Aachen (Aachen).

Source code

The following source codes were used for automated image analysis in FIJI

For automated nuclei count:

```
run("Z Project...", "projection=[Sum Slices]");  ← only inserted for the z-stack images
setAutoThreshold("Li dark");
//run("Threshold...");
setOption("BlackBackground", true);
run("Convert to Mask", "method=Li background=Default black");
run("Watershed");
run("Analyze Particles...", "size=4-Infinity show=[Overlay Outlines] display summarize
slice");
//run("Close");
```

For β1 integrin area evaluation:

```
run("Next Slice [>]");
run("Subtract...", "value=635.483 stack");
setAutoThreshold("Moments dark");
//run("Threshold...");
run("Measure");
run("Next Slice [>]");
setAutoThreshold("Moments dark");
run("Measure");
```

For proteome profiler array evaluation:

```
var diameter = 6000.0;

function findMin(rt, colName) {
        var min = 0;
        var currMin = null;
        for (var j = 0; j < rt.getCounter(); j++) {
                val = rt.getValue(colName, j);
                if ((currMin == null) || (currMin >  val)) {
```

```
                        currMin = val;
                        min = j;
                }
        }
        return min;
}
var imp = IJ.getImage();
var width = imp.getWidth() * imp.getCalibration().pixelWidth;
var height = imp.getHeight() * imp.getCalibration().pixelHeight;

IJ.run(imp, "Select None", "");
IJ.setAutoThreshold(imp, "Otsu dark");
//IJ.run("Set Measurements...", "  center redirect=None decimal=3");
//IJ.run(imp, "Analyze Particles...", "  display clear");

var rt2 = new ResultsTable();
var pa = new ParticleAnalyzer(ParticleAnalyzer.SHOW_NONE,
Measurements.CENTER_OF_MASS, rt2, 0, Double.POSITIVE_INFINITY); // try rt =
null?
pa.analyze(imp);

//rt = ResultsTable.getResultsTable();
for (var i=0; i<rt2.getCounter(); i++) {
        var xm = rt2.getValue("XM", i);
        var ym = rt2.getValue("YM", i);
        rt2.setValue("upperLeft", i, Math.pow(xm, 2) + Math.pow(ym, 2));
        rt2.setValue("upperRight", i, Math.pow(width - xm, 2) + Math.pow(ym, 2));
        rt2.setValue("lowerLeft", i, Math.pow(xm, 2) + Math.pow(height - ym, 2));
}

var a1 = findMin(rt2, "upperLeft");
var a24 = findMin(rt2, "upperRight");
var f1 = findMin(rt2, "lowerLeft");
```

```
var rm = RoiManager.getInstance();
if (rm==null) var rm = new RoiManager();

//rt = ResultsTable.getResultsTable();
//if (rt==null) rt = new ResultsTable();
rm.runCommand("Deselect");
if (rm.getCount() > 0) rm.runCommand("Delete");
rm.runCommand("Show All with labels");
rm.runCommand("Show All");

var xCenterA1 = rt2.getValue("XM", a1);
var yCenterA1 = rt2.getValue("YM", a1);
var xCenterA24 = rt2.getValue("XM", a24);
var yCenterA24 = rt2.getValue("YM", a24);
var xCenterF1 = rt2.getValue("XM", f1);
var yCenterF1 = rt2.getValue("YM", f1);

var colArray = [0,1,2,3, 4.5,5.5,6.5,7.5, 9,10,11,12, 13.5,14.5,15.5,16.5, 18,19,20,21,
22.5,23.5,24.5,25.5];
var rowArray = [0, 1.5,2.5,3.5,4.5, 6.0];
var colHeaders = [1,2,3,4,5,6,7,8,9,10,11,12,13,14,15,16,17,18,19,20,21,22,23,24];
var rowHeaders = ["A", "B", "C", "D", "E", "F"];

var colStepX = (xCenterA24 - xCenterA1) / 25.5;
var colStepY = (yCenterA24 - yCenterA1) / 25.5;
var rowStepX = (xCenterF1 - xCenterA1) / 6.0;
var rowStepY = (yCenterF1 - yCenterA1) / 6.0;

IJ.run("Set Measurements...", "  mean integrated display redirect=None decimal=3");

for (row = 0; row < rowArray.length; row++) {
        for (col = 0; col < colArray.length; col++) {
                x = xCenterA1 + colArray[col] * colStepX + rowArray[row] * rowStepX;
                y = yCenterA1 + colArray[col] * colStepY + rowArray[row] * rowStepY;
```

```
                IJ.run(imp, "Specify...", "width=" + diameter + " height=" + diameter + "
x=" + x + " y=" + y + " oval constrain centered scaled");
                roi = imp.getRoi();
                roi.setName("" + rowHeaders[row] + colHeaders[col]);
                rm.addRoi(roi);
                //IJ.run(imp, "Measure", "");
                //rt.addLabel("" + rowHeaders[row] + colHeaders[col]);
        }
}
//rt.show("Results");
rm.runCommand("Deselect");
rm.runCommand("Measure");
IJ.run("Labels...", "color=white font=8 show use draw");
```

Copyright

Permission to publish figures was approved online via Copyright Clearence Center (https://www.copyright.com/)

Figure 1: Unmodified from Mitchell & Willenbring, Nature Protocols, 2008[7]

Figure 2 and 3: Unmodified from Buschmann et al. in Liver Regeneration, Editor D. Häussinger, DeGruyter, 2011[10]

NATURE PUBLISHING GROUP LICENSE
TERMS AND CONDITIONS

Nov 21, 2016

This Agreement between Tobias Buschmann ("You") and Nature Publishing Group ("Nature Publishing Group") consists of your license details and the terms and conditions provided by Nature Publishing Group and Copyright Clearance Center.

License Number	3993831181905
License date	Nov 21, 2016
Licensed Content Publisher	Nature Publishing Group
Licensed Content Publication	Nature Protocols
Licensed Content Title	A reproducible and well-tolerated method for 2/3 partial hepatectomy in mice
Licensed Content Author	Claudia Mitchell and Holger Willenbring
Licensed Content Date	Jun 19, 2008
Licensed Content Volume Number	3
Licensed Content Issue Number	7
Type of Use	reuse in a dissertation / thesis
Requestor type	academic/educational
Format	print and electronic
Portion	figures/tables/illustrations
Number of figures/tables/illustrations	1
High-res required	no
Figures	Figure 3
Author of this NPG article	no
Your reference number	

Title of your thesis / dissertation	Communication of Blood Vessels and Hepatic Cell Types During Liver Regeneration
Expected completion date	Jan 2017
Estimated size (number of pages)	90
Requestor Location	Tobias Buschmann Universitätsstr. 1 Geb. 26.12.00.70 Düsseldorf, 40225 Germany Attn: Tobias Buschmann
Billing Type	Invoice
Billing Address	Tobias Buschmann Universitätsstr. 1 Geb. 26.12.00.70 Düsseldorf, Germany 40225 Attn: Tobias Buschmann
Total	0.00 EUR

Terms and Conditions

Terms and Conditions for Permissions
Nature Publishing Group hereby grants you a non-exclusive license to reproduce this material for this purpose, and for no other use,subject to the conditions below:

NPG warrants that it has, to the best of its knowledge, the rights to license reuse of this material. However, you should ensure that the material you are requesting is original to Nature Publishing Group and does not carry the copyright of another entity (as credited in the published version). If the credit line on any part of the material you have requested indicates that it was reprinted or adapted by NPG with permission from another source, then you should also seek permission from that source to reuse the material.

Permission granted free of charge for material in print is also usually granted for any electronic version of that work, provided that the material is incidental to the work as a whole and that the electronic version is essentially equivalent to, or substitutes for, the print version.Where print permission has been granted for a fee, separate permission must be obtained for any additional, electronic re-use (unless, as in the case of a full paper, this has already been accounted for during your initial request in the calculation of a print run).NB: In all cases, web-based use of full-text articles must be authorized separately through the 'Use on a Web Site' option when requesting permission.

Permission granted for a first edition does not apply to second and subsequent editions and for editions in other languages (except for signatories to the STM Permissions Guidelines, or where the first edition permission was granted for free).

Nature Publishing Group's permission must be acknowledged next to the figure, table or abstract in print. In electronic form, this acknowledgement must be visible at the same time as the figure/table/abstract, and must be hyperlinked to the journal's homepage.

The credit line should read:
Reprinted by permission from Macmillan Publishers Ltd: [JOURNAL NAME] (reference citation), copyright (year of publication)
For AOP papers, the credit line should read:
Reprinted by permission from Macmillan Publishers Ltd: [JOURNAL NAME], advance online publication, day month

year (doi: 10.1038/sj.[JOURNAL ACRONYM].XXXXX)

Note: For republication from the *British Journal of Cancer,* the following credit lines apply.
Reprinted by permission from Macmillan Publishers Ltd on behalf of Cancer Research UK: [JOURNAL NAME]

(reference citation), copyright (year of publication)For AOP papers, the credit line should read:
Reprinted by permission from Macmillan Publishers Ltd on behalf of Cancer Research UK: [JOURNAL NAME],

advance online publication, day month year (doi: 10.1038/sj.[JOURNAL ACRONYM].XXXXX)

Adaptations of single figures do not require NPG approval. However, the adaptation should be credited as follows:

Adapted by permission from Macmillan Publishers Ltd: [JOURNAL NAME] (reference citation), copyright (year of publication)

Note: For adaptation from the *British Journal of Cancer,* the following credit line applies.
Adapted by permission from Macmillan Publishers Ltd on behalf of Cancer Research UK: [JOURNAL NAME] (reference citation), copyright (year of publication)

Translations of 401 words up to a whole article require NPG approval. Please visit http://www.macmillanmedicalcommunications.com for more information.Translations of up to a 400 words do not require NPG approval. The translation should be credited as follows:

Translated by permission from Macmillan Publishers Ltd: [JOURNAL NAME] (reference citation), copyright (year of publication).

Note: For translation from the *British Journal of Cancer,* the following credit line applies.
Translated by permission from Macmillan Publishers Ltd on behalf of Cancer Research UK: [JOURNAL NAME] (reference citation), copyright (year of publication)

We are certain that all parties will benefit from this agreement and wish you the best in the use of this material. Thank you.
Special Terms:
v1.1

Questions? customercare@copyright.com or +1-855-239-3415 (toll free in the US) or +1-978-646-2777.

DE GRUYTER LICENSE TERMS AND CONDITIONS

Nov 21, 2016

This Agreement between Tobias Buschmann ("You") and De Gruyter ("De Gruyter") consists of your license details and the terms and conditions provided by De Gruyter and Copyright Clearance Center.

License Number
3993811186077
License date
Oct 31, 2016
Licensed Content Publisher
De Gruyter
Licensed Content Publication

DeGruyter Book
Licensed Content Title
Liver Regeneration
Licensed Content Author
Ed. Häussinger, Dieter
Licensed Content Date
Jul 7, 2011
Type of Use
Thesis/Dissertation
Requestor type
Academic institution
Format
Print, Electronic
Portion
chart/graph/table/figure
Number of charts/graphs/tables/figures
3
Rights for
Main product
Duration of use
Life of current/future editions
Creation of copies for the disabled
no
With minor editing privileges
no
For distribution to
Worldwide
In the following language(s)
Original language of publication
With incidental promotional use
yes
The lifetime unit quantity of new product
0 to 499
The requesting person/organization is:
Tobias Buschmann
Order reference number
Title of your thesis / dissertation
Communication of Blood Vessels and Hepatic Cell Types During Liver Regeneration
Expected completion date
Jan 2017
Expected size (number of pages)
90
Publisher VAT
DE 136 320 747
Requestor Location
Tobias Buschmann
Universitätsstr. 1
Geb. 26.12.00.70

Düsseldorf, 40225
Germany
Attn: Tobias Buschmann
Billing Type
Invoice
Billing Address
Tobias Buschmann
Universitätsstr. 1
Geb. 26.12.00.70

Düsseldorf, Germany 40225
Attn: Tobias Buschmann
Total
0.00 EUR
Terms and Conditions

STANDARD TERMS AND CONDITIONS FOR REPRODUCTION OF MATERIAL

Preamble
The publisher for this copyrighted material is Walter De Gruyter GmbH. By clicking "accept" in connection with completing this licensing transaction, you agree that the following terms and conditions apply to this transaction (along with the Billing and Payment terms and conditions established by Copyright Clearance Center, Inc. ("CCC"), at the time that you opened your CCC account and that are available at any time at http://myaccount.copyright.com).
1 Scope of Application
Limited License
Publisher hereby grants to you a non-exclusive license to use this material. Licenses are for one-time use only with a maximum distribution equal to the number that you identified in the licensing process; any form of granted republication must be completed within one (1) year from the date hereof (although copies prepared before then may be distributed thereafter); and any electronic posting is limited to a period of one (1) year. This permission shall automatically terminate if fail to comply with the terms of this license.
Geographic Rights: Scope
Licenses may be exercised anywhere in the world.
Altering/Modifying Material: Not Permitted
You may not alter or modify the material in any manner (except that you may use, within the scope of the license granted, one or more excerpts from the copyrighted material, provided that the process of excerpting does not alter the meaning of the material or in any way reflect negatively on the publisher or any writer of the material), nor may you translate the material into another language
Reservation of Rights
Publisher reserves all rights not specifically granted in the combination of (i) the license details provided by you and accepted in the course of this licensing transaction, (ii) these terms and conditions and (iii) CCC's Billing and Payment terms and conditions.
License Contingent on Payment
While you may exercise the rights licensed immediately upon issuance of the license at the end of the licensing process for the transaction, provided that you have disclosed complete and accurate details of your proposed use, no license is finally effective unless and until full payment is received from you (either by publisher or by CCC) as provided in CCC's Billing and Payment terms and conditions. If full payment is not received on a timely basis, then any license preliminarily granted shall be deemed automatically revoked and shall be void as if never granted. Further, in the event that you breach any of these terms and conditions or any of CCC's Billing and Payment terms and conditions, the license is automatically revoked and shall be void as if never granted. Use of materials as described in a revoked license, as well as any use of the materials beyond the scope of an unrevoked license, may constitute copyright infringement and publisher reserves the right to take any and all action to protect its copyright in the materials.
Copyright Notice: Disclaimer
You must include the following copyright and permission notice in connection with any reproduction of the licensed material: "De Gruyter [Insert Title of Publication], Walter De Gruyter GmbH Berlin Boston, [Insert Year of Publication]. Copyright and all rights reserved. Material from this publication has been used with the permission of Walter De Gruyter GmbH."
Warranties: None
Publisher makes no representations or warranties with respect to the licensed material and adopts on its own behalf the limitations and disclaimers established by CCC on its behalf in its Billing and Payment terms and conditions for this licensing transaction.
Indemnity
You hereby indemnify and agree to hold harmless publisher and CCC, and their respective officers, directors, employees and agents, from and against any and all claims arising out of your use of the licensed material other than as specifically authorized pursuant to this license.
No Transfer of License
This license is only granted you and your company (if noted in the license) and may not be sublicensed, assigned, or transferred by you to any other person without publisher's written permission.
No Amendment Except in Writing
This license may not be amended except in a writing and signed by both parties (or, in the case of publisher, by CCC on publisher's behalf).
Objection to Contrary Terms
Publisher hereby objects to any terms contained in any purchase order, acknowledgment, check endorsement or other writing prepared by you, which terms are inconsistent with these terms and conditions or CCC's Billing and Payment terms and conditions. These terms and conditions, together with CCC's Billing and Payment terms and conditions (which are incorporated herein), comprise the entire agreement between you and publisher (and CCC) concerning this licensing transaction. In the event of any conflict between your obligations established by

References

1 Häussinger, D. in *Metabolism of Human Diseases* Vol. 1 (eds E. Lammert & M. Zeeb) Ch. Overview, 173-179 (Springer, 2014).

2 Si-Tayeb, K., Lemaigre, F. P. & Duncan, S. A. Organogenesis and development of the liver. *Dev. Cell* **18**, 175-189, doi:10.1016/j.devcel.2010.01.011 (2010).

3 Marquard, J. *et al.* Characterization of pancreatic NMDA receptors as possible drug targets for diabetes treatment. *Nat. Med.* **21**, 363-+, doi:10.1038/nm.3822 (2015).

4 Remmer, H. The role of the liver in drug metabolism. *The American Journal of Medicine* **49**, 617-629, doi:10.1016/s0002-9343(70)80129-2 (1970).

5 Ishibashi, H., Nakamura, M., Komori, A., Migita, K. & Shimoda, S. Liver architecture, cell function, and disease. *Semin. Immunopathol.* **31**, 399-409, doi:10.1007/s00281-009-0155-6 (2009).

6 Rogers, A. B. & Dintzis, R. Z. in *Comparative Anatomy and Histology A Mouse and Human Atlas* (eds Piper M. Treuting & Renee Z. Dintzis) Ch. 13, 193-201 (Elsevier Inc., 2012).

7 Mitchell, C. & Willenbring, H. A reproducible and well-tolerated method for 2/3 partial hepatectomy in mice. *Nat. Protoc.* **3**, 1167-1170, doi:10.1038/nprot.2008.80 (2008).

8 Pinzani, M., Rosselli, M. & Zuckermann, M. Liver cirrhosis. *Best Pract. Res. Clin. Gastroenterol.* **25**, 281-290, doi:10.1016/j.bpg.2011.02.009 (2011).

9 Tilg, H., Moschen, A. R. & Roden, M. NAFLD and diabetes mellitus. *Nat. Rev. Gastroenterol. Hepatol.*, doi:10.1038/nrgastro.2016.147 (2016).

10 Buschmann, T., Eglinger, J. & Lammert, E. in *Liver Regeneration* (ed D. Häussinger) Ch. 10, 145-158 (De Gruyter, 2011).

11 Guyot, C. *et al.* Hepatic fibrosis and cirrhosis: the (myo)fibroblastic cell subpopulations involved. *Int. J. Biochem. Cell Biol.* **38**, 135-151, doi:10.1016/j.biocel.2005.08.021 (2006).

12 Fernandez, M. *et al.* Angiogenesis in liver disease. *J Hepatol* **50**, 604-620, doi:10.1016/j.jhep.2008.12.011 (2009).

13 Kleinman, R. *et al. Pediatric Gastrointestinal Disease*. 5 edn, Vol. 1 751 (2008).

14 Partin, J. S., Lane, B. P., Partin, J. C., Edelstein, L. R. & Priebe, C. J. Plexiform neurofibromatosis of the liver and mesentery in a child. *Hepatology* **12**, 559-564, doi:10.1002/hep.1840120318 (1990).

15 Shibayama, Y., Urano, T. & Nakata, K. Changes in hepatic lymph vessels in endotoxaemia. *J. Pathol.* **168**, 325-330, doi:10.1002/path.1711680313 (1992).

16 Aird, W. C. Phenotypic heterogeneity of the endothelium: II. Representative vascular beds. *Circ. Res.* **100**, 174-190, doi:10.1161/01.RES.0000255690.03436.ae (2007).

17 Aird, W. C. Phenotypic heterogeneity of the endothelium: I. Structure, function, and mechanisms. *Circ. Res.* **100**, 158-173, doi:10.1161/01.RES.0000255691.76142.4a (2007).

18 Oda, M., Yokomori, H. & Han, J. Y. Regulatory mechanisms of hepatic microcirculation. *Clin. Hemorheol. Microcirc.* **29**, 167-182 (2003).

19 Ivanov, K. P., Kalinina, M. K. & Levkovich Yu, I. Blood flow velocity in capillaries of brain and muscles and its physiological significance. *Microvasc. Res.* **22**, 143-155 (1981).

20 Duncan, A. W. *et al.* The ploidy conveyor of mature hepatocytes as a source of genetic variation. *Nature* **467**, 707-710, doi:10.1038/nature09414 (2010).

21 Haussinger, D. Hepatocyte Heterogeneity in Glutamine and Ammonia Metabolism and the Role of an Intercellular Glutamine Cycle during Ureogenesis in Perfused Rat Liver. *Eur. J. Biochem.* **133**, 269-275, doi:10.1111/j.1432-1033.1983.tb07458.x (1983).
22 Jungermann, K. Metabolic zonation of liver parenchyma: significance for the regulation of glycogen metabolism, gluconeogenesis, and glycolysis. *Diabetes Metab. Rev.* **3**, 269-293 (1987).
23 Planas-Paz, L. *et al.* The RSPO-LGR4/5-ZNRF3/RNF43 module controls liver zonation and size. *Nat. Cell Biol.* **18**, 467-479, doi:10.1038/ncb3337 (2016).
24 Steffan, A. M., Gendrault, J. L. & Kirn, A. Increase in the number of fenestrae in mouse endothelial liver cells by altering the cytoskeleton with cytochalasin B. *Hepatology* **7**, 1230-1238 (1987).
25 Fraser, R., Clark, S. A., Day, W. A. & Murray, F. E. Nicotine decreases the porosity of the rat liver sieve: a possible mechanism for hypercholesterolaemia. *Br. J. Exp. Pathol.* **69**, 345-350 (1988).
26 Horn, T., Christoffersen, P. & Henriksen, J. H. Alcoholic liver injury: Defenestration in noncirrhotic livers—a scanning electron microscopic study. *Hepatology* **7**, 77-82, doi:10.1002/hep.1840070117 (1987).
27 Wisse, E., De Zanger, R. B., Jacobs, R. & McCuskey, R. S. Scanning electron microscope observations on the structure of portal veins, sinusoids and central veins in rat liver. *Scan. Electron Microsc.*, 1441-1452 (1983).
28 Zhao, X. *et al.* Spontaneous immortalization of mouse liver sinusoidal endothelial cells. *Int. J. Mol. Med.* **35**, 617-624, doi:10.3892/ijmm.2015.2067 (2015).
29 Mouta Carreira, C. *et al.* LYVE-1 is not restricted to the lymph vessels: expression in normal liver blood sinusoids and down-regulation in human liver cancer and cirrhosis. *Cancer Res.* **61**, 8079-8084 (2001).
30 Ding, B. S. *et al.* Inductive angiocrine signals from sinusoidal endothelium are required for liver regeneration. *Nature* **468**, 310-315, doi:10.1038/nature09493 (2010).
31 Lalor, P. F., Lai, W. K., Curbishley, S. M., Shetty, S. & Adams, D. H. Human hepatic sinusoidal endothelial cells can be distinguished by expression of phenotypic markers related to their specialised functions in vivo. *World J. Gastroenterol.* **12**, 5429-5439 (2006).
32 Ju, C. & Mandrekar, P. Macrophages and Alcohol-Related Liver Inflammation. *Alcohol Research : Current Reviews* **37**, 251-262 (2015).
33 Klein, I. *et al.* Kupffer cell heterogeneity: functional properties of bone marrow derived and sessile hepatic macrophages. *Blood* **110**, 4077-4085, doi:10.1182/blood-2007-02-073841 (2007).
34 Lehner, P. J. & Cresswell, P. Recent developments in MHC-class-I-mediated antigen presentation. *Curr. Opin. Immunol.* **16**, 82-89, doi:10.1016/j.coi.2003.11.012 (2004).
35 Bayon, L. G. *et al.* Role of Kupffer cells in arresting circulating tumor cells and controlling metastatic growth in the liver. *Hepatology* **23**, 1224-1231, doi:10.1002/hep.510230542 (1996).
36 Bosch, J., Abraldes, J. G., Fernandez, M. & Garcia-Pagan, J. C. Hepatic endothelial dysfunction and abnormal angiogenesis: new targets in the treatment of portal hypertension. *J Hepatol* **53**, 558-567, doi:10.1016/j.jhep.2010.03.021 (2010).
37 Senoo, H., Kojima, N. & Sato, M. Vitamin A‐Storing Cells (Stellate Cells). **75**, 131-159, doi:10.1016/s0083-6729(06)75006-3 (2007).

38 Imai, K. *et al.* Intercellular Adhesive Structures Between Stellate Cells - An Analysis in Cultured Human Hepatic Stellate Cells. *Comp. Hepatol.* **3 Suppl 1**, S13, doi:10.1186/1476-5926-2-S1-S13 (2004).
39 Trautwein, C., Friedman, S. L., Schuppan, D. & Pinzani, M. Hepatic fibrosis: Concept to treatment. *J Hepatol* **62**, S15-24, doi:10.1016/j.jhep.2015.02.039 (2015).
40 Kordes, C., Sawitza, I., Gotze, S., Herebian, D. & Haussinger, D. Hepatic stellate cells contribute to progenitor cells and liver regeneration. *J. Clin. Invest.* **124**, 5503-5515, doi:10.1172/JCI74119 (2014).
41 Kordes, C. & Haussinger, D. Hepatic stem cell niches. *J. Clin. Invest.* **123**, 1874-1880, doi:10.1172/JCI66027 (2013).
42 Wisse, E., van't Noordende, J. M., van der Meulen, J. & Daems, W. T. The pit cell: description of a new type of cell occurring in rat liver sinusoids and peripheral blood. *Cell Tissue Res.* **173**, 423-435 (1976).
43 Trinchieri, G. Biology of natural killer cells. *Adv. Immunol.* **47**, 187-376 (1989).
44 Michalopoulos, G. K. Liver regeneration. *J. Cell. Physiol.* **213**, 286-300, doi:10.1002/jcp.21172 (2007).
45 Rabes, H. Kinetics of hepatocellular proliferation as a function of the microvascular structure and functional state of the liver. *Ciba Found Symp.* **55**, 31-53 (1977).
46 Szawlowski, A. W., Saint-Aubert, B., Gouttebel, M. C., Astre, C. & Joyeux, H. Experimental Model of Extended Repeated Partial Hepatectomy in the Dog. *Eur. Surg. Res.* **19**, 375-380, doi:10.1159/000128725 (1987).
47 Kahn, D., Hickman, R., Terblanche, J. & von Sommoggy, S. Partial hepatectomy and liver regeneration in pigs--the response to different resection sizes. *J. Surg. Res.* **45**, 176-180 (1988).
48 Winters, Z. *et al.* The changes in circulating hepatocyte growth factor after partial hepatectomy in the baboon. *S Afr J Surg.* **37**, 31-37 (1999).
49 Lacaze, L. & Scotte, M. Surgical treatment of intra hepatic recurrence of hepatocellular carcinoma. *World J. Hepatol.* **7**, 1755-1760, doi:10.4254/wjh.v7.i13.1755 (2015).
50 Michalopoulos, G. K. Liver Regeneration. *Science* **276**, 60-66, doi:10.1126/science.276.5309.60 (1997).
51 Freimuth, J. *et al.* Loss of caspase-8 in hepatocytes accelerates the onset of liver regeneration in mice through premature nuclear factor kappa B activation. *Hepatology* **58**, 1779-1789, doi:10.1002/hep.26538 (2013).
52 Michalopoulos, G. K. Liver regeneration after partial hepatectomy: critical analysis of mechanistic dilemmas. *Am. J. Pathol.* **176**, 2-13, doi:10.2353/ajpath.2010.090675 (2010).
53 Shah, S. A., Levy, G. A., Adcock, L. D., Gallagher, G. & Grant, D. R. Adult-to-adult living donor liver transplantation. *Can. J. Gastroenterol.* **20**, 339-343 (2006).
54 Hackl, C., Schlitt, H. J., Melter, M., Knoppke, B. & Loss, M. Current developments in pediatric liver transplantation. *World J. Hepatol.* **7**, 1509-1520, doi:10.4254/wjh.v7.i11.1509 (2015).
55 Hashimoto, K. *et al.* Split liver transplantation in adults. *World J. Gastroenterol.* **22**, 7500-7506, doi:10.3748/wjg.v22.i33.7500 (2016).
56 Broelsch, C. *et al.* Application of reduced-size liver transplants as split grafts, auxiliary orthotopic grafts, and living related segmental transplants. *Ann. Surg.* **212**, 368-375 (1990).

57 Morita, T. *et al.* Mechanism of postoperative liver failure after excessive hepatectomy investigated using a cDNA microarray. *J. Hepatobiliary. Pancreat. Surg.* **9**, 352-359, doi:10.1007/s005340200039 (2002).
58 Kragl, M. *et al.* Cells keep a memory of their tissue origin during axolotl limb regeneration. *Nature* **460**, 60-65, doi:10.1038/nature08152 (2009).
59 Blachier, M., Leleu, H., Peck-Radosavljevic, M., Valla, D. C. & Roudot-Thoraval, F. The burden of liver disease in Europe: a review of available epidemiological data. *J Hepatol* **58**, 593-608, doi:10.1016/j.jhep.2012.12.005 (2013).
60 Pinzani, M., Rombouts, K. & Colagrande, S. Fibrosis in chronic liver diseases: diagnosis and management. *J Hepatol* **42 Suppl**, S22-36, doi:10.1016/j.jhep.2004.12.008 (2005).
61 Bataller, R. & Brenner, D. A. Liver fibrosis. *J. Clin. Invest.* **115**, 209-218, doi:10.1172/jci24282 (2005).
62 Tsukamoto, H., Zhu, N. L., Wang, J., Asahina, K. & Machida, K. Morphogens and hepatic stellate cell fate regulation in chronic liver disease. *J. Gastroenterol. Hepatol.* **27 Suppl 2**, 94-98, doi:10.1111/j.1440-1746.2011.07022.x (2012).
63 Dirchwolf, M. & Ruf, A. E. Role of systemic inflammation in cirrhosis: From pathogenesis to prognosis. *World J. Hepatol.* **7**, 1974-1981, doi:10.4254/wjh.v7.i16.1974 (2015).
64 Gines, P., Cardenas, A., Arroyo, V. & Rodes, J. Management of cirrhosis and ascites. *N. Engl. J. Med.* **350**, 1646-1654, doi:10.1056/NEJMra035021 (2004).
65 Gressner, A. M. & Bachem, M. G. Cellular sources of noncollagenous matrix proteins: role of fat-storing cells in fibrogenesis. *Semin. Liver Dis.* **10**, 30-46, doi:10.1055/s-2008-1040455 (1990).
66 Surani, S. R., Mendez, Y., Anjum, H. & Varon, J. Pulmonary complications of hepatic diseases. *World J. Gastroenterol.* **22**, 6008-6015, doi:10.3748/wjg.v22.i26.6008 (2016).
67 Moreau, R. Acute-on-chronic liver failure: a new syndrome in cirrhosis. *Clin Mol Hepatol* **22**, 1-6, doi:10.3350/cmh.2016.22.1.1 (2016).
68 Yang, P. C. *et al.* Prophylactic liver transplantation for high-risk recurrent hepatocellular carcinoma. *World J. Hepatol.* **8**, 1309-1317, doi:10.4254/wjh.v8.i31.1309 (2016).
69 Raza, A. & Sood, G. K. Hepatocellular carcinoma review: current treatment, and evidence-based medicine. *World J. Gastroenterol.* **20**, 4115-4127, doi:10.3748/wjg.v20.i15.4115 (2014).
70 Berretta, M. *et al.* Angiogenesis Inhibitors for the Treatment of Hepatocellular Carcinoma. *Front. Pharmacol.* **7**, 428, doi:10.3389/fphar.2016.00428 (2016).
71 Allemann, P., Demartines, N., Bouzourene, H., Tempia, A. & Halkic, N. Long-term outcome after liver resection for hepatocellular carcinoma larger than 10 cm. *World J. Surg.* **37**, 452-458, doi:10.1007/s00268-012-1840-5 (2013).
72 Hu, J. *et al.* Endothelial cell-derived angiopoietin-2 controls liver regeneration as a spatiotemporal rheostat. *Science* **343**, 416-419, doi:10.1126/science.1244880 (2014).
73 Ding, B. S. *et al.* Divergent angiocrine signals from vascular niche balance liver regeneration and fibrosis. *Nature* **505**, 97-102, doi:10.1038/nature12681 (2014).
74 Ding, B. S. *et al.* Endothelial-derived angiocrine signals induce and sustain regenerative lung alveolarization. *Cell* **147**, 539-553, doi:10.1016/j.cell.2011.10.003 (2011).

75 Hedhli, N. *et al.* Endothelium-derived neuregulin protects the heart against ischemic injury. *Circulation* **123**, 2254-2262, doi:10.1161/CIRCULATIONAHA.110.991125 (2011).
76 Rafii, S., Butler, J. M. & Ding, B. S. Angiocrine functions of organ-specific endothelial cells. *Nature* **529**, 316-325, doi:10.1038/nature17040 (2016).
77 Matsumoto, K., Yoshitomi, H., Rossant, J. & Zaret, K. S. Liver organogenesis promoted by endothelial cells prior to vascular function. *Science* **294**, 559-563, doi:10.1126/science.1063889 (2001).
78 Lammert, E., Cleaver, O. & Melton, D. Induction of pancreatic differentiation by signals from blood vessels. *Science* **294**, 564-567, doi:10.1126/science.1064344 (2001).
79 Ramasamy, S. K., Kusumbe, A. P. & Adams, R. H. Regulation of tissue morphogenesis by endothelial cell-derived signals. *Trends Cell Biol.* **25**, 148-157, doi:10.1016/j.tcb.2014.11.007 (2015).
80 Calandra, T. & Roger, T. Macrophage migration inhibitory factor: a regulator of innate immunity. *Nat. Rev. Immunol.* **3**, 791-800, doi:10.1038/nri1200 (2003).
81 Flieger, O. *et al.* Regulated secretion of macrophage migration inhibitory factor is mediated by a non-classical pathway involving an ABC transporter. *FEBS Lett.* **551**, 78-86, doi:10.1016/s0014-5793(03)00900-1 (2003).
82 Cheng, Q. *et al.* Macrophage migration inhibitory factor increases leukocyte-endothelial interactions in human endothelial cells via promotion of expression of adhesion molecules. *J. Immunol.* **185**, 1238-1247, doi:10.4049/jimmunol.0904104 (2010).
83 Lee, C. Y. *et al.* Macrophage migration inhibitory factor increases cell motility and up-regulates alphavbeta3 integrin in human chondrosarcoma cells. *J. Cell. Biochem.* **113**, 1590-1598, doi:10.1002/jcb.24027 (2012).
84 Bernhagen, J. *et al.* MIF is a noncognate ligand of CXC chemokine receptors in inflammatory and atherogenic cell recruitment. *Nat. Med.* **13**, 587-596, doi:10.1038/nm1567 (2007).
85 Heinrichs, D. *et al.* Macrophage migration inhibitory factor (MIF) exerts antifibrotic effects in experimental liver fibrosis via CD74. *Proc. Natl. Acad. Sci. U. S. A.* **108**, 17444-17449, doi:10.1073/pnas.1107023108 (2011).
86 Heinrichs, D. *et al.* Protective role of macrophage migration inhibitory factor in nonalcoholic steatohepatitis. *FASEB J.* **28**, 5136-5147, doi:10.1096/fj.14-256776 (2014).
87 Makino, A. *et al.* High plasma levels of macrophage migration inhibitory factor are associated with adverse long-term outcome in patients with stable coronary artery disease and impaired glucose tolerance or type 2 diabetes mellitus. *Atherosclerosis* **213**, 573-578, doi:10.1016/j.atherosclerosis.2010.09.004 (2010).
88 Toso, C., Emamaullee, J. A., Merani, S. & Shapiro, A. M. The role of macrophage migration inhibitory factor on glucose metabolism and diabetes. *Diabetologia* **51**, 1937-1946, doi:10.1007/s00125-008-1063-3 (2008).
89 Avraamides, C. J., Garmy-Susini, B. & Varner, J. A. Integrins in angiogenesis and lymphangiogenesis. *Nat. Rev. Cancer* **8**, 604-617, doi:10.1038/nrc2353 (2008).
90 Legate, K. R., Montanez, E., Kudlacek, O. & Fassler, R. ILK, PINCH and parvin: the tIPP of integrin signalling. *Nat. Rev. Mol. Cell Biol.* **7**, 20-31, doi:10.1038/nrm1789 (2006).
91 Qin, J. & Wu, C. ILK: a pseudokinase in the center stage of cell-matrix adhesion and signaling. *Curr. Opin. Cell Biol.* **24**, 607-613, doi:10.1016/j.ceb.2012.06.003 (2012).

92 Hynes, R. O. Integrins: bidirectional, allosteric signaling machines. *Cell* **110**, 673-687 (2002).
93 Humphries, M. J. Integrin structure. *Biochem. Soc. Trans.* **28**, 311-339 (2000).
94 Brakebusch, C. *et al.* Skin and hair follicle integrity is crucially dependent on beta 1 integrin expression on keratinocytes. *EMBO J.* **19**, 3990-4003, doi:10.1093/emboj/19.15.3990 (2000).
95 Varner, J. A., Emerson, D. A. & Juliano, R. L. Integrin alpha 5 beta 1 expression negatively regulates cell growth: reversal by attachment to fibronectin. *Mol. Biol. Cell* **6**, 725-740 (1995).
96 Zhang, Z., Vuori, K., Reed, J. C. & Ruoslahti, E. The alpha 5 beta 1 integrin supports survival of cells on fibronectin and up-regulates Bcl-2 expression. *Proc. Natl. Acad. Sci. U. S. A.* **92**, 6161-6165 (1995).
97 Ross, T. D. *et al.* Integrins in mechanotransduction. *Curr. Opin. Cell Biol.* **25**, 613-618, doi:10.1016/j.ceb.2013.05.006 (2013).
98 Ishida, T., Peterson, T. E., Kovach, N. L. & Berk, B. C. MAP Kinase Activation by Flow in Endothelial Cells: Role of 1 Integrins and Tyrosine Kinases. *Circ. Res.* **79**, 310-316, doi:10.1161/01.res.79.2.310 (1996).
99 Planas-Paz, L. *et al.* Mechanoinduction of lymph vessel expansion. *EMBO J.* **31**, 788-804, doi:10.1038/emboj.2011.456 (2012).
100 Speicher, T. *et al.* Knockdown and knockout of beta1-integrin in hepatocytes impairs liver regeneration through inhibition of growth factor signalling. *Nat Commun* **5**, 3862, doi:10.1038/ncomms4862 (2014).
101 Xiao, X., Mruk, D. D. & Cheng, C. Y. Intercellular adhesion molecules (ICAMs) and spermatogenesis. *Hum. Reprod. Update* **19**, 167-186, doi:10.1093/humupd/dms049 (2013).
102 Amin, M. A. *et al.* Migration inhibitory factor up-regulates vascular cell adhesion molecule-1 and intercellular adhesion molecule-1 via Src, PI3 kinase, and NFkappaB. *Blood* **107**, 2252-2261, doi:10.1182/blood-2005-05-2011 (2006).
103 Long, E. O. ICAM-1: getting a grip on leukocyte adhesion. *J. Immunol.* **186**, 5021-5023, doi:10.4049/jimmunol.1100646 (2011).
104 Karenberg, K., Hudalla, H. & Frommhold, D. Leukocyte recruitment in preterm and term infants. *Mol Cell Pediatr* **3**, 35, doi:10.1186/s40348-016-0063-5 (2016).
105 Selzner, N. *et al.* ICAM-1 triggers liver regeneration through leukocyte recruitment and Kupffer cell-dependent release of TNF-alpha/IL-6 in mice. *Gastroenterology* **124**, 692-700, doi:10.1053/gast.2003.50098 (2003).
106 Duarte, S., Baber, J., Fujii, T. & Coito, A. J. Matrix metalloproteinases in liver injury, repair and fibrosis. *Matrix Biol.* **44-46**, 147-156, doi:10.1016/j.matbio.2015.01.004 (2015).
107 Reinstadler, S. J. *et al.* Combined biomarker testing for the prediction of left ventricular remodelling in ST-elevation myocardial infarction. *Open Heart* **3**, e000485, doi:10.1136/openhrt-2016-000485 (2016).
108 Fingerle-Rowson, G. *et al.* A tautomerase-null macrophage migration-inhibitory factor (MIF) gene knock-in mouse model reveals that protein interactions and not enzymatic activity mediate MIF-dependent growth regulation. *Mol. Cell. Biol.* **29**, 1922-1932, doi:10.1128/MCB.01907-08 (2009).
109 Wang, Y. *et al.* Ephrin-B2 controls VEGF-induced angiogenesis and lymphangiogenesis. *Nature* **465**, 483-486, doi:10.1038/nature09002 (2010).
110 Potocnik, A. J., Brakebusch, C. & Fassler, R. Fetal and adult hematopoietic stem cells require beta1 integrin function for colonizing fetal liver, spleen, and bone marrow. *Immunity* **12**, 653-663 (2000).

111 Haussiner, D. & Sies, H. Hepatic Glutamine Metabolism under the Influence of the Portal Ammonia Concentration in the Perfused Rat Liver. *Eur. J. Biochem.* **101**, 179-184, doi:10.1111/j.1432-1033.1979.tb04230.x (1979).
112 *COMPARATIVE ANATOMY AND HISTOLOGY - A MOUSE AND HUMAN ATLAS*. (Academic Press, 2012).
113 Schrage, A. *et al.* Murine CD146 is widely expressed on endothelial cells and is recognized by the monoclonal antibody ME-9F1. *Histochem. Cell Biol.* **129**, 441-451, doi:10.1007/s00418-008-0379-x (2008).
114 Schindelin, J. *et al.* Fiji: an open-source platform for biological-image analysis. *Nat Methods* **9**, 676-682, doi:10.1038/nmeth.2019 (2012).
115 Schmittgen, T. D. & Livak, K. J. Analyzing real-time PCR data by the comparative CT method. *Nat. Protoc.* **3**, 1101-1108, doi:10.1038/nprot.2008.73 (2008).
116 Noh, J. K. *et al.* Live cell-imaging perfusion culture system of liver sinusoidal endothelial cells to mimic stem cell engraftment in liver. *Transplant. Proc.* **44**, 1116-1119, doi:10.1016/j.transproceed.2012.03.007 (2012).
117 Gross JF, A. J. Mathematical models of capillary flow: a critical review. *Biorheology* **9**, 225-264 (1972).
118 vom Dahl, S. *et al.* Involvement of integrins in osmosensing and signaling toward autophagic proteolysis in rat liver. *J. Biol. Chem.* **278**, 27088-27095, doi:10.1074/jbc.M210699200 (2003).
119 Schliess, F., Reissmann, R., Reinehr, R., vom Dahl, S. & Haussinger, D. Involvement of integrins and Src in insulin signaling toward autophagic proteolysis in rat liver. *J. Biol. Chem.* **279**, 21294-21301, doi:10.1074/jbc.M313901200 (2004).
120 Hans, F. & Dimitrov, S. Histone H3 phosphorylation and cell division. *Oncogene* **20**, 3021-3027, doi:10.1038/sj.onc.1204326 (2001).
121 Buetow, M. A. L. M. M. S. B. S. in *COMPARATIVE ANATOMY AND HISTOLOGY - A MOUSE AND HUMAN ATLAS* (ed Suzanne Dintzis Piper M. Treuting, Denny Liggitt and Charles W. Frevert) Ch. 10, 135-153 (Academic Press, 2012).
122 Griffioen, A. W. *et al.* The angiogenic factor bFGF impairs leukocyte adhesion and rolling under flow conditions. *Angiogenesis* **2**, 235-243, doi:10.1023/A:1009237324501 (1998).
123 Luu, N. T., Glen, K. E., Egginton, S., Rainger, G. E. & Nash, G. B. Integrin-substrate interactions underlying shear-induced inhibition of the inflammatory response of endothelial cells. *Thromb. Haemost.* **109**, 298-308, doi:10.1160/TH12-06-0400 (2013).
124 Burger-Kentischer, A. *et al.* Reduction of the aortic inflammatory response in spontaneous atherosclerosis by blockade of macrophage migration inhibitory factor (MIF). *Atherosclerosis* **184**, 28-38, doi:10.1016/j.atherosclerosis.2005.03.028 (2006).
125 Yeh, T. M. *et al.* Dengue virus enhances thrombomodulin and ICAM-1 expression through the macrophage migration inhibitory factor induction of the MAPK and PI3K signaling pathways. *PLoS One* **8**, e55018, doi:10.1371/journal.pone.0055018 (2013).
126 Jin, X. Y. & Khan, T. M. Quality of life among patients suffering from cholestatic liver disease-induced pruritus: A systematic review. *J. Formos. Med. Assoc.* **115**, 689-702, doi:10.1016/j.jfma.2016.05.006 (2016).
127 Institute of Medicine Committee on the, P. & Control of Viral Hepatitis, I. in *Hepatitis and Liver Cancer: A National Strategy for Prevention and Control of Hepatitis B and C* (eds H. M. Colvin & A. E. Mitchell) (National Academies Press (US)

128 Akamatsu, N. & Kokudo, N. Liver transplantation for hepatocellular carcinoma from living-donor vs. deceased donor. *Hepatobiliary Surg Nutr* **5**, 422-428, doi:10.21037/hbsn.2016.08.03 (2016).
129 Reinehr, R., Gohlke, H., Sommerfeld, A., Vom Dahl, S. & Haussinger, D. Activation of integrins by urea in perfused rat liver. *J. Biol. Chem.* **285**, 29348-29356, doi:10.1074/jbc.M110.155135 (2010).
130 Janostiak, R., Pataki, A. C., Brabek, J. & Rosel, D. Mechanosensors in integrin signaling: the emerging role of p130Cas. *Eur. J. Cell Biol.* **93**, 445-454, doi:10.1016/j.ejcb.2014.07.002 (2014).
131 Hannigan, G. E. *et al.* Regulation of cell adhesion and anchorage-dependent growth by a new beta 1-integrin-linked protein kinase. *Nature* **379**, 91-96, doi:10.1038/379091a0 (1996).
132 Gkretsi, V. *et al.* Liver-specific ablation of integrin-linked kinase in mice results in abnormal histology, enhanced cell proliferation, and hepatomegaly. *Hepatology* **48**, 1932-1941, doi:10.1002/hep.22537 (2008).
133 Lathia, J. D. *et al.* Pivotal role for beta-1 integrin in neurovascular remodelling after ischemic stroke. *Exp. Neurol.* **221**, 107-114, doi:10.1016/j.expneurol.2009.10.007 (2010).
134 Liu, A., Fang, H., Dirsch, O., Jin, H. & Dahmen, U. Early release of macrophage migration inhibitory factor after liver ischemia and reperfusion injury in rats. *Cytokine* **57**, 150-157, doi:10.1016/j.cyto.2011.11.009 (2012).
135 Lemasters, J. J. & Thurman, R. G. Reperfusion injury after liver preservation for transplantation. *Annu. Rev. Pharmacol. Toxicol.* **37**, 327-338, doi:10.1146/annurev.pharmtox.37.1.327 (1997).
136 Feng, A. C., Fan, H. L., Chen, T. W. & Hsieh, C. B. Hepatic hemodynamic changes during liver transplantation: a review. *World J. Gastroenterol.* **20**, 11131-11141, doi:10.3748/wjg.v20.i32.11131 (2014).

Erklärung

An Eidesstatt erkläre ich, dass

- ich die vorgelegte Dissertation selbstständig und ohne unzulässige fremde Hilfe unter der Beachtung der "Grundsätze zur Sicherheit guter wissenschaftlicher Praxis an der Heinrich-Heine-Universität Düsseldorf" angefertigt habe und dass ich diese in der jetzigen oder einer ähnlichen Form noch keiner anderen Fakultät eingereicht habe;

- die Dissertation noch nicht veröffentlicht wurde (Veröffentlichungen nach § 6 (3) der Promotionsordnung bleiben hiervon ausgenommen).

Tobias Buschmann, Düsseldorf 2017

Danksagung

Ich danke...

Prof. Eckhard Lammert für die Betreuung, die Diskussionen und die Unterstützung während der Arbeit.

Prof. Hermann Aberle, der immer ein offenes Ohr und hilfreiche Tipps für mich hatte.

Prof. Dieter Häussinger und den Mitarbeiten des SFB974, vor allem Ute Albrecht und Prof. Verena Keitel, für das tolle Arbeitsumfeld.

Prof. Jürgen Bernhagen und Prof. Christian Trautwein für die Kooperation und freundliche Beratung.

Daniel Eberhard für die Beratung, wissenschaftliche Diskussionen und umfassenden seelsorgerischen Tätigkeiten.

Bengt Belgardt für seine umfassende Beratung und Diskussionen, sowohl über Wissenschaft als auch Unterhaltungselektronik.

Jennifer Axnick für die tolle Zusammenarbeit und ihre Freundschaft.

Jaqueline Kinold für die vielen wertvollen Tipps und das geteilte Leid.

Paul, Lena und Isabelle für die tolle Teamarbeit.

Silke Jakob und Barbara Bartosinska für die Hilfsbereitschaft und das schaffen einer tollen Arbeitsatmosphäre.

Nicole Eichhorst und Vanessa Herbertz für die gute Zusammenarbeit, Aufopferung und Offenheit für neue Ideen.

Den anderen Mitgliedern des Instituts für Stoffwechselphsiologe, Jessica, Carina, Okka, Haiko, Sofia, Esther, Linda, Anna und Silke.

Den ehemaligen Mitgliedern des Instituts: Astrid Wies, Jan Eglinger, Lara Planas-Paz und Martin Kragl.

Und vor allem meiner Frau, meinen Söhnen und meiner Familie für die Liebe und Unterstützung.